IL
NUOVO CIMENTO
ORGANO DELLA SOCIETÀ ITALIANA DI FISICA
SOTTO GLI AUSPICI DEL CONSIGLIO NAZIONALE DELLE RICERCHE

VOL. X, N. 3 *Serie decima* 1° Novembre 1958

On the Consistency of Schwinger's Action Principle.

T. W. B. KIBBLE (*)

Tait Institute of Mathematical Physics - University of Edinburgh - Edinburgh

(ricevuto il 17 Aprile 1958)

Summary. — The conditions for consistency of the equations of motion and commutation relations derived from Schwinger's action principle are investigated. For consistency, it is, in particular, necessary that the time-derivative of equal-time c-number commutators should vanish. It is shown that, under certain assumptions, the theory is consistent if the interaction terms in the Lagrangian are written in a suitably symmetrized form, identical with that required for invariance under SR, and that in general only theories which are equivalent to such «symmetrized» theories can be consistent.

1. – Introduction.

Schwinger's action principle [1] has been extensively used to provide a concise logical foundation from which equations of motion and commutation relations may be derived, given the Lagrangian function $L(x)$. The purpose of this paper is to examine certain requirements which must be satisfied by this function, to ensure consistency.

(*) Present address: Norman Bridge Laboratory of Physics, California Institute of Technology.

(1) J. SCHWINGER: *Phys. Rev.*, **82**, 914 (1951); **91**, 713 (1953).

We consider a system described by a set of Hermitian field variables $\chi_r(x)$, with the Lagrangian,

$$(1) \qquad \begin{cases} L = \frac{1}{4}(\tilde{\chi}A^\mu \partial_\mu \chi - \partial_\mu \tilde{\chi} A^\mu \chi) - H\,, \\ H = \frac{1}{2}\tilde{\chi} M \chi + H_I\,. \end{cases}$$

A^μ and M are c-number matrices of the form

$$A^\mu = A^\mu_B \oplus A^\mu_F, \qquad M = M_B \oplus M_F\,,$$

corresponding to the partition of χ into Bose and Fermi variables, and

$$(2) \qquad \begin{cases} A^{\mu *}_B = A^\mu_B = -\tilde{A}^\mu_B\,, & M^*_B = M_B = \tilde{M}_B\,, \\ -A^{\mu *}_F = A^\mu_F = \tilde{A}^\mu_F\,, & -M^*_F = M_F = -\tilde{M}_F\,. \end{cases}$$

Here the complex conjugate (or operator Hermitian conjugate) of a matrix A is A^*; the transpose is $\tilde{A}$; and the Hermitian conjugate is $A^+ = \tilde{A}^*$.

If F and G are products of field variables, we define their generalized commutator $(F; G)$ to be equal to the commutator $[F, G]$ unless F and G are both odd in the Fermi variables, in which case it is the anticommutator $\{F, G\}$. In Sect. **2**, some notations are introduced to enable $(F; G)$ to be expressed in terms of the individual commutators $(\chi_r; G)$. Derivatives with respect to χ are also defined.

The equations of motion and commutation relations are written down in Sect. **3**, for a restricted class of theories, in a form appropriate to the subsequent discussion.

The commutation relations on any spacelike surface may be evaluated by using the equations of motion and the commutation relations on another given spacelike surface. For consistency, these must have the same form as those obtained directly from the action principle. Hence one must require that

$$(3) \qquad \partial_0 (\chi_r(\boldsymbol{x}, x^0); \chi_s(\boldsymbol{x}, x^0)) = 0\,,$$

whenever this commutator is a c-number. The conditions under which this relation holds are investigated in Sect. **4**, and it is shown that theories which do not satisfy (3) have other disadvantages, including the appearance of infinite terms in the equations of motion. In Sect. **5** it is shown that theories (of our restricted class) for which H is suitably symmetrized are consistent. This symmetrization requirement is identical with that assumed by PAULI [2] in his proof of invariance under SR. Thus for theories of this class the con-

[2] W. PAULI: *Niels Bohr and the Development of Physics* (1955), pp. 30-51.

sistency requirement is equivalent to SR invariance. The possibility of such symmetrization was also used by KIBBLE and POLKINGHORNE ([3]) in a discussion of the role of linear variations of the field variables in the action principle. The proof of consistency of these theories is based on a theorem on symmetrized products whose proof is given in an Appendix.

The conclusions, and their possible extension to other cases, are discussed in Sect. **6**.

2. – Definitions.

Let F and G be products of field variables. Then the operator $G\delta_r F$ is defined to be the sum of all terms in which one occurrence of χ_r in F is replaced by G, multiplied by the sign factor $(-1)^{(g+p)q}$, where g, p and q are the numbers of Fermi factors in G, in χ_r, and in F to the left of the deleted χ_r, respectively. We define $F\delta_r^* G$ in the same way, but with «right» in place of «left». As the notation suggests,

$$(G\delta_r F)^* = F^* \delta_r^* G^* . \tag{4}$$

We note that

$$(F; G) = F\delta^+(\chi; G) = (F; \tilde{\chi})\delta G . \tag{5}$$

Left and right derivatives of F are defined by

$$\delta_r F = 1\delta_r F , \qquad F\delta_r^* = F\delta_r^* 1 .$$

It is important to note that in general $G\delta_r F$ and $G(\delta_r F)$ are different operators (unless G is a c-number). Now

$$(\delta_r F)\delta_s^* = \delta_r (F\delta_s^*) .$$

Thus we may define unambiguously the matrix operator $\delta F\delta^+$.

It is clear that (5) is only self-consistent if

$$F\delta^+\{(\chi; \tilde{\chi})\delta G\} = \{F\delta^+(\chi; \tilde{\chi})\}\delta G . \tag{6}$$

One may easily verify, however, that this is always an identity.

If the matrix A^0 is singular, we write it, by a suitable real non-singular transformation of the χ, as

$$A^0 = \begin{bmatrix} A_{11}^0 & 0 \\ 0 & 0 \end{bmatrix} ,$$

([3]) T. W. B. KIBBLE and J. C. POLKINGHORNE: *Proc. Roy. Soc.*, A **242**, 252 (1957).

where A^0_{11} is non-singular. The corresponding partitions of χ and of any matrix B will be denoted by

$$\chi = \begin{bmatrix} \chi_1 \\ \chi_2 \end{bmatrix} \quad \text{and} \quad B = \begin{bmatrix} B_{11} & B_{12} \\ B_{21} & B_{22} \end{bmatrix}.$$

It will be convenient to redefine H_I in (1) to include the terms

$$\tfrac{1}{2}(\tilde{\chi}_1 M_{12} \chi_2 + \tilde{\chi}_2 M_{21} \chi_1),$$

so that we now have

$$H = (\tfrac{1}{2}\tilde{\chi}_1 M_{11} \chi_1 + \tilde{\chi}_2 M_{22} \chi_2) + H_I .$$

3. – Equations of motion and commutation relations.

From the action principle (1), the equations of motion are

$$A^\mu \partial_\mu \chi = M\chi + \delta H_I \tag{7}$$

or

$$-\partial_\mu \tilde{\chi} A^\mu = \tilde{\chi} M + H_I \delta^+ . \tag{8}$$

In order that (7) and (8) be consistent, it is necessary that H_I be restricted to be even in the Fermi variables. The commutation relations are

$$A^0(\chi(\boldsymbol{x}, x^0); \tilde{\chi}(\boldsymbol{x}', x^0))A^0 = iA^0\delta(\boldsymbol{x} - \boldsymbol{x}') .$$

Using the decomposition of Sect. 2, these equations become

$$A^0_{11}\partial_0\chi_1 + A^k_{11}\partial_k\chi_1 + A^k_{12}\partial_k\chi_2 = M_{11}\chi_1 + \delta_1 H_I , \tag{9}$$

$$A^k_{21}\partial_k\chi_1 + A^k_{22}\partial_k\chi_2 = M_{22}\chi_2 + \delta_2 H_I , \tag{10}$$

$$(\chi_1(\boldsymbol{x}, x^0); \tilde{\chi}_1(\boldsymbol{x}', x^0)) = i(A^0_{11})^{-1}\delta(\boldsymbol{x} - \boldsymbol{x}') . \tag{11}$$

The commutation relations for χ_2 must follow from (11) by use of (10). In order to avoid infinite series in derivatives of the δ-function, we shall assume that $A^k_{22} = 0$. This assumption is certainly valid for all the usual theories (*). We shall also make the simplifying assumption that M_{22} is non-singular: this too is valid in all the familiar theories. Then

$$\chi_2 = M^{-1}_{22}(A^k_{21}\partial_k\chi_1 - \delta_2 H_I) . \tag{12}$$

(*) *E.g.*, the Kemmer β-matrices contain no non-zero elements connecting φ^k and φ^l.

If we define a matrix operator K by the implicit relation

$$K = \delta H_I \delta^+ - (\delta H_I)\delta^+ NK\,, \tag{13}$$

where

$$N = \begin{bmatrix} 0 & 0 \\ 0 & M_{22}^{-1} \end{bmatrix},$$

then the commutators $(\chi_2, \tilde{\chi}_1)$ may be expressed in terms of K. If $x = (\boldsymbol{x}, x^0)$ and $x' = (\boldsymbol{x}', x^0)$ then it is easy to verify that

$$(\chi_2(x);\, \tilde{\chi}(x'))\, A_{11}^0 = iC_{21}(x)\,\delta(\boldsymbol{x} - \boldsymbol{x}') + iC_{21}^k(x)\partial_k \delta(\boldsymbol{x} - \boldsymbol{x}')\,, \tag{14}$$

where

$$\begin{cases} C_{21} = -M_{22}^{-1} K_{21}\,, \\ C_{21}^k = (M_{22}^{-1} - M_{22}^{-1} K_{22} M_{22}^{-1})\, A_{21}^k\,. \end{cases} \tag{15}$$

We note that K has the iterative expansion

$$K = \delta H_I \delta^+ - (\delta H_I)\delta^+ N(\delta H_I \delta^+) + (\delta H_I)\delta^+ N\{(\delta H_I)\delta^+ N(\delta H_I \delta^+)\} - \dots\,, \tag{16}$$

if this converges.

In the restricted case where H_I is linear in χ_2, the relation (12) becomes an explicit equation for χ_2 in terms of χ_1, and (15) becomes

$$\begin{cases} C_{21} = -M_{22}^{-1}(\delta_2 H_I \delta_1^+)\,, \\ C_{21}^k = M_{22}^{-1} A_{21}^k\,. \end{cases} \tag{17}$$

Note that from (14) there follows

$$\begin{aligned} A_{11}^0(\chi_1(x);\, \tilde{\chi}_2(x')) &= iC_{21}^+(x')\delta(\boldsymbol{x} - \boldsymbol{x}') - iC_{21}^{k+}(x')\partial\,\delta_k(\boldsymbol{x} - \boldsymbol{x}') = \\ &= i\{C_{21}^+(x) - \partial_k C_{21}^{k+}(x)\}\delta(\boldsymbol{x} - \boldsymbol{x}') - iC_{21}^{k+}(x)\partial_k \delta(\boldsymbol{x} - \boldsymbol{x}')\,. \end{aligned} \tag{18}$$

4. – Consistency conditions.

According to (3), one requires for consistency that, since (11) is a c-number,

$$A_{11}^0(\partial_0 \chi_1(x);\, \tilde{\chi}_1(x'))\, A_{11}^0 + A_{11}^0(\chi_1(x);\, \partial_0 \tilde{\chi}_1(x'))A_{11}^0 = 0\,.$$

Expressing $\partial_0 \chi_1$ in terms of χ_1 and χ_2 by (9), and using (5), (11), (14), (17)

and (18), this condition may be written in the form

$$
\left\{
\begin{aligned}
&A^k_{12} M^{-1}_{22} \partial_k (K_{21} - K^+_{12}) + (K_{11} - K^+_{11}) = 0 \,, \\
&A^k_{12} M^{-1}_{22} (K_{21} - K^+_{12}) + (K_{12} - K^+_{21}) M^{-1}_{22} A^k_{21} + \\
&\qquad\qquad + A^l_{12} M^{-1}_{22} \partial_l (K_{22} - K^+_{22}) M^{-1}_{22} A^k_{21} = 0 \,, \\
&A^k_{12} M^{-1}_{22} (K_{22} - K^+_{22}) M^{-1}_{22} A^l_{21} + A^l_{12} M^{-1}_{22} (K_{22} - K^+_{22}) M^{-1}_{22} A^k_{21} = 0 \,.
\end{aligned}
\right. \tag{19}
$$

It is clear that a sufficient condition for (19) to hold is

$$K = K^+ \,. \tag{20}$$

In general, this will also be a necessary condition, although it may be possible to choose the matrices A^k_{12} in such a way that a less stringent condition would suffice. Note that the leading term in the expansion (16) of K is automatically Hermitian.

If H_I is linear in χ_2, then (20) reduces to

$$(\delta_1 H_I) \delta^+_2 M^{-1}_{22} (\delta_2 H_I \delta^+_1) = (\delta_1 H_I \delta^+_2) M^{-1}_{22} \delta_2 (H_I \delta^+_1) \,. \tag{21}$$

Moreover, this is now a necessary, as well as a sufficient, condition for consistency. Since, in this case, (12) is an explicit solution for χ_2, any function of χ may be expressed as a function of χ_1 only. The condition (6) for functions F and G of χ_1 becomes

$$F \delta^+_1 (A^0_{11})^{-1} (\delta_1 G) = (F \delta^+_1)(A^0_{11})^{-1} \delta_1 G \,, \tag{22}$$

which bears a formal resemblance to (19). This resemblance is, however, illusory, since (22) is identically satisfied, whereas (21) is not.

To see more clearly the meaning of (21), we consider the special case

$$H_I = f^+_2 \chi_2 + \tilde{\chi}_2 f_2 + g \,. \tag{23}$$

where f_2 and g are functions of χ_1 only, and $g^* = g$. Then a straighforward calculation shows that (21) may be expressed in the form

$$\mathrm{tr}\{M^{-1}_{22} (\delta_r f_2 ; \tilde{f}_2 \delta^*_s)\} = \mathrm{tr}\{M^{-1}_{22} (\delta_r f^*_2 ; f^+_2 \delta^*_s)\} \,, \tag{24}$$

for every pair of components χ_r and χ_s of χ_1. Here the trace is taken over the components of χ_2. It is worth noting that the interaction terms usually considered are consistent, because every f corresponding to a Bose variable

is Hermitian, and every f corresponding to a Fermi variable anti-Hermitian. Of course, one might take the Bose f's anti-Hermitian, or the Fermi f's Hermitian, but it is easy to see that such interaction terms are vacuous, in that they contribute nothing to the equations of motion. Inconsistencies only arise when the f's are neither Hermitian nor anti-Hermitian.

One may easily find examples of inconsistent theories. If we consider a scalar field represented by φ and φ^μ, and two spinor fields ψ^1 and ψ^2 (all Hermitian), then the interaction term (*)

$$H_I = c\varphi^\mu \tilde{\psi}^1 i\beta\gamma_\mu \psi^2 + c^* \tilde{\psi}^2 i\beta\gamma_\mu \psi^1 \varphi^\mu , \tag{25}$$

where $c = a + ib$ is inconsistent if neither a nor b is zero. It may be verified that, for example, $\partial_0\{\psi^1(x), \tilde{\psi}^1(x')\}$ is non-zero (and in fact infinite). The theory is in any case highly pathological, as can be seen from writing the equations of motion for the spinor fields, using the commutation relations, in the form

$$\begin{cases} i\gamma^\mu \partial_\mu \psi^1 = m\psi^1 + ai\gamma_\mu \{\varphi^\mu, \psi^2\} - 6ab i\gamma_0 \psi^1 \delta(0) , \\ i\gamma^\mu \partial_\mu \psi^2 = m\psi^2 - ai\gamma_\mu \{\varphi^\mu, \psi^1\} - 6ab i\gamma_0 \psi^2 \delta(0) . \end{cases} \tag{26}$$

The only terms depending on b contain the infinite factor $\delta(0)$. It is clear that the peculiarities of the theory stem from the attempt to include in H_I a term of the form of a commutator of two expressions, each even in the Fermi variables. It is interesting to note that, if one uses the commutation relations, this term in H_I actually vanishes, and one finds

$$H_I = a\{\varphi^\mu, \tilde{\psi}^1 i\beta\gamma_\mu \psi^2\} . \tag{27}$$

Of course, the theory obtained by starting with (27) differs from that given by (25), and is perfectly consistent.

It is useful to consider also the theory with

$$H_I = c\varphi\tilde{\psi}^1 \beta\psi^2 + c^* \tilde{\psi}^2 \beta\psi^1 \varphi . \tag{28}$$

Since (28) contains no components of χ_2, the theory is consistent, despite its close resemblance to (25). This is essentially due to the fact that φ exactly commutes with ψ^1 and ψ^2, so that the terms in ab, analogous to those in (26) are zero. The consistency of this theory is thus rather accidental, and is closely related to the fact that the theory is identical with that obtained by

(*) We use the $(1, -1, -1, -1)$ metric, and pure imaginary Dirac matrices.

choosing

$$H_I = a\{\varphi, \tilde{\psi}^1 \beta \psi^2\}, \tag{29}$$

which corresponds to (27). The expressions (27) and (29) may be regarded as symmetrized forms of (25) and (28), and it thus appears that an interaction term is only consistent if it is equivalent to its symmetrized form. Note that (25) with $a = 0$ gives a consistent theory, equivalent to that with $H_I = 0$.

5. – Symmetrization of H_I.

In this section we shall discuss in greater detail the general rule roughly formulated at the end of Sect. **4**.

Let $a_1, ..., a_n$ be n given operators. Their symmetrized product is defined to be

$$S[a_1 ... a_n] = \frac{1}{n!} \sum_P \alpha(P) a_{P1} ... a_{Pn}, \tag{30}$$

where the sum is over all permutations P of $(1 ... n)$, and $\alpha(P)$ is $+1$ or -1 according as the number of interchanges of Fermi variables on going from the order $a_1, ..., a_n$ to $a_{P1}, ..., a_{Pn}$ is even or odd: $\alpha(P)$ may be termed the Fermi signature of the permutation P. We shall require the following theorem, whose proof is given in an Appendix:

Theorem. *If $a_1, ..., a_n$ and $b_1, ..., b_m$ are operators such that*

$$(a_i; b_j) = c_{ij}, \tag{31}$$

where each c_{ij} is a c-number which vanishes unless a_i and b_j are variables of the same type (both Bose or both Fermi), then

$$S[a_1 ... a_n S[b_1 ... b_m]] = S[S[a_1 ... a_n] b_1 ... b_m]. \tag{32}$$

We shall now show that if H_I is symmetrized (that is, written as a sum of terms, each a symmetrized product of field variables), and is linear in χ_2, then the resulting theory satisfies the consistency conditions (21). This restriction on H_I is identical with the « ordering of operators » assumed by PAULI [2] in his proof of invariance under SR. It is a remarkable fact that the consistency conditions found here appear to be equivalent to SR invariance.

Now, if H_I is symmetrized, then each element of the matrix $\delta_2 H_I \delta_1^+$ will itself be a symmetrized function of χ_1 only. Consider the term

$$(\delta_{1r} H_I) \delta^*_{2s} (M^{-1}_{22})_{st} (\delta_{2t} H_I \delta^*_{1u}) \tag{33}$$

of the left side of (21). It is clear that (apart from the c-number factor $(M_{22}^{-1})_{st}$) this is equal to the left side of (32) with $a_1 \dots a_n$ replaced by $\delta_{1r} H_I \delta_{2s}^*$ and $b_1 \dots b_m$ by $\delta_{2t} H_I \delta_{1u}^*$. The corresponding term

$$(\delta_{1r} H_I \delta_{2s}^*)(M_{22}^{-1})_{st} \delta_{2t} (H_I \delta_{1u}^*) \tag{34}$$

from the right side of (21) is the same multiple of the right side of (32). But, since these expressions involve χ_1 only, the relations (31) are satisfied. Hence, by the theorem, (33) and (34) are equal, and the consistency condition (21) is satisfied.

The symmetrized form of any theory is obtained by replacing every product by the corresponding symmetrized product, and evidently any theory which is equivalent to its symmetrized form is consistent. It is probable that the converse is also true, since any non-symmetrized terms in H_I will contribute to the equations of motion terms involving generalized commutators as factors, and these terms may be replaced by expressions which either vanish or contain the infinite factor $\delta(0)$.

It is easy to show that for theories of the special form (23), the condition (24) is equivalent to the requirement that the theory be equivalent to its symmetrized form.

6. – Conclusions.

It is not certain to what extent the considerations of this paper might be extended to cases in which H_I is more than linear in χ_2, but it may be conjectured that the symmetrization condition would ensure consistency in that case also. The preceding discussion leads us to conjecture that the following conditions are each equivalent to the self-consistency of the theory:

i) the consistency condition (25), or (27), holds;

ii) the theory is equivalent to its symmetrized form;

iii) the theory is invariant under SR.

In view of the present interest in the TCP theorem, the last condition may be of considerable importance.

There would be no difficulty in extending the discussion to include commuting sets of kinematically independent Fermi fields, provided that H is even in each set separately. (Indeed, one may also allow anticommuting Bose fields, provided that H is even in those variables which anticommute with each given variable).

It is worth remarking that the non-interaction terms in L are already symmetrized functions, in view of the conditions (2) on A^μ and M.

* * *

I wish to thank Dr. J. C. POLKINGHORNE for many interesting discussions and helpful suggestions.

APPENDIX

We now prove the theorem stated in Sect. 5. Define

$$\alpha_{ij} = \begin{cases} -1, & \text{if } a_i \text{ and } b_j \text{ are both Fermi variables;} \\ +1, & \text{otherwise.} \end{cases}$$

Let P and Q denote permutations of $(1 \ldots n)$ and $(1 \ldots m)$. Then

$$\text{(A.1)} \qquad f \equiv S[a_1 \ldots a_n S[b_1 \ldots b_m]] =$$

$$= \frac{1}{(n+1)!}\frac{1}{m!}\sum_P \sum_Q \alpha(P)\alpha(Q)\{a_{P1} \ldots a_{Pn} b_{Q1} \ldots b_{Qm} +$$

$$+ (\alpha_{Pn,Q1} \ldots \alpha_{Pn,Qm}) a_{P1} \ldots a_{P(n-1)} b_{Q1} \ldots b_{Qm} a_{Pn} + \ldots$$

$$+ (a_{P1,Q1} \ldots \alpha_{P1,Qm}) \ldots (\alpha_{Pn,Q1} \ldots \alpha_{Pn,Qm}) b_{Q1} \ldots b_{Qm} a_{P1} \ldots a_{Pn}\}.$$

Now

$$\sum_Q \alpha(Q)(\alpha_{i,Q1} \ldots \alpha_{i,Qm}) b_{Q1} \ldots b_{Qm} a_i = \sum_Q \alpha(Q)\{a_i b_{Q1} \ldots b_{Qm} - c_{i,Q1} b_{Q2} \ldots b_{Qm} -$$

$$- (\alpha_{i,Q1}) c_{i,Q2} b_{Q1} b_{Q3} \ldots b_{Qm} - \ldots - (\alpha_{i,Q1} \ldots \alpha_{i,Q(m-1)}) c_{i,Qm} b_{Q1} \ldots b_{Q(m-1)}\}.$$

But, in virtue of the fact that $c_{ij} = 0$ unless a_i and b_j are of the same type,

$$\text{(A.2)} \qquad \alpha_{ik} c_{ij} = \alpha'_{jk} c_{ij},$$

where α'_{jk} refers to b_j and b_k. Hence making a permutation of the indices (Qj) in each term, and absorbing the appropriate « Fermi signature »,

$$\sum_Q \alpha(Q)(\alpha_{i,Q1} \ldots \alpha_{i,Qm}) b_{Q1} \ldots b_{Qm} a_i = \sum_Q \alpha(Q)\{a_i b_{Q1} \ldots b_{Qm} - m c_{i,Q1} b_{Q2} \ldots b_{Qm}\}.$$

Thus each term within the braces in (A.1) may be expressed in terms of the preceding one. Using (A.2) again, and making a suitable permutation in the

indices (P_i), one finds

$$f = S[a_1 \dots a_n]\, S[b_1 \dots b_m] - \frac{1}{(n+1)!}\,\frac{1}{m!}\sum_P \sum_Q \alpha(P)\alpha(Q) m c_{Pn,Q1} \cdot$$

$$\cdot \Big\{ n a_{P1} \dots a_{P(n-1)} b_{Q2} \dots b_{Qm} +$$

$$+ (n-1)(\alpha_{P(n-1),Q2} \dots \alpha_{P(n-1),Qm}) a_{P1} \dots a_{P(n-2)} b_{Q2} \dots b_{Qm} a_{P(n-1)} +$$

$$+ \dots + (\alpha_{P1,Q2} \dots \alpha_{P1,Qm}) \dots (\alpha_{P(n-1),Q2} \dots \alpha_{P(n-1),Qm}) b_{Q2} \dots b_{Qm} a_{P1} \dots a_{P(n-1)} \Big\}.$$

This process may be repeated, and each term again expressed in terms of the preceding one. We obtain in this way

$$f = S[a_1 \dots a_n]\, S[b_1 \dots b_m] - \frac{1}{(n+1)!}\,\frac{1}{m!}\sum_P \sum_Q \alpha(P)\alpha(Q) \cdot$$

$$\cdot \Big\{ m \binom{n+1}{2} a_{P1} \dots a_{P(n-1)} b_{Q2} \dots b_{Qm} c_{Pn,Q1} -$$

$$- m(m-1) \binom{n+1}{3} a_{P1} \dots a_{P(n-2)} b_{Q3} \dots b_{Qm} c_{P(n-1),Q2} c_{Pn,Q1} + \dots \Big\} =$$

$$= S[a_1 \dots a_n]\, S[b_1 \dots b_n] + \sum_P \sum_Q \alpha(P)\alpha(Q) \cdot$$

$$\cdot \sum_{i=1}^{\min(m,n)} (-1)^i \frac{a_{P1} \dots a_{P(n-1)}}{(n-i)!} \cdot \frac{b_{Q(i+1)} \dots b_{Qm}}{(m-i)!} \cdot \frac{c_{P(n-i-1),Qi} \dots c_{Pn,Q1}}{(i+1)!}.$$

In view of the obvious symmetry of this expression between the operators a_i and b_j, it is clear that

$$S[a_1 \dots a_n\, S[b_1 \dots b_m]] = S[S[a_1 \dots a_n] b_1 \dots b_m].$$

This completes the proof.

RIASSUNTO (*)

Si esaminano le condizioni per la compatibilità delle equazioni di moto colle relazioni di commutazione derivanti dal principio d'azione di Schwinger. Per la compatibilità è in particolare necessario che le derivate temporali di commutatori di numeri c contemporanei si annullino. Si dimostra che, in determinate ipotesi, la teoria è consistente se i termini di interazione del lagrangiano sono scritti in un'adatta forma simmetrizzata identica a quella richiesta per l'invarianza rispetto all'inversione dello spazio, e che, in generale, solo le teorie di questo tipo « simmetrizzato » o equivalenti possono essere consistenti.

(*) *Traduzione a cura della Redazione.*

IL NUOVO CIMENTO Vol. X, N. 3 1° Novembre 1958

Multiple Neutron Production in a Cosmic Ray Neutron Monitor Pile.

M. A. Collins (*)

Physics Department, Victoria University of Wellington - New Zealand

(ricevuto il 4 Luglio 1958)

Summary. — A measurement of the number of neutrons produced in the lead of a paraffin-lead cosmic-ray neutron detector of the Chicago design has been made. The experiment indicates that an average of nine neutrons are created per event.

1. – Introduction.

The cosmic ray neutron monitor developed by the Chicago group (Simpson *et al.* [1]) for the study of the nucleonic component of the cosmic radiation uses boron trifluoride counters to detect neutrons produced locally in the lead-paraffin pile.

The production of neutrons by cosmic ray interactions in various elements was studied by Cocconi *et al.* [2] and by Cocconi-Tongiorgi [3,4]. It was shown later by Cocconi *et al.* [5,6] and by Geiger [7] that the number of neutrons

(*) Now at Dominion Physical Laboratory Lower Hutt, New Zealand.

(1) J. A. Simpson, W. H. Fonger and S. B. Treiman: *Phys. Rev.*, **90**, 934 (1953).

(2) G. Cocconi, V. Cocconi-Tongiorgi and K. Greisen: *Phys. Rev.*, **74**, 1867 (1948).

(3) V. Cocconi-Tongiorgi: *Phys. Rev.*, **75**, 928 (1948).

(4) V. Cocconi-Tongiorgi: *Phys. Rev.*, **76**, 517 (1949).

(5) G. Cocconi, V. Cocconi-Tongiorgi and M. Widgoff: *Phys. Rev.*, **79**, 768 (1950).

(6) G. Cocconi and V. Cocconi-Tongiorgi: *Phys. Rev.*, **84**, 29 (1951).

(7) K. W. Geiger: *Can. Journ. Phys.*, **34**, 288 (1956).

produced in an interaction in lead depends on the thickness of the local « producer ». It is, however, difficult to predict from these measurements the average number of neutrons produced per interaction in a pile of the Chicago design, nor does it appear that any measurements of the neutron multiplicity in such a pile have been recorded.

The present paper describes some measurements made on a two-counter pile from which a value for the average neutron multiplicity can be found.

2. – Outline of method.

GEIGER (7) showed that for a nuclear evaporation process the average neutron multiplicity is given by:

$$\bar{v} = \left(\frac{1}{1 - \exp[-a]}\right). \tag{1}$$

This relation follows from the assumption that the number of events, $I(v)$, with multiplicity v is:

$$I(v) = (\exp[a] - 1)\exp[-av] \tag{2}$$

where « a » is a constant.

GEIGER (7) also developed the following expression which enables a to be evaluated in terms of measurable quantities:

$$\frac{\Delta \log R_m}{\Delta m} = \log \varepsilon f - a \log e - \log\{1 - (1 - \varepsilon f)\exp[-a]\}, \tag{3}$$

where R_m is the observed rate at which groups of m counts occur within a gate interval, initiated by the first count, ε is the neutron detection efficiency of the system, and f is the « gate efficiency » as defined in Sect. 6.

By measuring R_m for different values of m it is possible to evaluate a and so to find $\bar{v}$.

3. – Experimental details.

A cross-section of the pile is shown in Fig. 1.

The preamplifier, amplifier and discriminator circuits were similar to those suggested by ELLIOT (8).

(8) H. ELLIOT: *Cosmic Radiation Neutron Intensity Monitor* (ed. J. A. SIMPSON). The University of Chicago (Jan. 1955).

The pulse of the first detected neutron from an interaction in the lead was used to open a « gate » circuit of known interval, and the number of neutron counts occurring within that interval was recorded.

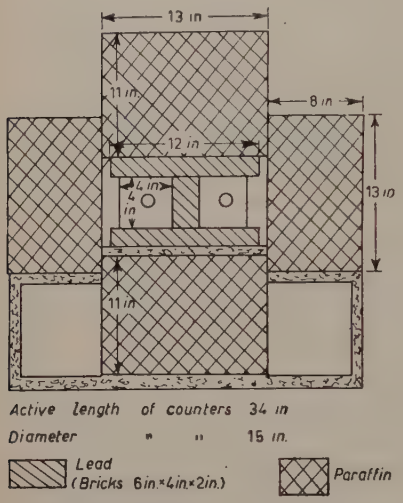

Fig. 1.

This was achieved by means of an integrating circuit described in a Philips Application Note No. EB 34-8, in which each pulse gave a step charge to a condenser. The integration network was followed by a univibrator which could be biased to trigger on any step of the integration condenser charge, that is after any given number of pulses had occurred. In the present experiment five such channels were provided which recorded the occurrence of at least 1, 2, 3, 4 or 5 pulses respectively within the period of the gate interval. All channels were reset at the end of the gate interval by blocking the input circuit and discharging the integrating condensers. The number of « single » events was therefore obtained by subtracting the count in channel 2 from the count in channel 1 and similarly for two- three- and four-fold events. Channel 5 recorded all events of five-fold or greater multiplicity. Because of the low count rate (40 counts per minute) there was only a very small probability of neutrons from more than one event being detected within the gate interval used.

To test the operation of the above equipment a pulse generator was used to give groups of 1 to 5 pulses, the groups being spaced at intervals slightly greater than the gate interval plus the time required to reset the equipment. Using this generator it was possible to test the operation by observing the output recorders for each channel, for a known number of pulses from the generator, or by displaying simultaneously the input and appropriate channel output on a double beam oscilloscope. A further test was made using a Ra-Be neutron source. In agreement with the assumption that the low energy neutrons from the source would produce a large preponderance of single-fold events, the use of the source gave a large increase in the channel 1 count but a negligible increase in all other channels.

4. – Results.

Table I shows the values obtained for R_m and m, as defined above, using a gate interval of 340 μs duration.

TABLE I. – *Observed multiplicity m.*

	1	2	3	4
Hourly rate	2141 ± 8	179 ± 3.5	27.5 ± 1.5	3.8 ± 0.50

Values of $\log_{10} R_m$ were plotted against m as shown in Fig. 2. From this curve the slope $(\Delta \log_{10} R_m)/\Delta m$ was obtained between the points $m = 1$ and $m = 2$.

Using equations (1) and (3) a number of points were calculated enabling a graph of $(\Delta \log_{10} R_m)/\Delta m$ against $\bar{\nu}$ to be drawn (Fig. 3), the values of ε (Sect. **5**) and f (Sect. **6**) having been obtained experimentally.

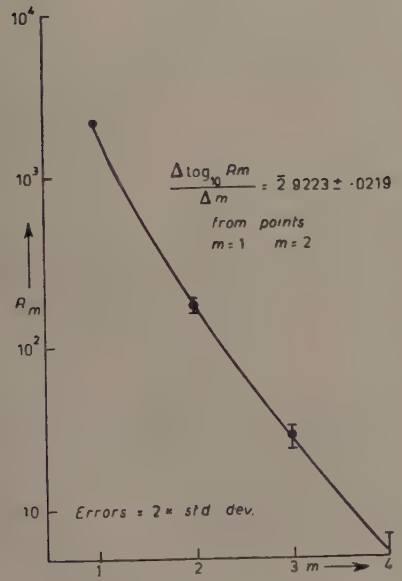

Fig. 2.

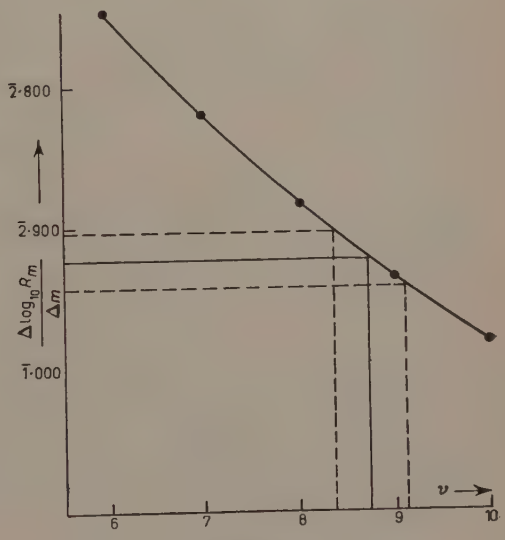

Fig. 3.

It was then possible to read off the value of $\bar{\nu}$ corresponding to the experimental value of $(\Delta \log_{10} R_m)/\Delta m$ obtained above.

The value obtained was $\bar{\nu} = (8.8 \pm 0.3)$ neutrons per event, the uncertainty quoted here being equivalent to the standard deviations of the count rates.

This value is, however, subject to a much greater uncertainty due to the large uncertainty in the detection efficiency of the pile.

Consideration of this factor indicates that the mean neutron multiplicity lies between 7 and 11 neutrons per event.

5. – Detection efficiency.

The neutron detection efficiency was determined experimentally using a radium beryllium neutron source. The value obtained was $\varepsilon = (1.3 \pm 0.2)\%$ the uncertainty being due chiefly to the uncertainty of the source calibration.

6. – Gate efficiency.

The « gate efficiency » f as defined by GEIGER [7] is given by:

$$f = \frac{N}{N_0},$$

where N_0 is the number of neutron counter pulses produced per event and N is the number of counts actually recorded within the gate interval.

Now the number of neutron counts occurring in a gate interval T, commencing at the first count, is:

$$N = N_0 \left(1 - \exp\left[\frac{-T}{\tau}\right]\right),$$

where τ is the mean life for absorption of the neutrons. The gate efficiency is then

$$f = \frac{N}{N_0} = \left(1 - \exp\left[\frac{-T}{\tau}\right]\right).$$

The determination of f therefore reduces to a determination of the mean life. This may be carried out as shown in the following section using the apparatus already described.

By using a value of $\tau = 150\ \mu s$ the gate efficiency was found to be 91% for the 340 μs gate.

7. – Mean life of neutrons in the pile.

If N_1 neutrons are present at a time t_1 when the gate opens, and N_2 remain at time t_2, when the gate closes, then the number absorbed is:

$$N = N_1 - N_2,$$

$$= N_0 \left(\exp\left[\frac{-t_1}{\tau}\right] - \exp\left[\frac{-t_2}{\tau}\right]\right) = N_0 \exp\left[\frac{-t_1}{\tau}\right]\left(1 - \exp\left[\frac{-T}{\tau}\right]\right),$$

where $T = (t_2 - t_1)$ is the gate interval.

For two gate intervals T_A and T_B the number of neutrons absorbed are in the ratio:

$$\frac{N_A}{N_B} = \frac{1 - \exp[-T_A/\tau]}{1 - \exp[-T_B/\tau]}, \tag{4}$$

as N_0 and t_1 are independent of the gate interval used.

Table II shows the counts in each channel for several gate intervals.

The gate intervals quoted represent the actual period of the gate circuit less 20 μs, the width of pulses from the pile. Because a 20 μs portion of the gate interval is masked for every pulse recorded an appropriate correction to the number of pulses observed in each channel has been made and the corrected counts are shown in the table.

TABLE II.

Gate	Corrected channel counts per 1000 events					Total 2 to 5
	1	2	3	4	5	
70 μs	1000	36.8±0.8	1.9±0.2	0	0	38.7±1.0
145 μs	1000	59.0±1.4	5.8±0.4	0.6±0.1	0.07±0.05	65.5±2.0
340 μs	1000	78.5±1.2	11.0±0.4	1.6±0.2	0.15±0.05	91.2±1.8

From the data in Table II and solving equation (4) graphically the following values of τ were obtained for the three possible ratios N_A/N_B.

For $T_A = 340$ μs and $T_B = 70$ μs $\tau = (145^{+25}_{-20})$ μs,

For $T_A = 340$ μs and $T_B = 145$ μs $\tau = (135^{+35}_{-30})$ μs,

For $T_A = 145$ μs and $T_B = 70$ μs $\tau = (165^{+100}_{-70})$ μs.

The limits quoted allow for an uncertainty of 5% in the values of T_A and T_B and for the standard deviation of the number of counts observed. The above values are in reasonable agreement with the measurements of COCCONI *et al.* (6), GEIGER (7) and GEIGER and ROSE (9). A mean life of 150 μs was used in the calculation of neutron multiplicity.

(9) K. W. GEIGER and D. C. ROSE: *Can. Journ. Phys.*, **32**, 498 (1954).

8. – Discussion.

The mean multiplicity found here ($\bar{v} = 9$) is rather larger than those values quoted by GEIGER ($\bar{v} = 6.5$), COCCONI *et al.* ($\bar{v} = 4.5$) and ORTEL ($\bar{v} = 6$). This could be explained by Cocconi's concept of a nucleon cascade process in the lead. In this case the relatively large thickness of lead in this experiment (about 5 cm as compared with 1.9 cm in GEIGER's work) would substantially increase the probability of secondary multiple events.

The method appears to be inherently sound and if the detection efficiency of the pile could be determined with greater accuracy more accurate multiplicity results could be obtained.

* * *

The author wishes to express his thanks to Mr. N. V. RYDER for his assistance in preparing this paper and together with Professor WALKER and Mr. R. W. HUMPHREY of the Physics Department, Victoria University of Wellington, for encouragement and advice.

RIASSUNTO (*)

Si è eseguita una misurazione del numero di neutroni prodotti nel piombo di un rivelatore di neutroni dei raggi cosmici a paraffina-piombo del tipo in uso a Chicago. L'esperimento indica una media di nove neutroni creati per evento.

(*) *Traduzione a cura della Redazione.*

IL NUOVO CIMENTO Vol. X, N. 3 1° Novembre 1958

Detailed Studies of an Event Involving the Multiple Production of Strange Particles.

TSAI-CHÜ

Faculté des Sciences - Sorbonne, Paris

(ricevuto il 10 Luglio 1958)

Summary. — Three strange particles are emitted from a cosmic ray star of the type 14+5p found in the Sardinia stack S36. They are: 1) a negative hyperon captured at rest; 2) a positive hyperon decaying in flight and 3) a negative K-meson interacting in flight. Detailed measurements of each particle are given in this study. The three strange particles are coplanar. Each has the same strangeness number. Evidently, there are three pairs of strange particles emitted in this interaction. But, if the negative hyperon were an anti-hyperon, then two pairs should be emitted. It seems very probable that the strange particles are produced through a multiple rather than a plural process. In conclusion, this paper gives a rough estimate of the frequency ratio between multiple production events and all associated events involving two or more identified strange particles. The ratio is of the order 0.02 to 0.07 for two-nucleon interactions in the energy range of about 15 GeV.

1. – Introduction.

Detailed studies (1) were made on the trajectory of a negative hyperon found in the Sardinia stack S 36 and on the capture star produced at its resting point. In our previous article, we mentioned that the other two prongs of the primary star (1) showed some interesting features and that their measurements were to be continued. Recent studies (2) have proved that one is a positive hyperon decaying in flight and the other a negative K-meson inter-

(1) TSAI-CHÜ: *Nuovo Cimento*, **3**, 921 (1956).
(2) TSAI-CHÜ and M. MORAND: *Phys. Rev.*, **104**, 1493 (1956).

acting in flight. The three strange particles are emitted nearly in the same plane but each of them has the same strangeness number. This event indicates that in high energy interactions more complicated processes exist than double production. It provides us with the first example of multiple production of strange particles. The hyperon pair, positive and negative, produced side by side, could indicate that the negative one might be an anti-hyperon.

It was maintained by theory that strange particles should be produced copiously in a single nuclear interaction. Experimentally, associated productions of strange particles were found in nuclear interactions caused by cosmic rays as well as by artificially accelerated particles. At present there exist about 130 cosmic ray examples (see Table VI in Appendix I). Associated events ([3,4]) involving a hyperon and a K-meson were also observed in π^--p interactions caused by the 1 GeV negative π-meson beam at Brookhaven. The number of such events ([5,6]) has been considerably increased from experiments by means of the bubble chambers. So far as the pair production of K-mesons is concerned, only a few examples ([7,8]) exist as it requires a higher threshold energy. Associated events produced by mesons ([9]), photons ([10,11]) and nucleons ([12]) have also been reported. In associated productions, two or more strange particles appear together in each nuclear interaction so that their strangeness number is always conserved.

The following paragraphs will give detailed measurements made on the three strange particles under study and on other prongs of the parent star. Probable reactions by which strange particles are produced will also be discussed.

([3]) W. B. Fowler, R. P. Shutt, A. M. Thorndike and W. L. Whittemore: *Phys. Rev.*, **91**, 1287 (1953); **93**, 861 (1954); **98**, 121 (1955).

([4]) W. D. Walker: *Phys. Rev.*, **98**, 1407 (1955); W. D. Walker and W. D. Shephard: *Phys. Rev.*, **101**, 1810 (1956).

([5]) R. Budde, M. Chretien, J. Leitner, N. Samios, M. Schwartz and J. Steinberger: *Phys. Rev.*, **103**, 1827 (1956).

([6]) R. Plano, N. Samios, M. Schwartz and J. Steinberger: *Nuovo Cimento*, **5**, 216 (1957). Also other reports in *Padua-Venice Conference* (1957).

([7]) M. Ceccarelli, M. Grilli, M. Merlin, G. Salandin and B. Sechi: *Nuovo Cimento*, **2**, 828 (1955).

([8]) W. B. Fowler, G. Maenchen, W. M. Powell, G. Saphir and R. W. Wright: *Phys. Rev.*, **103**, 208 (1956).

([9]) J. C. van der Velde, J. L. Brown, D. A. Glaser, D. I. Meyer, M. L. Perl, J. W. Crownin, S. Debenedetti and R. Cool: *Bull. Phys. Soc.*, II, **1**, 221 (1957).

([10]) Staff of the California Institute of Technology Synchrotron, *Padua-Venice Conference* (1957).

([11]) A. Silverman, R. R. Wilson and W. M. Woodward: *Padua-Venice Conference* (1957).

([12]) M. M. Block, E. M. Harth, W. B. Fowler, R. P. Shutt, A. M. Thorndike and W. L. Whittemore: *Phys. Rev.*, **99**, 261 (1955).

2. – Positive and negative hyperon pairs.

2·1. *Negative hyperon.* – A careful study of this negative hyperon has already appeared in a previous article (1). In order to give a complete idea of this multiple production event, it suffices to summarize the former results. The negative hyperon is represented by track 15 in Fig. 1 (Table V). It is ejected from the primary star at a dip angle of $1°45' \pm 10'$ relative to the emulsion surface and has a flat trajectory of length 876 μm. It comes to rest in the emulsion and produces a small star of three prongs; two of them can be identified as α-particles. The probability of an accidental coincidence between a radioactive α star and the end of a proton track is negligible. Further, the mass of this star producing particle measured by ionization and range is $(2\,830 \pm 560)\ m_e$ and by multiple scattering $(2\,560 \pm 1\,100)\ m_e$ (13). The small star can be explained as a result of the capture of a hyperon Σ^- by a nitrogen nucleus. However, if an anti-hyperon exists, it will be impossible to distinguish it from a negative hyperon by the observed small star. In nuclear interactions like

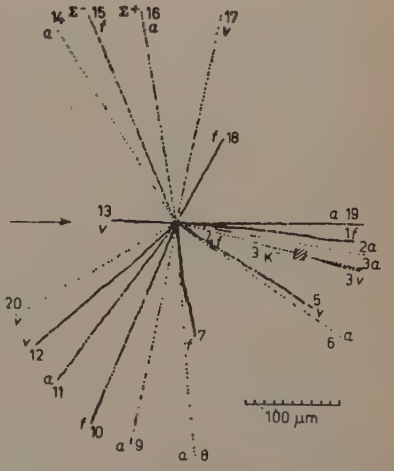

Fig. 1. – Primary star containing three strange particles.

(1) $$\Sigma^- + p \to \Lambda^0 + n$$

and

(2) $$\overline{\Sigma^-} + p \to \overline{\Lambda^0} + n$$

the conservation of strangeness, charge and baryon number obliges both hyperon and anti-hyperon to undergo charge exchange reactions; the anti-proton or -neutron could appear only after the decay of $\overline{\Lambda^0}$. A rapid scanning made within an area of $1 \times 3\ cm^2$ for each of the 10 plates next to the one containing the small star failed to reveal any decay event due to Λ^0 or $\overline{\Lambda^0}$. Considering this hyperon to be a Σ^- and to have a mass $(2342 \pm 1)\ m_e$ (14), the energy and momentum of the negative hyperon at emission are 14.6 MeV and 183 MeV/c respectively and the moderation time is $2.65 \cdot 10^{-11}$ s.

---

(13) The error of mass by scattering is increased according to M. HUYBRECHTS: *Suppl. Nuovo Cimento*, **4**, 903 (1956).

(14) K. M. CROWE: *Nuovo Cimento*, **5**, 541 (1957).

2·2. *Positive hyperon.* – The positive hyperon is represented by track 16 (Fig. 1, Table V) and appears at a projection angle of 13°.3 from the negative hyperon and a diple angle of $1°58' \pm 10'$ relative to the emulsion surface. After traversing 8.61 mm approximately parallel to the plane of the emulsion, the particle shows a large deflection of 35° and ends in the next plate. The dip angles are $-50'$ before and $-3°10'$ after deflection respectively; there exist distinct discontinuities in ionization and multiple scattering values of the two portions of the trajectory separated by the deflection. Points marked with (•) in Fig. 2 indicate the ionization before deflection and points with (×) the ionization after deflection. Ionization and multiple scattering measurements made on the 4 535 μm track after deflection prove it to be a proton. Ionization is measured by the blob-gap method, *i. e.* by counting the number of gaps $N(L)$, with L longer than 0.95 μm. The mass of the particle measured by ionization and range is $(1950 \pm 280)\ m_e$. Comparing the multiple scattering of this particle with the average scattering of a proton, we obtain $(1790 \pm 470)\ m_e$ for the mass of this particle.

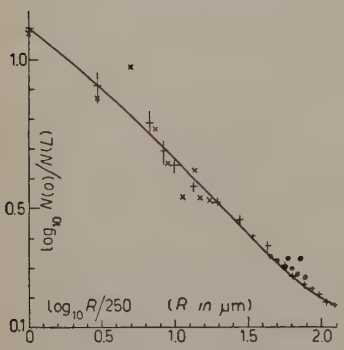

Fig. 2. – Ionization-range curve for protons and track 16.

The ionization of the particle before deflection decreases less rapidly along its trajectory than that of a proton (Fig. 2), so it must have a greater mass. The mass of this particle is measured by three different methods; each of these measurements proves it to be a hyperon Σ.

(*a*) Rate of change of ionization with range. Let the particle before deflection have a mass m_x and a residual range R_0 at the point of deflection; we have

$$r = \frac{m_x}{m_p} = \frac{R_0 + R_x}{R_p},$$

or

$$R_p = \frac{1}{r}(R_x + R_0), \tag{3}$$

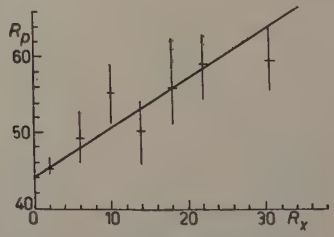

Fig. 3. – R_p against R_x curve for the positive hyperon.

where R_x is the distance given in units of 250 μm measured from the point of deflection; R_p the corresponding residual range of a proton with the ionization of the unknown particle. Equation (3) allows one to obtain the ratio (r) of masses from the reciprocal of the slope of a straight line and the

residual range from its intercept on the ordinate axis. From Fig. 3, we get $r = 1.50 \pm 0.37$, $R_0/r = (10\,930 \pm 420)$ μm and $m_x = (2\,765 \pm 670)\, m_e$.

(*b*) Multiple scattering against ionization. Multiple scattering of the trajectory before deflection is measured by constant cells of 50 μm. The average second difference of a 100 μm cell for this particle is about three times the noise value. Internal calibration of the scattering constant is made by doing the same measurements on about 10 cm of flat proton and deuteron tracks which are selected in the neighborhood of this trajectory and which have nearly the same ionization and the same direction. We have from scattering measurements, average $p_x v = (145 \pm 19)$ MeV for the particle and from ionization measurements, $p_p v = (121.2 \pm 3.0)$ MeV for a proton, therefore the mass of the particle before deflection is

$$m_x = (p_x v / p_p v) m_p = (2\,200 \pm 290)\, m_e .$$

(*c*) Q-value for the decay $\Sigma^+ \to p + \pi^0$. The direct measurements show that the particle before deflection has a value of mass greater than that of a proton but the particle after deflection has a mass of a proton. It is therefore reasonable to assume the deflection as due to the decay of a hyperon Σ^+ into a proton and a π^0 meson and then to deduce the mass of the hyperon from the Q-value. The Q-value is equal to the sum of kinetic energies of the proton and the π^0 meson in the system of the hyperon. For $\theta = 35°10' \pm 3°30'$, the angle made by the hyperon with the proton, $\beta = 0.330 \pm 0.003$, the hyperon velocity divided by the light velocity and the observed proton kinetic energy $E_p = (33.7 \pm 0.8)$ MeV, we obtain $Q = (116 \pm 13)$ MeV and the mass of the hyperon $(2\,328 \pm 26)\, m_e$, in excellent agreement with the mass of Σ^+. The energy and momentum of the positive hyperon at emission are 92.9 MeV and 479 MeV/c respectively and the time of flight $7.64 \cdot 10^{-11}$ s.

3. – Interaction in flight of a negative K-meson.

The third strange particle is represented by track number 3 in Fig. 1. It is emitted at a projection angle of 113°.8 from the positive hyperon and a dip angle of $-3°23' \pm 10'$ relative to the emulsion surface. It produces a nuclear interaction after traversing 285 μm. The interaction consists of two prongs separated by a small projection angle of one degree from each other and there could be a small nuclear recoil at their origin. To help the vision, the two prongs are shown slightly apart in the figure, but remain parallel to their original directions. The black one (3*v*) makes a large dip angle of 54°35', leaves the same plate at the glass side and ends in the emulsion after traversing five other plates. The other one (3*a*) has a dip angle of $-26°$ and leaves the stack after traversing 24 plates.

3·1. *Coplanarity of the three tracks.* – The angle between the incident track 3 and the normal to the plane containing the secondary prongs ($3a$, $3v$) is 90°2′ and the angle between the track $3v$ and the normal to the plane containing the other two tracks (3, $3a$) is 90°5′. It is remarkable how the coplanarity condition for the three tracks is satisfied, the errors arising from distortion, measurements and others may be much greater than 1°. The angle between 3 and $3a$ is 21°49′, that between 3 and $3v$ 59°44′.

3·2. *Measurements on incident track* 3. – Ionization is measured by the blob density and blob-gap ratio, $(N(0)/N(L)$, with L longer than 3.16 μm. Velocity calibration is made by comparing the above two quantities with those of π-meson tracks ending in the emulsion.

TABLE I.

	Ionization	R_p (cm)	E_p (MeV)
$N(0)$ per 100 μm	25.6 ± 3.0	$10.4^{+1.0}_{-2.6}$	202 ± 31
$N(0)/N(L)$	2.85 ± 0.05 (*)	10.12 ± 0.30	198.6 ± 5.1

(*) Weighted mean.

This particle has, therefore, an average value of $\beta = 0.566 \pm 0.017$. If it were a proton, the average energy corresponding to such a velocity would be (200 ± 16) MeV, momentum $pc = (644 \pm 28)$ MeV and $pv = (365 \pm 27)$ MeV.

As this track has only a short length of 285 μm, multiple scattering cannot give precise results. However, there is some evidence that it is lighter than a proton. For a proton with $pv = 365$ MeV, the mean angle of scattering is 4′ for a 100 μm cell, the probability of having a scattering 4 times larger than this value is less than 1%. Therefore the presence of two or more such angles may well exclude the possibility of this particle being a proton. Multiple scattering is first measured as usual in cells of 25 μm. Average second differences from five series of measurements are given in Table II. Second differences of larger cells are calculated with all the overlapping combinations possible.

TABLE II.

	$D(25)$	$D(50)$	$D(75)$	$D(100)$
Mean value in divisions	2.25	3.44	2.32	1.86
Independent cells	11	5	3	2

Among the second differences of various cells, $D(50)$ has the largest value. In fact two values of $D(50)$ give true scattering angles four times larger than

the average scattering of a proton. Incidentally, the dip angles of this particle are $-3°23' \pm 10'$ at emission and $-4°10' \pm 20'$ at interaction respectively. By attributing to each multiple cell a weight proportional to the number of independent second differences, we calculate the true scattering of the particle by the following formula

$$7K^2 s^3 = \frac{4[D(50)^2 - D(25)^2]}{7} + \frac{2[D(75)^2 - D(25)^2]}{26} + \frac{D(100)^2 - D(25)^2}{63},$$

$$K(2s)^{\frac{3}{2}} = (0.74 \pm 0.40)(2)^{\frac{3}{2}} = 2.1 \qquad \text{for } s = 25\ \mu\text{m}.$$

$K(2s)^{\frac{3}{2}} = 2.1$, given in arbitrary units, can be converted into the unit of degree for a 100 μm cell, by multiplying it with a constant factor $180 \times (100)^{\frac{1}{2}} \times \times 0.057\,94/\pi(50)^{\frac{3}{2}} = 0.093\,88$. Hence $pv = (142 \pm 77)$ MeV for the particle by scattering, and $(pv)_p = (365 \pm 27)$ MeV for a proton by ionization, the mass of the particle is $(714 \pm 320)\ m_e$.

More elaborate measurements of multiple scattering are made by applying Molière's method ([15]) of determining the c.g. of the ordinate of the grains inside a cell. Aligning the track along the x-axis, we measure in the centre of the eyepiece the ordinate y of the nearest grain or grains every 5 μm and calculate the arithmetic mean of the ordinate $(\bar{y})$ for a cell of 25 μm. The $\bar{y}$ of each cell is used for calculating the scattering differences. The absolute mean value of scattering between chords is calculated from the formula

$$Ks^{\frac{3}{2}} = \sqrt{\frac{2}{3}}\sqrt{\frac{2}{\pi}}\sqrt{\frac{8}{7}\left(\overline{D_i^2} + \frac{3}{2}\,\overline{D_i D_{i+1}}\right)}.$$

We have, as a mean of three measurements

$$Ks^{\frac{3}{2}} = 0.469\,, \quad pv = 22.1/0.469 \times (2)^{\frac{3}{2}} \times 0.093\,88 = (178 \pm 70)\ \text{MeV}\,.$$

$$\text{Mass of the particle} = 178 \times 1836\ m_e/365 = (894 \pm 400)\ m_e\,.$$

The scattering constant ([16]) for 25 μm cell is taken as 22.1. From the above measurements, track 3 can neither be a proton nor a π-meson; but very probably a K-meson.

3·3. *Measurements on secondary track 3v and 3a.* – The black track can be identified as a proton by grain counting. It ends in emulsion with a total range of 3 736 μm. Its energy and momentum at emission are 30 MeV and 240 MeV/c respectively.

([15]) See for example, B. D'ESPAGNAT: *Journ. Phys. et Rad.*, **13**, 74 (1952).

([16]) L. VOYVODIC and E. PICKUP: *Phys. Rev.*, **85**, 91 (1952).

The track 3*a* has a fairly large dip angle. It has a total length of 3.798 cm in emulsion and should have a residual range of a few thousand more microns if it were a proton. Ionization is measured in the same way as that of protons used for calibration (Fig. 2). However, it is carefully corrected for the possible variations of the minimum ionization among different plates, the variation with depth in each plate and for the dilatation of gaps due to distortion. The dilatation of range due to distortion ([17]) should also be corrected. The mass and residual range can be found from the rate of change of ionization with range by using equation (3). Points marked with (+) in Fig. 4 show the values (R_p, R_x) before correction; points with (×) the same values after correction. The mass of the particle is (1.29 ± 0.08) times that of a proton or is equal to (2 369 ± 150) m_e; it is slightly smaller than the value ([2]) found without correction. The residual range estimated from the average value of intercepts given by different pairs of experimental points is (3 503 ± 400) μm. Direct comparison of ionization of this particle in plate No. 1 with that of protons found in the same plate gives $R_0/r = (2\,666 \pm 1\,000)$ μm or a residual range $R_0 = (3\,438 \pm 1\,310)$ μm for $r = 1.29$.

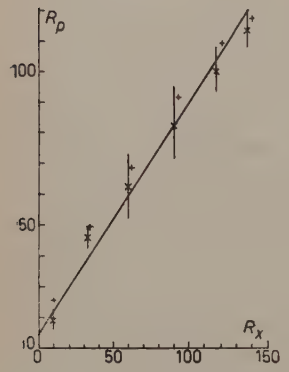

Fig. 4. – R_p against R_x curve for track 3*a*.

The mass of particle 3*a* can also be obtained by multiple scattering and ionization measurements. The multiple scattering of this particle is measured in constant cells of 50 μm. As distortion is not negligible in comparison with the multiple scattering in most plates, only third differences are used for mass calibration. The value of mass is found to be (2 275 ± 103) m_e (Table III).

TABLE III.

Plate No.	$(pv)_p$ MeV by ionization	$(pv)_x$ MeV by scattering	$M_x = (pv)_x M_p/(pv)_p$
24 to 21	183.2	237.6	2 382 m_e
20 to 17	171.0	186.3	2001
16 to 13	152.0	170.0	2078
12 to 9	127.0	154.2	2229
8 to 5	107.0	131.0	2247
4 to 1	62.5	94.4	2 712

([17]) TSAI-CHÜ: *Nuovo Cimento*, **5**, 1128 (1957).

3·4. *Nature of the interaction.* – From direct measurements, the incident particle 3 has a mass of the order of a K-meson and one secondary prong (3*a*) has a mass equal to that of a hyperon. Further, the incident particle can neither be a proton nor a π-meson, because none of these has sufficient energy to produce a hyperon. The interaction must be the capture of a K^--meson by a nucleus with the production of a hyperon. As shown above, the three particles K^-, p, and Σ lie in the same plane; the transversal momenta of proton and hyperon are nearly balanced (Table IV). So it seems plausible

TABLE IV.

Track	Particle	Energy (MeV)	Momentum (MeV/c)	Transversal momentum	Longitudinal momentum
3	K^-	105 ± 8	339 ± 15	0	339
3*v*	p	30	240	205	125
3*a*	Σ^-	130	573	-213	532

to presume a few neutral particles emitted in this interaction. The surplus energy and momentum could easily be balanced by assuming two neutrons moving in opposite directions: a slow one with a kinetic energy of about 30 MeV moving forward and a fast one with 150 MeV backward. The reaction could then be

$$K^- + n + n \rightarrow n + \Sigma^- ;$$

i.e. the capture of a K^- by two neutrons, with the production of a fast neutron and a negative hyperon, each of about 150 MeV. A part of the energy of the K^--meson is used to liberate the bound nucleons; the neutron and the hyperon slow down somewhat as they knock out another neutron and another proton, each about 30 MeV. Assuming the track 3*a* to be a Σ^-, the time of flight is $2.84 \cdot 10^{-10}$ s.

4. – Other prongs of the primary star.

The primary star of the strange particles is found in plate No. 24. Of the 20 prongs of this star (Fig. 1, Table V), six have an ionization below 1.5 times the plateau value. The three strange particles appear among the fourteen tracks with a higher ionization. Negative projection angles from 0 to 180° (Table V) represent the upper hemisphere; positive ones from 0 to 180° the lower hemisphere. During exposition, cosmic rays falling vertically traversed

TABLE V. – *Prongs of the Primary Star, 14 + 5p, containing three Strange Particles.*

Track No.	Projection angle	Dip angle	Length in Plate 24 μm	No. of plates traversed	Range or total length	Nature of Particle	Energy MeV	REMARKS
1	83.8°	17°	205	1	205 (R)	p	5.6	—
2	80.3°	—19°	1235	22	40425	π	233 ± 40	Grain density $= (12.06 \pm 0.18)$ grains per 100 μm. Energy deduced from scattering measurements.
3	76.4°	— 3°23′	285	1	285	K^-	105	Strange particle. Interacting in flight.
4	61.4°	35°	17	1	17 (R)	α	4.3	—
5	58.3°	40°	143	5	3227 (R)	D	37	—
6	54°	—41°	695	—	—	—	—	Grain density $= 14 \pm 2$; too inclined to be measured.
7	8.2°	—66°	333	1	333 (R)	α(?)	26	May be heavier than α-particle.
8	4.4°	—12°	2004	22	70770	π	126 ± 20	Grain density $= 12.63 \pm 0.13$. Energy deduced from scattering measurements.
9	— 6°	— 2°30′	9955	7	33037 (R)	π^-	47.5	Made a large angle deflection of 16° 30′ after traversing 1.45 cm and captured at rest with a σ star of 2 prongs.
10	— 23.5°	—15°	306	1	306 (R)	p	7	—
11	— 38.3°	—31°	854	4	3918 (R)	D	42	—
12	— 48.5°	28°	356	2	949 (R)	D	18.5	—
13	— 93.2°	63°	150	6	3374 (R)	p	28.4	—
14	—149°	—62°	481	—	—	—	—	Grain density $= 12 \pm 2$; too inclined to be measured.
15	—156.5°	1°45′	876	1	876 (R)	Σ^-	14.6	Strange particle, captured at rest.
16	—169.8°	1°58′	8610	1	8610	Σ^+	92.9	Strange particle, $\Sigma^+ \rightarrow p + \pi^0$, decay in flight.
17	167°	27°	285	16	21395 (R)	p	82	—
18	140.7°	— 4°30′	100	1	100 (R)	D(?)	4.7	—
18	88.7°	—25°	62	2	203 (R)	p(?)	5.5	—
20	— 60.4°	30°	280	—	—	—	—	Grain density $= 9 \pm 2$, too inclined to be measured.

the stack parallel to the plane of the emulsion and along the direction of projection angle $-90°$ to $90°$ (Fig. 1). The primary star has been considered as the type 14+5p, because there are two minimum ionization tracks (No. 14 and No. 20) present in the upper hemisphere. However, these tracks show such large dip angles that it would be impossible for any one of them to be responsible for this multiple production event.

We measure preliminarly the grain density and multiple scattering of each track by means of an ordinary microscope. Any track susceptible of being a strange particle is studied in great detail. No positive K-meson is found among the slow prongs. The eleven prongs consisting of protons, deuterons and α-particles (Table V) have a total kinetic energy of 265 MeV and a total energy of 120 MeV was expended when they were released from the nucleus. The latter is obtained by assuming a separation energy of 8 MeV per nucleon for proton and deuteron and a separation energy of the same value for an α-particle. The neutral prongs could have a total energy of 1.25(265+120) ([18]) or 481 MeV. Altogether, the total sum of energy expended in emitting the heavy prongs is 0.866 GeV. The three strange particles have a total kinetic energy of 212.5 MeV, a rest energy of 1001.5 MeV (supposing Σ^+, Σ^- to be created from neutrons) plus the separation energy of a neutron from the parent nucleus 8 MeV, *i.e.* a total of 1222 GeV.

Among six tracks at minimum ionization, half of them with dip angles greater than 30° cannot be identified. The other half, tracks 2, 8, and 9 with smaller dip angles can be identified as π-mesons. Track 9 has a length of 1 cm in plate 24, shows a large deflection in the next plate and comes to end in the emulsion with a two prong σ-star. This negative π-meson traverses six plates and has a kinetic energy of 47.5 MeV. Ionization and scattering measurements made on the 1.45 cm trajectory before deflection prove it as well to be a π-meson. Tracks 2 and 8 at minimum ionization traverse the 24 plates of the stack, and can be followed through 22 plates. Track 2 has a mean dip angle of $-19°$, a mean grain density of (12.06 ± 0.18) grains per 100 μm and a mean scattering angle of $0°.088\,5$ for a 100 μm cell (see Appendix II). Ionization and scattering identify this track as a π-meson, and energy at emission is (233 ± 40) MeV. Track 8 is emitted at a dip angle of $-12°$ and becomes less steep, $-5°$, in the last few plates. It has a mean grain density of (12.63 ± 0.13) grains per 100 μm. The mean scattering, 0.158° for a 100 μm cell, indicates a π-meson. Energy at emission is (126 ± 20) MeV. The average energy, kinetic plus rest energy, of the identified π-mesons in this interaction is 275 MeV. Supposing all the shower particles of this star are π-mesons with the same average energy as the identified ones, then the

---

([18]) R. H. Brown, U. Camerini, P. H. Fowler, H. Heitler, D. T. King and C. F. Powell: *Phil. Mag.*, **40**, 862 (1949).

total energy of the minimum ionization tracks will be 5×275 or 6×275 MeV, depending on the presence of a charged or neutral primary. Assuming three neutral π-mesons to be emitted with the same kinetic energy as the charged ones, we have an energy of 3×271 for all of them. The energy for all π-mesons is then 2188 or 2463 GeV. The total energy of all the prongs of the primary star, except the neutral strange particles, is 4276 to 4551 GeV.

5. – Conclusion.

The measurements show that each strange particle is emitted nearly parallel to the emulsion surface. The direction of the negative K-meson makes a small angle of 3° with its projection in the plane containing the hyperon pairs. Since no track parallel to the emulsion surface could be taken for the primary, the strange particles must be produced either by a neutral primary or by a secondary particle resulting from the first collision. If one considers, as usual practice, the captured hyperon to be a Σ^-, then each of the strange particles should have strangeness -1. If conservation of strangeness holds for multiple production as in the case of associated production, then three pairs of strange particles should be emitted. In addition to the three strange particles observed, there should be a simultaneous emission of another three with strangeness $+1$, *i.e.* θ^0, K^0 or K^+ mesons. If there is any positive K meson, it could only occur among the three minimum ionization tracks with large dip angles. As the interaction involves the production of two hyperons, it should take place in a collision between two nucleons, *e.g.*

$$\text{neutron} + \text{nucleon} \rightarrow \Sigma^+ + \Sigma^- + K^- + 3\,\theta^0 + n\pi\,.$$

The strange particles must be produced simultaneously through a multiple process from a single nuclear collision rather than through a plural process from three successive collisions inside the same nucleus. It seems unlikely that the production plane—the plane containing the producing particle and the charged strange particle—remains parallel to one another in the collisions. Besides, if one assumes a cross-section for double production 1/1000 times the geometrical cross-section of the nucleus, the probability of observing such a plural production event will be 10^{-6} times smaller than that of observing a double production event.

The threshold energy for the production of the above three pairs of strange particles is 2.48 GeV in the C.M. system of two nucleons and it will be 4.95 GeV in the laboratory system by non-relativistic calculations. The minimum energy of the primary neutron should be 8 GeV, a relativistic correction will bring it to about 14 GeV. So, the primary particle responsible for this star must have an energy greater than 14 GeV.

If the negative hyperon were an anti-hyperon, an alternative interpretation might apply. The interaction involves the creation of a pair of hyperons in association with another pair of K-mesons, *i.e.*

$$\text{neutron} + \text{nucleon} \rightarrow \Sigma^+ + \overline{\Sigma^-} + K^- + \theta^0 + n\pi + \text{neutron} + \text{nucleon}\,.$$

It is more probable to consider this interaction as a plural process. A hyperon pair is produced in the first collision, and a secondary from the first collision produces the K-meson pair. The probability for a plural process is increased by a factor 10^3, but the coplanarity of strange particles can only be explained as purely accidental.

Another probable example ([19]) found recently in the G-stack was produced by a cosmic primary with an energy more than 15 GeV. Four strange particles were emitted in this interaction: a positive K-meson decaying at rest, a hyperon Y decaying in flight and a pair of K-mesons identified by ionization and scattering. This event may be interpreted as the production of a K^+-meson in association with a hyperon and a pair of K-mesons. The strange particles in the photograph ([19]) appear to have small dip angles relative to the emulsion surface, *i.e.* to say, the two production planes do not differ very much from each other. This example together with ours is in favor of a multiple production.

It is still premature to calculate the relative frequency between multiple and double production events from an estimation based on a small number of examples actually available. There is one multiple production event among 15 associated events in the G-stack. The ratio between multiple and all associated events is greater than 1/14, if we eliminate one event in which the primary has not enough energy to produce more than two strange particles and keep the others of which we have no information about the primary star. On the other hand, if we take all cosmic ray associated events observed in nuclear emulsions (Table VI, Appendix I), except a few where the primary has not sufficient energy, we obtain 30 associated events against 2 multiple events; the ratio is 2/30, or 0.07. This ratio will decrease to about 2/130 or 0.02, if we include all the associated cosmic ray events observed in cloud chambers (Table VI, Appendix I). The latter comparison may not be adequate, because the technique of detection by cloud chambers is quite different from that by nuclear emulsions, and furhter, in most cloud chamber examples, the primary star was not observed, so we have no idea about the primary energy. At present, the large ratio, 0.07 would seem more probable. Therefore in two-

---

([19]) D. F. Falla, M. W. Friedlander, F. Anderson, W. D. B. Greening, S. Limentani, B. Sechi-Zorn, C. Cernigoi, G. Iernetti and G. Poiani: *Nuovo Cimento*, **5**, 1203 (1957).

nucleon interactions in the energy region of 15 or more GeV, there may be an appreciable proportion of multiple production events. Some theoretical studies of multiple production process have been done by DOMOKOS ([20]). With the development of high energy accelerators, we may expect to have more examples of multiple production events in the future.

* * *

I wish to express my sincere thanks to Professor MAX MORAND for his direction and interest in my work and my deep gratitude to the French Centre National de la Recherche Scientifique for the research fellowship. I wish also to express my appreciation to Mrs. HILDA M. TSAI for her invaluable assistance and constant encouragement.

APPENDIX I

TABLE VI. – *Associated production events observed in cosmic rays.*

	Inter-action	Strange particles	Cases	Remarks	References
1	C.R.	(Ch) $3\,V^0$	1	2 originated in gas	McCUSKER *et al.* ([21])
2	$13+10\alpha$	(Em) $\tau^+ + \Sigma$	1	$\Sigma \rightarrow \pi + n$	LAL *et al.* ([22])
	$14+2n$	(Em) $K^+ + K^-$	1	K^- 308 μm	»
3	C.R.+Pb	(Ch) $\Lambda^0 + \theta^0$	1	Λ^0 identified	BRIDGE *et al.* ([23])
4	$27+9p$	(Em) $K^+ + V^0$	1	V^0 may be Λ^0 or θ^0	DEBENEDETTI *et al.* ([24])
	$21+7p$	(Em) ${}^3_1H^* + \tau^+$	1	—	»
5	$p+\pi^-$	(Ch) $\theta^0 + \Lambda^0$	1	—	THOMPSON *et al.* ([25])

([20]) G. DOMOKOS: private communication.

([21]) C. B. A. McCUSKER and D. D. MILLER: *Nuovo Cimento*, **8**, 289 (1951).

([22]) D. LAL, YASH PAL and B. PETERS: *Conference of Bagnère-de-Bigorre* (1953); *Proc. Acad. Sci. Ind.*, **38**, 398 (1953).

([23]) H. BRIDGE and B. ROSSI: *Conference of Bagnère-de-Bigorre* (1953).

([24]) A. DEBENEDETTI, C. M. GARELLI, L. TALLONE and M. VIGONE: *Nuovo Cimento*, **12**, 369, 466 (1954); *Suppl. Nuovo Cimento*, **1**, 249 (1955).

([25]) R. W. THOMPSON, J. R. BURWELL, R. W. HUGGET and C. J. KARZMARK: *Phys. Rev.*, **95**, 1576 (1955).

TABLE VI (*continued*).

	Interaction	Strange particles	Cases	Remarks	References
6	19+3n	(Em) $K^+ + \Sigma$	1	$\Sigma \to \pi + n$	DAHANAYAKE *et al.* [26]
	13+3p	(Em) $K^+ + \Sigma$	1	$\Sigma \to \pi + n$	»
7	28+29p	(Em) $\tau^+ + \Sigma$	1	$\Sigma \to \pi + n$	GOTTSTEIN [27]
8	C.R.+Cu	(Ch) $\Lambda^0 + \theta^0$	1	—	BALLAM *et al.* [28]
	»	$\theta^0 + \theta^0$	1	—	»
	»	$V^0 + V^0$	5	—	»
9	18+4p	(Em) $K^+ + \Sigma^-$	1	Σ^- 96 μm, to a capture star	FRIEDLANDER *et al.* [29]
	1+2p	(Em) $K^+ + \Sigma$	1	K^+ 2 interactions, decays as $K^+_{\mu 3}$	»
	6+5p	(Em) $K + K^-$	1	—	»
	22+3p	(Em) $K + {}^4_1H^*$	1	—	»
10	$\pi^- + p$	(Em) $K^+ + K^- + n$	1	π^- 1.5 GeV, K^- captured	CECCARELLI *et al.* [7]
11	22+36α	(Em) $K^+_{\mu 2} + \Sigma$	1	$\Sigma \to \pi + n$	FOWLER *et al.* [30]
12	18+20α	(Em) $K^+_{\mu 2} + \Sigma$	1	$\Sigma \to \pi + n$	FOWLER *et al.* [31]
13	C.R.+Pb	(Ch) $V^0 + V^0$	13	—	JAMES *et al.* [32]
	»	$V^0 + V^\pm$	6	—	»
14	C.R.+Pb	(Ch) $\Xi^- + \theta^0 + \theta^0$	1	—	SORRELS *et al.* [33]
15	C.R.+Pb	(Ch) $\Lambda^0 + \theta^0$	36	—	TRILLING *et al.* [34]
	»	$\Lambda^0 + K^+$	4	1 certain	»
	»	$\Sigma^- + \theta^0$	4	Σ^- probable	»
	»	$\Xi^- + \theta^0$	1	—	»
	»	$K^+ + \theta^0$	1	—	»
	»	$V^\pm + V^0$	6	2 θ^0; 1 Λ^0	»

([26]) C. DAHANAYAKE, P. E. FRANÇOIS, Y. FUJIMOTO, P. IREDALE, C. J. WADDINGTON and M. YASIN: *Phil. Mag.*, **45**, 855 (1954); *Nuovo Cimento*, **1**, 888 (1955).

([27]) K. GOTTSTEIN: *Nuovo Cimento*, **1**, 284 (1955).

([28]) J. BALLAM, A. L. HODSON, M. W. MARTIN, R. R. RAU, G. T. REYNOLDS and S. B. TREIMAN: *Phys. Rev.*, **97**, 245 (1955).

([29]) M. W. FRIEDLANDER, D. KEEFE and M. G. K. MENON: *Nuovo Cimento*, **1**, 482, 694 (1955); **2**, 663, 666 (1955).

([30]) P. H. FOWLER and W. C. ORTEL: *Nuovo Cimento*, **2**, 864 (1955).

([31]) P. H. FOWLER and D. H. PERKINS: *Nuovo Cimento*, **2**, 874 (1955).

([32]) G. D. JAMES and R. A. SALMERON: *Phil. Mag.*, **46**, 571 (1955).

([33]) J. D. SORRELS, R. B. LEIGHTON and C. D. ANDERSON: *Phys. Rev.*, **100**, 1457 (1955).

([34]) G. H. TRILLING and R. B. LEIGHTON: *Phys. Rev.*, **104**, 1703 (1956).

TABLE VI (*continued*).

	Interaction	Strange particles	Cases	Remarks	References
16	C.R.	(Ch) $K^+_{\mu 2}+\Lambda^0$	1	—	BARKER *et al.* [35]
17	C.R.	(Ch) Λ^0+V^0	1	—	LLOYD *et al.* [36]
18	C.R.+C	(Ch) K^0+V^0	2	$n+p \to K^0+\overline{K}^0+n+p$ 1 case	COOPER *et al.* [37]
	C.R.+Cu	(Ch) V^0+V^0	3	K^0+K^0 1 case	»
	»	V^0+V^+	3	$n+p \to K^+ + \overline{K}^0+n+p$ 1 case	»
19	15+5n	(Em) $K^+ + \Sigma^-$	1	Σ^- captured at rest	GOTTSTEIN *et al.* [38]
20	4+1 (?)	(Em) $K^+ + \Sigma^-$	1	Σ^- captured at rest (probable)	BACCHELLA *et al.* [39]
21	38+4p	(Em) K+F*	1	—	CIOK *et al.* [40]
22	22+9p	(Em) $K^+ + Y + 2K$	1	—	FALLA *et al.* [19]
		$K^+ + \Sigma^\pm$	4	1 Σ^+; 1 Σ^-	»
		$K^+_{\mu 2} + \Sigma^-$	2	Σ^- captured at rest	»
		$K^+_{\pi 2} + \Sigma^\pm$	2	1 event in reference (31)	»
		$K^+ + F^*$	2	1 $^4He_\Lambda$ or $^5He_\Lambda$; 1 F* (?)	»
		$K^+ + K$	2	1 $K^+_{\mu 2}$	»
		$K^+ + Y^\pm$ (or K)	1	—	»
		$\tau + Y^\pm$ (or K)	1	—	»
23	7+1n	(Em) $K^+ + F^*$	1	$\gamma + p \to K^+ + \Lambda^0$	TSAI *et al.* [41]

C.R. = Cosmic Rays, Ch = Cloud Chamber, Em = Nuclear Emulsion.

[35] K. H. BARKER, M. S. COATES and B. R. FRENCH: *Suppl. Nuovo Cimento*, **4**, 319 (1956).

[36] J. L. LLOYD and A. W. WOLFENDALE: *Phil. Mag.*, **1**, 93 (1956).

[37] W. A. COOPER, H. FILTHUTH, J. A. NEWTH, G. PETRUCCI, R. A. SALMERON and A. ZICHICHI: *Nuovo Cimento*, **5**, 1388 (1957).

[38] K. GOTTSTEIN, B. ROEDERER, J. VARSHNEYA and P. WALOSCHEK: *Suppl. Nuovo Cimento*, **4**, 440 (1956).

[39] L. BACCHELLA, M. DI CORATO, M. LADU, R. LEVI SETTI, L. SCARSI and G. TOMASINI: *Suppl. Nuovo Cimento*, **4**, 465 (1956).

[40] P. CIOK, M. DANYSZ, J. GIERULA, E. SKRZYPCZAK and A. WROBLEWSKI: *Suppl. Nuovo Cimento*, **4**, 619 (1956).

[41] TSAI-CHÜ, B. CHEMEL and S. DESPREZ-REBAUD: *Nuovo Cimento*, **9**, 192 (1958).

Appendix II

For inclined tracks with low grain density, it is more convenient to measure multiple scattering by the tangent method. The scattering angle for a double cell is equal to the mean angle of two successive basic cells. Let $\Delta\theta_1$, $\Delta^2\theta_1$ and $\Delta\theta_2$, $\Delta^2\theta_2$ be the scattering differences corresponding to second and third ordinate differences of basic and double cells, we eliminate the noise (e) by the following formulas:

$$(\Delta\theta_1)^2 = (K_1 s^{\frac{1}{2}})^2 + e^2 ,$$

$$(\Delta\theta_2)^2 = 2(K_2 s^{\frac{1}{2}})^2 + \frac{e^2}{4} ,$$

and for higher order difference

$$(\Delta^2\theta_1)^2 = \tfrac{3}{2}(1.06 K_1 s^{\frac{1}{2}})^2 + e'^2 ,$$

$$(\Delta^2\theta_2) \ = 3(1.06 K_2 s^{\frac{1}{2}})^2 + \frac{e'^2}{4} .$$

Scattering of inclined tracks (track 2) is calculated from the last two formulas.

RIASSUNTO (*)

Tre particelle strane sono emesse da una stella del tipo 14 + 5p trovata nel Sardinia stack S36. Sono: 1) un iperone negativo catturato a riposo; 2) un iperone positivo che decade in volo e 3) un mesone K negativo che interagisce in volo. Nel presente studio si danno misurazioni dettagliate di ognuna di tali particelle. Le tre particelle strane sono coplanari. Ognuna ha lo stesso numero di stranezza. Evidentemente in questa interazione sono emesse tre coppie di particelle strane. Ma, se l'iperone negativo fosse un antiiperone le coppie emesse dovrebbero essere due. Sembra molto probabile che le particelle strane siano prodotte tramite un processo multiplo anzichè plurimo. In conclusione il presente lavoro dà un valore di massima del rapporto di frequenza tra eventi da produzione multipla e tutti gli eventi associati interessanti due o più particelle strane identificate. Il rapporto è dell'ordine di 0.02 a 0.07 per interazioni fra due nucleoni nell'intervallo di energia di circa 15 MeV.

(*) *Traduzione a cura della Redazione.*

IL NUOVO CIMENTO Vol. X, N. 3 1° Novembre 1958

The Kinematics of Meson Interactions within Nuclei (*).

K. M. Watson and C. Zemach

Physics Department, University of California - Berkeley, Cal.

(ricevuto l'11 Luglio 1958)

Summary — The optical model of the nucleus, which has proved useful in the study of coherent scattering processes, is applied here to the inelastic scattering of π-mesons by nuclei. Various aspects of meson and nucleon kinematics as modified by the presence of the optical model potential are discussed. Formulae and numerical results which relate free pion-nucleon cross sections to cross sections for pion-nucleon collisions within nuclei are also given. They indicate that the coherent effects described by the optical model play an important role in the inelastic scattering of mesons.

1. – Introduction.

The interactions in which π-mesons are scattered by atomic nuclei are qualitatively of two kinds, those which leave the nuclear state unaltered (elastic or coherent) and those which excite the nucleus, or are inelastic. The elastic scattering results from interference of coherent waves scattered from all parts of the nucleus, and reflects the properties of the nuclear medium as a whole. These properties are expressed by means of a potential well, conventionally termed the « optical model potential » (1), which serves to describe how a pion propagates through a nucleus without loss of energy.

In addition to these elastic processes, the scattering of high energy pions is often accompanied by energy transfers large enough to excite one or more nucleons above the nuclear Fermi energy. Such inelastic events are commonly attributed to a sequence of pion collisions with single nucleons within the nucleus, with interaction strengths given by the known free pion-nucleon

(*) This work was supported in part by the National Science Foundation.

(1) S. Fernbach, R. Serber and T. B. Taylor: *Phys. Rev.*, **75**, 1352 (1949).

cross-sections. If coherent effects are ignorable, then inelastic cross-sections may be obtained by the « Monte Carlo » technique which computes the classical trajectories of a beam of pions that scatter incoherently from an assembly of nucleon targets ([2,3]). In this scheme, the exclusion principle forbids collisions which place the recoiling nucleon in a momentum state already occupied by a similar nucleon. The consequence is to limit the number of inelastic collisions a pion may suffer; a pion with, say, 100 MeV kinetic energy is seldom scattered more than once or twice in its journey through a heavy nucleus. There is, of course, no limitation of this kind on the elastic scattering processes.

We wish to suggest that the coherent processes in the nuclear medium, as evidenced by the elastic cross-sections and characterized by the optical model potential, may affect significantly the calculation of inelastic cross-sections by the Monte Carlo method. Not only is the effective kinetic energy at which pion-nucleon collisions occur displaced, but the dispersive nature of the medium (the variation of the potential with pion energy) alters the magnitudes of pion flux and the density of states. Expressed differently, the optical model potential may give the meson an « effective mass » which varies with energy and is quite different from its actual mass. This view-point is, of course, familiar in the study of transport phenomena involving electrons in solids.

In the present work we shall pursue the implications of this point. That is, we shall use the optical model potential, as inferred from dispersion relations, to determine the modified kinematics of meson propagation in nuclei. The results will be applied to a discussion of pion scattering by neutrons and protons within nuclei and some comparisons with experiment will be given. We find that the dispersion in the nuclear medium affects markedly the energy spectrum of mesons emitted at a given angle, as well as the magnitude and angular distribution of cross-sections for incident pion energies up to a few hundred MeV.

Although calculated results are presented for this entire energy range, we must emphasize that near the « resonance » energy for pion nucleon scattering, the very strong interactions limit the accuracy of the approximations upon which our simple model is based. In this region, the elementary theory described here must be regarded as qualitative at best. Nevertheless, we expect that in the resonance region as elsewhere, no theory which aims at quantitative agreement with experiments on nuclear scattering of mesons can afford to neglect the role of coherent effects.

([2]) R. Serber: *Phys. Rev.*, **72**, 1114 (1947).

([3]) M. L. Goldberger: *Phys. Rev.*, **74**, 1269 (1948); N. Metropolis *et al.*: *Phys. Rev.*, **110**, 204 (1958).

2. – The optical model.

From a formal point of view, the optical model treats the elastic scattering of pions by nuclei exactly. We contemplate, in the present paper, pion energies quite small compared to nuclear rest energies. Hence we neglect at the outset the recoil of the nucleus in an elastic interaction. Then such interactions are described rigorously if we choose a suitable potential V and write a Schrödinger equation for the meson wave function $\psi(\boldsymbol{r})$:

$$\omega\psi(\boldsymbol{r}) + \int \langle \boldsymbol{r} | V | \boldsymbol{r}' \rangle \, \mathrm{d}^3\boldsymbol{r}' \psi(\boldsymbol{r}') = E\psi(\boldsymbol{r}) \,. \tag{1}$$

The energy ω is $(p^2+\mu)^{\frac{1}{2}}$ where p is the momentum operator for the pion and μ its rest mass. The potential is expected to be non-local and, in consequence of absorbtive processes, non-Hermitian.

From a practical standpoint, it is desirable that the form of the potential be simple and, moreover, that it be related to the dynamics of pion-nucleon interactions. For these reasons, the potential is written in an approximate form [4]

$$\langle \boldsymbol{r} | V | \boldsymbol{r}' \rangle = \varrho\left(\frac{\boldsymbol{r}+\boldsymbol{r}'}{2}\right) W(\boldsymbol{r}-\boldsymbol{r}') \,, \tag{2}$$

where $\varrho(\boldsymbol{r})$ is the nuclear density. As a further simplification, $\varrho(\boldsymbol{r})$ is normalized to unity when $\boldsymbol{r}$ lies within the nucleus and is zero otherwise.

The « well depth » V_0 of the optical model potential is the Fourier transform of W:

$$V_0(K) = \int \exp\left[-i\boldsymbol{K}\cdot\boldsymbol{r}\right] W(\boldsymbol{r}) \, \mathrm{d}^3\boldsymbol{r} \,. \tag{3}$$

Thus, when the potential acts upon a plane wave $\exp\left[i\boldsymbol{K}\cdot\boldsymbol{r}\right]$, we have, if the nuclear radius is large compared to K^{-1}:

$$V \exp\left[i\boldsymbol{K}\cdot\boldsymbol{r}\right] \approx \varrho(\boldsymbol{r}) V_0(K) \exp\left[i\boldsymbol{K}\cdot\boldsymbol{r}\right] \,. \tag{4}$$

Approximate solutions to (1) may then be sought in which an incident plane wave is coupled to a plane wave within the nucleus:

$$\begin{cases} \psi(\boldsymbol{r}) \sim \exp\left[i\boldsymbol{q}_0\cdot\boldsymbol{r}\right] \,, & \boldsymbol{r} \text{ outside the nucleus,} \\ \psi(\boldsymbol{r}) \sim \exp\left[i\boldsymbol{K}\cdot\boldsymbol{r}\right] \,, & \boldsymbol{r} \text{ inside the nucleus.} \end{cases} \tag{5}$$

[4] For a derivation of this equation, see R. M. FRANK, J. L. GAMMEL and K. M. WATSON: *Phys. Rev.*, **101**, 891 (1956).

The energy-momentum relations now have the form

$$E = (q_0^2 + \mu^2)^{\frac{1}{2}} \equiv \varepsilon_0 + \mu \tag{6}$$

and

$$E = (K^2 + \mu^2)^{\frac{1}{2}} + V_0(K) \equiv \varepsilon(K) + \mu \,. \tag{7}$$

Taken together, Eq. (6) and (7) determine the momentum change suffered by a pion upon entering a nucleus. The well depth V_0 may be regarded, equi-

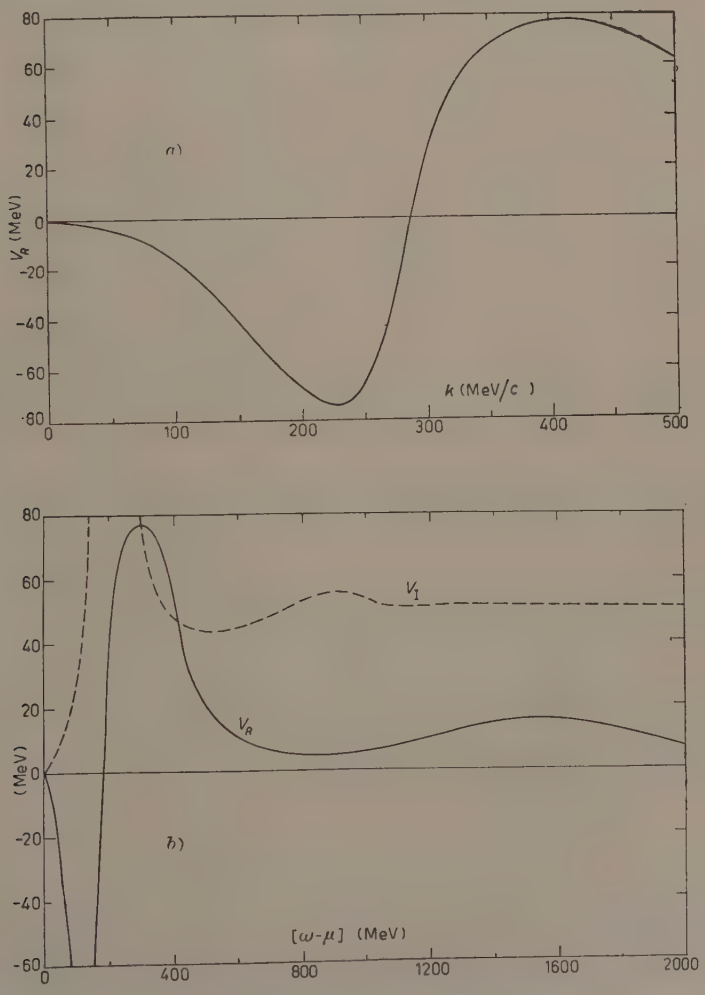

Fig. 1. – (*a*) V_R is shown as a function of the pion momentum k within the nucleus. (*b*) V_R and V_I are shown as functions of $(\omega(k) - \mu)$.

valently, as a function of the incident pion kinetic energy $\varepsilon_0 = E - \mu$, or of q_0, or of K. It is, in general, complex; the real and imaginary parts of V_0 are specified by the notation

$$V_0 = V_R - iV_I . \tag{8}$$

On the basis of the Serber model (2), one can relate V_0 to the pion-nucleon interaction. Indeed, to a reasonable approximation, V_0 is proportional to $f(K)$, the amplitude for *forward* scattering of pions by nucleons (4). Further, $V_0(K)$ is an analytic function of the complex variable $(K^2 + \mu^2)^{\frac{1}{2}}$ in the upper half plane, and may be explicitly calculated from the dispersion relations of GOLDBERGER (5). The quantities V_R and V_I so calculated are shown (with the inclusion of a correction for true absorption of pions (3,4) in Fig. 1).

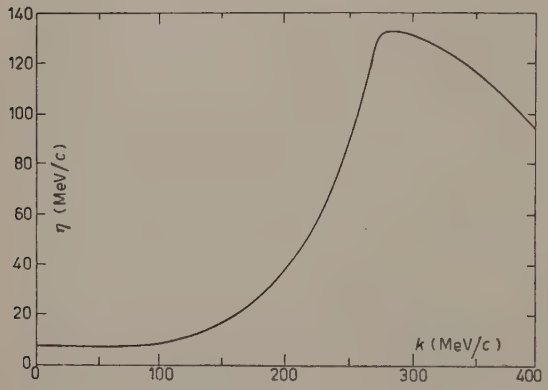

Fig. 2. – The imaginary part of the momentum K is shown as a function of k.

It is clear from (7) and (8) that the pion momentum K within the nucleus is complex. Setting $K = k + i\eta$, we see that η and V_I have the same sign and, from Fig. 1, both are positive. The plane wave $\exp[i\boldsymbol{K}\cdot\boldsymbol{r}]$ is exponentially damped as the pion propagates through the nucleus. The quantity $(2\eta)^{-1}$ is then identified as the mean free path λ for the absorbtive effects characterized by V_I. In Fig. 2, η is given as a function of the pion momentum k within the nucleus. This is taken from Table I of reference (4). In Figs. 1*a* and 2 we have increased the quantities of reference (4) by a factor of 1.6. This corresponds to changing the nuclear radius parameter r_0 from 1.4 to 1.2, which now seems a better value. For the purposes of the present paper, we accept as correct the optical model parameters given in these figures.

---

(5) M. L. GOLDBERGER: *Phys. Rev.*, **99**, 979 (1955); M. L. GOLDBERGER, H. MIYAZAWA and R. OEHME: *Phys. Rev.*, **99**, 986 (1955). The numerical values for the dispersion integrals were taken from H. L. ANDERSON, W. C. DAVIDON and U. E. KRUSE: *Phys. Rev.*, **100**, 339 (1955) and from R. COOL, O. PICCIONI and D. CLARK: *Phys. Rev.*, **103**, 1082 (1956). Similar evaluations have been made by R. STERNHEIMER: *Phys. Rev.*, **101**, 384 (1956).

3. – Pion kinematics in nuclei.

The calculation of a cross-section entails, first of all, a knowledge of the velocity of the particles which make up the incident beam. In a quantum treatment, one ordinarily constructs wave packets of fairly well defined energy and makes use of the mean group velocity $\mathrm{d}E(K)/\mathrm{d}K$ of the waves. As is well known, the group velocity coincides with the classically defined particle velocity when $E(K)$ denotes the energy of a free particle. We must now consider in what sense this proceedure is applicable to the pion-nucleon collisions which occur in a nuclear medium.

In order to use the model discussed in the previous section, we must require that the breadth of a meson packet be small compared to a nuclear diameter. Otherwise, one cannot specify whether the meson is truly inside or outside of the nucleus during its time of interaction. A further limitation is that the packet breadth not exceed a mean free path for absorbtion, for it is difficult to speak of the propagation of a particle when it is already half absorbed, initially. On the other hand, the packet must maintain its localization at least until is has an opportunity for a collision. Consequently, the spread of a packet in the time needed to cover a mean free path length must be small compared to the breadth itself.

We consider, for simplicity, a one dimensional packet $\psi(x, t)$, wholly within the nucleus, which at $t = 0$ is represented as

$$\psi(x, 0) = \int_{-\infty}^{+\infty} a(K - Q) \exp [iQx] \, \mathrm{d}Q \, . \tag{9}$$

For illustrative purposes, we select a Gaussian packeting function

$$a(K - Q) = (\Delta p \sqrt{2\pi})^{-1} \exp \left[- \frac{(K - Q)^2}{2(\Delta p)^2} \right], \tag{10}$$

so that

$$\psi(x, 0) = \exp [iKx] \exp \left[- \frac{x^2}{2(\Delta x)^2} \right], \tag{11}$$

with $\Delta x = (\Delta p)^{-1}$.

To obtain the time dependence of ψ, we first deform the path of integration into the upper half plane so that the variable Q passes through all values $Q_1 + iQ_2$ which, by Eq. (7), appear as momenta corresponding to a real energy. The wave function is now represented as a superposition of eigenwaves in

the nucleus. Consequently,

$$\psi(x, t) = \int a(K - Q) \exp\left[i(Qx - E(Q)t)\right] \mathrm{d}Q \,. \tag{12}$$

We approximate $E(Q)$ within the region of integration by the initial terms of a Taylor series about K:

$$E(Q) = E(K) + (Q - K)\frac{\mathrm{d}E}{\mathrm{d}K} + \frac{1}{2}(Q - K)^2 \frac{\mathrm{d}^2E}{\mathrm{d}K^2} \,. \tag{13}$$

The integral remains of gaussian type so that

$$\psi(x, t) = \exp\left[i(Kx - E(K)t)\right] \exp\left[-\frac{(x - (\mathrm{d}E/\mathrm{d}K)t)^2}{2\alpha}\right], \tag{14}$$

with

$$\alpha = (\Delta p)^{-2} + it\frac{\mathrm{d}^2E}{\mathrm{d}K^2} \,.$$

Equation (14) suggests that $\mathrm{d}E/\mathrm{d}K$ be interpreted as the velocity of the packet, but this is only possible when $\mathrm{d}E/\mathrm{d}K$ is real. If not, we separate the derivative into real and imaginary parts, and define a « group velocity » v_G by

$$\frac{\mathrm{d}E}{\mathrm{d}K} = v_G + iw_G \,. \tag{15}$$

Thus, v_G represents an approximate propagation velocity of the packet if we may suppose w_G small and if, further, the packet does not spread so rapidly as to lose its meaning. Even if $\mathrm{d}E/\mathrm{d}K \approx v_G$ and $\mathrm{d}^2E/\mathrm{d}K^2 \approx v_G'$ were real, the width Δp in momentum space must still be narrow enough to permit the expansion (13). The latter leads to

$$|\psi(x, t)|^2 = \exp\left[-\frac{(x - v_G t)^2}{(\Delta_t x)^2}\right], \tag{16}$$

where the spread $\Delta_t x$ at time t is given by

$$(\Delta_t x)^2 = (\Delta x)^2 + \left[\frac{\mathrm{d}v_G}{\mathrm{d}k}\frac{t}{\Delta x}\right]^2. \tag{17}$$

Imposing the conditions that Δx be less than the mean free path λ, and that $(v_G' t/\Delta x)$ be less than Δx if $t < \lambda/v_G$, we are led to a consistency requirement:

$$\frac{1}{v_G}\frac{\mathrm{d}v_G}{\mathrm{d}k} < \lambda \,. \tag{18}$$

To obtain numerical values from these quantities, we rewrite Eq. (7) as

$$(7') \qquad E(K) = E(k + i\eta) \approx E(k) + iv_G\eta = \varepsilon_0 + \mu \,.$$

From Eqs. (7) and (8), we obtain $V_I = v_g\eta$ and $\omega(k) + V_R = \varepsilon_0 + \mu$. Strictly speaking, the mean-free-path and thus η should now be recalculated from the cross-sections of Sect. **6** and V_I should be obtained from this. Since it is not important for our conclusions, we shall use the values of η taken from Fig. 2. In Fig. 3 are given the resulting values of V_I and V_R as functions of ε_0.

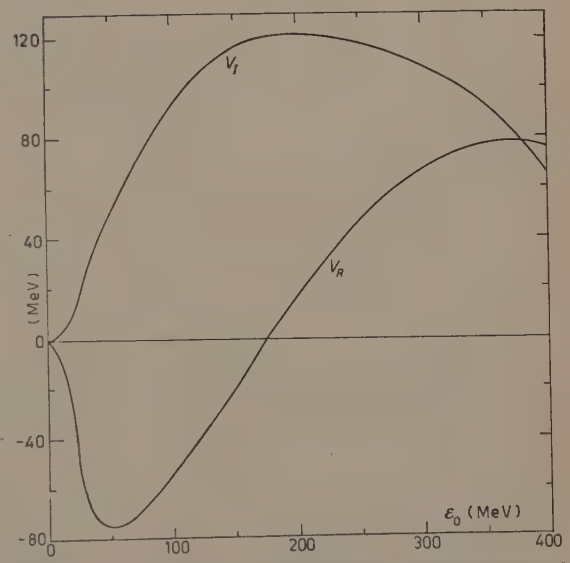

Fig. 3. — V_I and V_R are shown as functions of $\varepsilon_0 = \omega(q_0) - \mu$, the kinetic energy of the pion outside of the nucleus.

In Fig. 4 are shown the momentum k *vs.* ε_0 and (for comparison) the free particle momentum q_0 *vs.* $\varepsilon_0 = (q_0^2 + \mu^2)^{\frac{1}{2}} - \mu$.

In Fig. 5, the group velocity defined by (15) is displayed as a function of the pion momentum within the nucleus. The limitations upon the values of v_G are not met in the resonance region where $V_R(K)$ has a positive slope. This interval is, in optical terminology, the region of « anomalous dispersion ». It is the region in which absorption is large, where the group velocity exceeds the particle velocity and may exceed the velocity of light. As in the optical case, the identification of v_G with a velocity of energy transport fails under such circumstances.

Although the given theory breaks down in the region of anomalous dispersion, it is desirable that some qualitative guide to the magnitudes of particle fluxes and inelastic cross-sections be obtained for energies near resonance. An analogous situation has been considered long ago by Brillouin [6]: the propagation of the wave front of a half infinite light wave through a dispersive medium. Brillouin made use of the known analytic form of the index of refraction (due to resonating bound electrons), a form similar to that of the optical model well depth. He showed that the wave front propagates with a fairly well-defined velocity for all frequencies. This « signal velocity »

[6] L. Brillouin: *Ann. Phys.*, **44**, 203 (1914).

agrees with the group velocity for normal dispersion, but parts company with it, remaining close to, but less than, the speed of light in the anomalous region.

Motivated by this example, we shall likewise « smooth out » the group velocity curve, obtaining the dashed curve in Fig. 5 which approximates the speed of light in the anomalous region. There is, indeed, no necessity for a

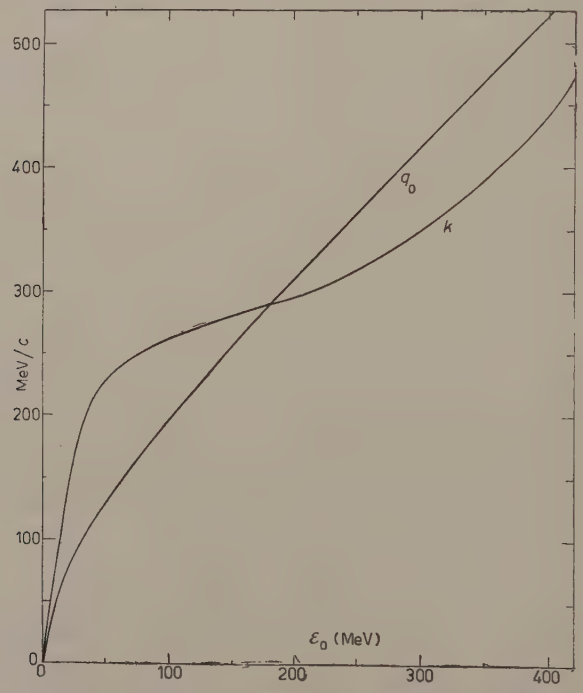

Fig. 4. – The momentum k of a pion in the nucleus is shown as a function of the energy ε_0 (Eq. (71)). For comparison, the momentum q_0 of a free pion is also shown as a function of ε_0 (Eq. (6)).

packet to have a well-defined velocity such as possessed by the wave front in Brillouin's example. We hope, however, that this adjustment of v_G approximates a relatistic velocity with which to calculate particle fluxes and that a qualitative indication of dispersive effects in inelastic scattering near resonance may thereby be obtained.

We note, finally, that a conservation equation for meson current may be obtained for wave packets described as in (12). The meson probability density $P(x)$ is proportional to $\psi^*\psi$, so that

$$(19) \qquad P(x) \approx \int \mathrm{d}Q\, \mathrm{d}Q' a(K-Q)a^*(K-Q') \exp\left[i(Qx - E(Q)t)\right] \cdot \exp\left[-i(Q'x - E^*(Q')t)\right].$$

The Q and Q' integrations may be carried out along the real axis. The application of $i(\partial/\partial t)$ to $P(x)$ brings under the integral sign in (9) a factor of

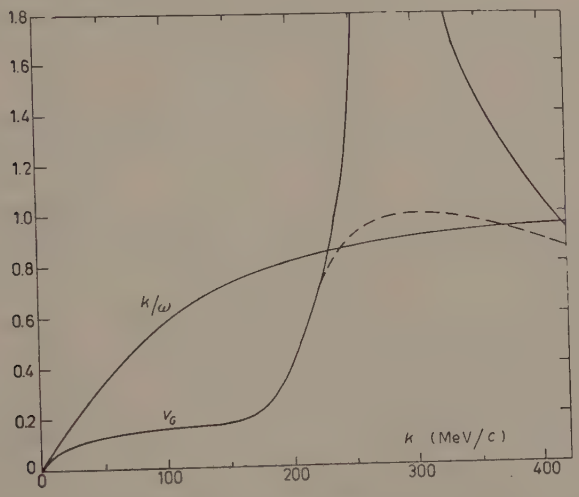

Fig. 5. – The pion group velocity V_G is shown as a function of the momentum k within the nucleus (Eq. (15)). The corresponding free particle velocity k/ω is also shown. The dashed curves represent conjectured values, consistent with $v_G \leqslant c$.

$E(Q) - E(Q')$, while an application of $-i(\partial/\partial x)$ yields a factor of $(Q - Q')$. Separating E into real and imaginary parts, $E = E_1 + iE_2$, we have

$$E(Q) - E^*(Q') = E_1(Q) - E_1(Q') + i[E_2(Q) + E_2(Q')] \approx (Q - Q')\, v_G(K) - 2iV_I(K)\,,$$

subject to the limitations previously discussed. Hence, we infer that

$$\frac{\partial}{\partial t} P(x) + \frac{\partial}{\partial x}[V_G(K)P(x)] = -2V_I(K)P(x)\,, \tag{20}$$

which shows, for sufficiently narrow packets, how the instantaneous change in density in a small region is due to a flow of probability with velocity v_G and to an absorbtion of probability into the medium.

4. – The cross section for pion-nucleon scattering within nuclei.

Consider first the scattering of a meson of momentum k_0 against a free nucleon at rest. Let the scattered pion have momentum K and the nucleon a momentum

$$\boldsymbol{Q} = \boldsymbol{k}_0 - \boldsymbol{K}\,.$$

The final energy is

$$\omega(K) + (Q^2 + M^2)^{\frac{1}{2}} = \omega(k_0) + M \,. \tag{21}$$

The differential scattering cross-section is

$$\left(\frac{\mathrm{d}\sigma}{\mathrm{d}\Omega}\right)_{\text{free}} = \left\{\int K^2 \mathrm{d}K\, \delta[\omega(K) + (Q^2 + M^2)^{\frac{1}{2}} - \omega(k_0) - M]\right\} (2\pi)^4 \frac{\omega(k_0)}{k_0} |t|^2 \,.$$

Here t is the « scattering operator » ([7]) and an average and sum over initial and final nucleon spin states is implied. Carrying out the integration over K gives

$$\left(\frac{\mathrm{d}\sigma}{\mathrm{d}\Omega}\right)_{\text{free}} = (2\pi)^4 F_f |t|^2 \,, \tag{22}$$

where

$$\begin{cases} F_f \equiv \dfrac{\omega(k_0)}{k_0} \dfrac{K^2}{B_f} \,, \\ B_f = \hat{K} - \left[\dfrac{\boldsymbol{K}}{\omega} - (Q^2 + M^2)^{-\frac{1}{2}}(\boldsymbol{k}^0 - \boldsymbol{K})\right] . \end{cases} \tag{23}$$

In these equations the value of K is defined by Eq. (21).

To obtain the cross-section when the nucleon is bound in a nucleus, we assume that t is the same as for a free nucleon. This may be justified in a qualitative way: First, if the scattering interaction is weak, so t is given in Born approximation from some potential, the assumption is evidently valid. On the other hand, if the pion-nucleon interaction is very strong and of short range (as actually seems to be true), we argue that high energy virtual transitions determine t. For these, however, the optical model potential should be relatively unimportant. We shall actually take

$$t_{\text{bound}}(\theta) = t_{\text{free}}(\theta) \,. \tag{24}$$

That is, the free and bound quantities t are considered equal for the same *scattering angle* θ. This is somewhat arbitrary, but seems consistent with our semi-quantitative discussion.

It is useful to define the « effective mass » of a pion as μ^*, where

$$\frac{1}{\mu^*} = 2\frac{\mathrm{d}E}{\mathrm{d}k^2} \,. \tag{25}$$

([7]) M. Gell-Mann and M. L. Goldberger: *Phys. Rev.*, **91**, 3953).

Thus $v_g = k/\mu^*$, if w_G is negligible in Eq. (15). The energy E is defined by Eq. (7). In Fig. 6 we display μ^* as a function of the pion momentum.

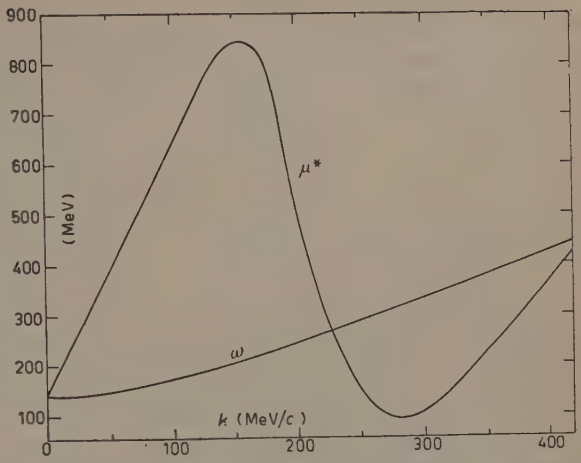

Fig. 6. – The effective mass μ^* of the pion is shown as a function of the momentum k within the nucleus. Also shown is the relativistic « free particle mass » ω.

The energy conservation equation (21) is now replaced by

$$E(k)+(Q^2+M^2)^{\frac{1}{2}}= \\ = \omega(k_0) + M\,, \tag{26}$$

where again $\boldsymbol{Q} = \boldsymbol{k}_0 - \boldsymbol{k}$. We suppose the imaginary part of E to be neglected and write the cross-section for scattering from a *bound* nucleon [$(v_g)_0$ is the group velocity of the incident pion] as:

$$\left(\frac{\mathrm{d}\sigma}{\mathrm{d}\Omega}\right)_{\text{bound}} = \left\{\int k^2\,\mathrm{d}k\,\delta[E(k) + (Q^2 + M^2)^{\frac{1}{2}} - \omega(k_0) - M]\right\}\frac{(2\pi)^4}{(v_g)_0}|t|^2\,.$$

Evaluation of the integral above leads to (the scattering angle θ is the angle between $\boldsymbol{k}_0$ and $\boldsymbol{k}$)

$$\frac{\mathrm{d}\sigma(\theta)}{\mathrm{d}\Omega} = (2\pi)^4 F\,|t|^2\,, \tag{27}$$

in analogy to Eq. (22). Here

$$\begin{cases} F \equiv \dfrac{k^2}{(v_g)_0}\,\dfrac{1}{B}\,, \\ B = \hat{k} - \left[\dfrac{\boldsymbol{k}}{\mu^*} - \dfrac{1}{M}\,(\boldsymbol{k}_0 - \boldsymbol{k})\right]. \end{cases} \tag{28}$$

The expression for B may be improved by replacing M by the effective nucleon mass M^* in nuclear matter. For the computation of the next section we have used Brueckner's and Wada's [8] value $M^* = .6\,M$ at very low energies and joined this to that obtained from the nucleon optical model potential at higher energies.

[8] K. A. Brueckner and W. Wada: *Phys. Rev.*, **103**, 1008 (1956).

The relation (27) has also been obtained in the course of a discussion of quantum mechanical transport phenomena (9).

Equation (22) and (27) may be combined to give

$$\left(\frac{d\sigma}{d\Omega}\right)_{\text{bound}} = \frac{F}{F_f}\left(\frac{d\sigma}{d\Omega}\right)_{\text{free}}. \tag{29}$$

5. – Calculated cross sections.

The function F_f of Eq. (23) is given in Fig. 7 for several incident momenta k_0 and scattering angle θ. In Fig. 8 we give corresponding values for the function F of Eq. (28). From these we may relate the « free » and « bound » scattering cross-sections, as given by Eq. (29).

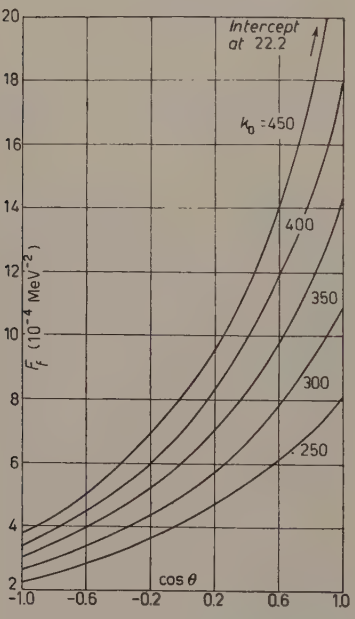

Fig. 7. – The function F_f of Eq. (23) is shown for several values of k_0 and the scattering angle θ.

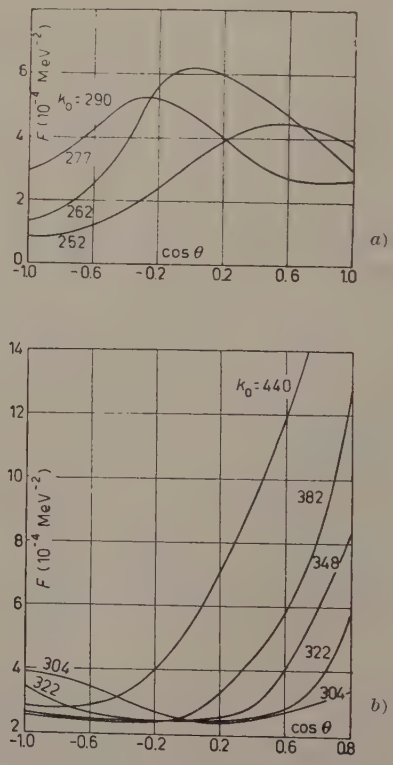

Fig. 8. – *a*), *b*) The function F of Eq. (28) is shown for several values of k_0 and scattering angle θ.

From Eq. (29) we have obtained the cross-section for inelastic scattering of 125 MeV pions on carbon. Multiple scattering corrections were neglected,

(9) K. M. WATSON: submitted to the *Phys. Rev.*

except for a simple exponential attenuation of the incident wave. In Fig. 9 the resulting calculated cross-section is compared with that measured by KESSLER and LEDERMAN ([10]). It is evident from Fig. 9 that the absolute magnitude of the cross-section is not very well obtained from our calculation.

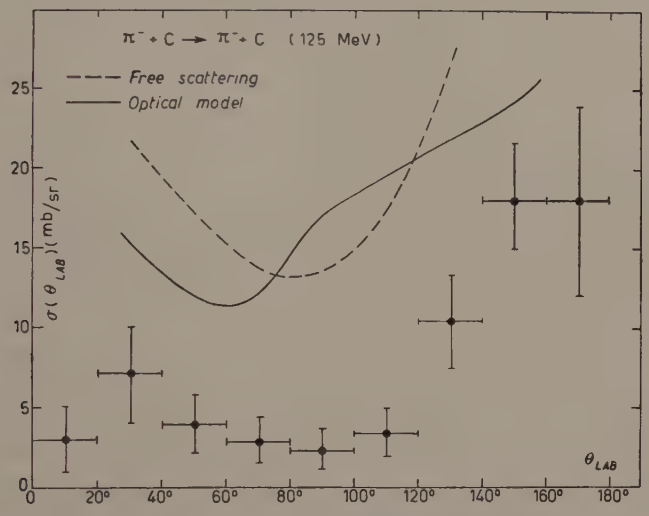

Fig. 9. – Comparison is made of calculated inelastic scattering of 125 MeV pions with measurements of KESSLER and LEDERMAN on carbon.

This is very sensitive, however, to the value of the mean free path. It is also not at all evident that our corrections are reflected in the experimental cross-sections. It is unfortunate for our comparison that the energy at which this experiment was done corresponds so closely to the resonance energy for scattering in nuclei. At this energy we do not anticipate any quantitative reliability for our calculation.

6. – Discussion of results.

We have seen that dispersive corrections to pion scattering in nuclei are by no means negligible. Indeed, near the resonance energy for pion-nucleon scattering these are too large to be handled adequately by the conventional, simple theory which has been used.

Our discussion has assumed that each inelastically scattered wave interacts continuously with a quiescent nuclear medium. When the particles in the

---

([10]) J. O. KESSLER and L. M. LEDERMAN: *Phys. Rev.*, **94**, 689 (1954).

medium are strongly correlated, the local disturbance caused by an inelastic scattering may modify the medium, causing our arguments to be invalid. The conditions under which this is expected to occur have been discussed before ([11]). From this discussion we may expect our assumption of an undisturbed medium to be valid when the deBroglie wavelength of the scattered particle is large compared to the distance over which nucleons are *correlated* in nuclei. For a degenerate Fermi gas model this distance is roughly $\hbar/P_F$, where $P_F = 270$ MeV/c. Thus for pion energies below resonance, for which the dispersive corrections are most important, we expect our assumption of an undisturbed nuclear medium to be valid.

Finally, our evaluation of the optical model potential has been based on the first approximation, which gives the potential as linear function of the forward scattering amplitude for pions on free nucleons. The second approximation is also rather simple at high energies (see, for example, Eq. (83), reference ([11])).

To write this out, we must first introduce the nuclear pair correlation function $G(r)$: Let $P_1(\boldsymbol{Z}_1)$ be the probability of finding nucleon « 1 » at $\boldsymbol{Z}_1$ within the nucleus and let $P_2(\boldsymbol{Z}_1, \boldsymbol{Z}_2)$ be the joint probability of finding nucleon « 1 » at $\boldsymbol{Z}_1$ and nucleon « 2 » at $\boldsymbol{Z}_2$. Then

$$P_2(\boldsymbol{Z}_1, \boldsymbol{Z}_2) = P_1(\boldsymbol{Z}_1) P_1(\boldsymbol{Z}_2) [1 + G(|\boldsymbol{Z}_1 - \boldsymbol{Z}_2|)] \tag{30}$$

defines G. Let

$$R_G \equiv \int_0^\infty G(r)\, \mathrm{d}r\,, \tag{31}$$

$$\begin{cases} \Delta_R = - V_R R_G \dfrac{E}{k_0}\,, \\ \Delta_I = - V_I R_G \dfrac{E}{k_0}\,, \end{cases} \tag{32}$$

where E is given by Eq. (6). Then the optical model potential, correct to second order is

$$V_{op} = [V_R - iV_I](1 + i\Delta_R + \Delta_I)\,. \tag{33}$$

The quantities V_R and V_I here and in Eq. (32) are those of Eq. (8) and Figs. 1*a* and 1*b*.

([11]) K. M. WATSON: *Phys. Rev.*, **105**, 1388 (1957).

Except near the resonance energy, the quantities Δ_R adn Δ_I do not give a very important correction to Eq. (33).

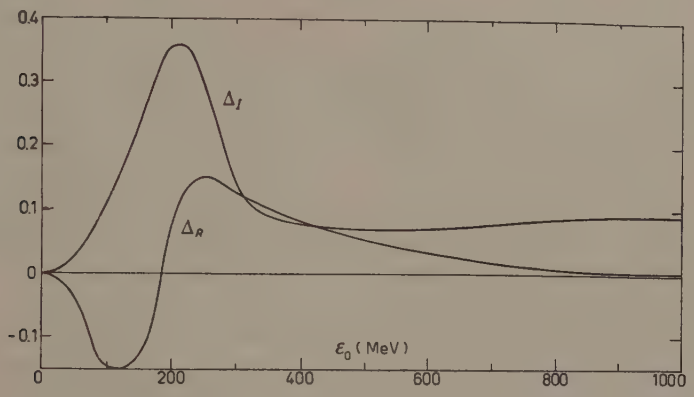

Fig. 10. – The functions Δ_R and Δ_I of Eq. (32) are given as functions of ε_0.

For example, assuming a degenerate Fermi gas model of the nucleus, we estimate $R_c \approx -\frac{1}{3} r_0$ (where r_0 is the mean radius per nucleon). For this value the resulting quantities Δ_R and Δ_I are plotted in Fig. 10.

* * *

We are indebted to Professor L. M. LEDERMAN for informing us that he also has considered the effect of the optical potential on inelastic pion corrections ([12]).

([12]) Unpublished.

RIASSUNTO (*)

Si applica qui il modello ottico del nucleo, che si è dimostrato utile nello studio dei processi di scattering coerenti, allo studio dello scattering anelastico dei mesoni μ da parte dei nuclei. Si discutono vari aspetti della cinematica dei mesoni e dei nucleoni in quanto risulterebbero modificati dalla presenza del potenziale derivante dal modello ottico. Si danno anche formule e risultati numerici che mettono in relazione le sezioni d'urto pione-nucleone libere con le sezioni d'urto delle collisioni pione-nucleone entro i nuclei. Se ne trae l'indicazione che gli effetti coerenti descritti dal modello ottico hanno notevole importanza nello scattering anelastico dei mesoni.

(*) *Traduzione a cura della Redazione.*

IL NUOVO CIMENTO Vol. X, N. 3 1° Novembre 1958

Bubble Chamber Study of Unstable Particle Production in π^--p Collisions at 910, 960, 1200 and 1300 MeV (*).

F. Eisler, R. Plano, A. Prodell, N. Samios, M. Schwartz and J. Steinberger

Columbia University and Brookhaven National Laboratory, New York - N. Y.

P. Bassi, V. Borelli, G. Puppi, H. Tanaka, P. Waloschek and V. Zoboli

Istituto di Fisica dell'Università - Bologna

M. Conversi, P. Franzini, I. Mannelli, R. Santangelo and V. Silvestrini

Istituto di Fisica dell'Università - Pisa

(ricevuto il 17 Luglio 1958)

Summary. — Results are reported on the total and differential cross-sections for the reactions $\pi^- + p \to \begin{matrix}\Lambda^0 + \theta^0 \\ \Sigma^0 + \theta^0 \\ \Sigma^- + K^+\end{matrix}$ at 910, 960, 1200 and 1300 MeV using hydrogen and propane bubble chambers in a magnetic field of 13.4 kG. The chambers and their operation, as well as the method of analysis are described in detail.

1. – Introduction.

The associated production of heavy mesons and hyperons in pion-proton collisions was first observed in the Brookhaven diffusion cloud chamber (1). Since then these « strange particle » producing collisions have been studied by various groups (2-4)using bubble chamber techniques. It is our purpose

(*) This research is supported by the Atomic Energy Commission and the Office of Naval Research.

(1) W. B. Fowler, R. P. Shutt, A. M. Thorndike and W. L. Whittemore: *Phys. Rev.*, **98**, 121 (1954).

(2) R. Budde, M. Chretien, J. Leitner, N. Samios, M. Schwartz and J. Steinberger: *Phys. Rev.*, **103**, 1827 (1956).

(3) L. Leipuner and R. K. Adair: *Phys. Rev.*, **109**, 1358 (1958).

(4) G. L. Brown, D. A. Glaser and M. L. Perl: *Phys. Rev.*, **108**, 1036 (1957).

here to report on an extension of this work toward higher statistical validity and to other pion energies. In all cases, a bubble chamber, filled with either propane (C_3H_8) or hydrogen was used, and the reactions studied were:

1) $\pi^- + p \to \Lambda^0 + \theta^0$
2) $\pi^- + p \to \Sigma^0 + \theta^0$ where
3) $\pi^- + p \to \Sigma^- + K^+$

a) $\Lambda^0 \to \pi^- + p$ or $\pi^0 + n$
b) $\theta^0 \to \pi^- + \pi^+$ or $2\pi^0$
c) $\Sigma^0 \to \Lambda^0 + \gamma$
d) $\Sigma^- \to \pi^- + n$.

Only the work on the cross-sections themselves is reported here. Results on decay modes of the Λ^0 and θ^0 ([5]) as well as the angular correlations in production and decay of the hyperons which are the basis of studies on the hyperon spins ([6]) and the question of parity conservation in hyperon decay ([7]) have already been reported. The results on the question of leptonic decay of hyperons and on the strange particle lifetimes are in preparation.

The experimental details, not previously reported, are presented in this paper. Some particulars of the various exposures (*i.e.* chamber type and size, beam energy, magnetic field, number of pictures taken) are given in Table I.

TABLE I. – *Exposure details.*

Incident pion kinetic energy (MeV)	Chamber size	Chamber filling	Magnetic field (kG)	Number of pictures	Analyzing group
910	12 in. diam. × 8 in.	Propane	13.4	24000	Bologna
960	12 in. diam. × 6 in.	Hydrogen	13.4	15000	C.U.-B.N.L.
1200	12 in. diam. × 8 in.	Propane	13.4	20000	Pisa
1300	12 in. diam. × 8 in.	Propane	13.4	18000	C.U.-B.N.L.
1300	6 in. diam. × 4 in.	Propane	—	25000	C.U.-B.N.L.

([5]) F. EISLER, R. PLANO, N. SAMIOS, M. SCHWARTZ and J. STEINBERGER: *Nuovo Cimento*, **5**, 1700 (1957).

([6]) F. EISLER, R. PLANO, A. PRODELL, N. SAMIOS, M. SCHWARTZ, J. STEINBERGER, P. BASSI, V. BORELLI, G. PUPPI, H. TANAKA, P. WALOSCHEK, V. ZOBOLI, M. CONVERSI, P. FRANZINI, I. MANNELLI, R. SANTANGELO, V. SILVESTRINI, G. L. BROWN, D. A. GLASER and C. GRAVES: *Nuovo Cimento*, **7**, 222 (1958).

([7]) F. EISLER, R. PLANO, A. PRODELL, N. SAMIOS, M. SCHWARTZ, J. STEINBERGER, P. BASSI, V. BORELLI, G. PUPPI, H. TANAKA, P. WALOSCHEK, V. ZOBOLI, M. CONVERSI, P. FRANZINI, I. MANNELLI, R. SANTANGELO, V. SILVESTRINI, G. L. BROWN, D. A. GLASER and C. GRAVES: *Phys. Rev.*, **108**, 1353 (1957).

2. – Description of the bubble chambers.

Two different propane chambers and one hydrogen chamber were used in the course of the experiment. The 6 in. propane chamber has been previously described ([2]). It was used without magnetic field.

2·1. *12 in. Propane chamber.* – A photograph of this chamber, 12 in. in diameter and 8 in. deep is shown in Fig. 1. In most respects it was similar to the 6 in. chamber in construction and operation.

The liquid propane was maintained at a temperature of 57 °C (and a vapor pressure of ~ 300 p.s.i.g.) by means of two main heating elements around the chamber and an auxiliary heating element below the neck. Temperatures were detected by means of thermo-couples attached to the chamber at various points. The output of one of these thermocouples was fed to a commercial control unit, which regulated the voltage to the main heater. The stability of the chamber temperature was $\sim \pm .1$ °C.

The propane communicated through a 5 in. diameter opening with a diaphragm located below the chamber. This diaphragm was made of a layer of nylon reinforced rubber faced with a layer of .007 in. mylar. Below the diaphragm was a perforated hold plate and a chamber filled with thin oil, followed by another diaphragm. The chamber was actuated by means of compressed air acting on the lower diaphragm. The basic purpose of the oil was to thermally insulate the chamber from the incoming compressed air.

Operation of the chamber proceeded as follows:

1) The chamber was overcompressed to a pressure of 325 p.s.i.g.

2) Upon receipt of a timing pulse from the Cosmotron, the chamber was allowed to expand. The expansion was completed in 10 milliseconds, at which time the beam was introduced. About 1 millisecond later the light was flashed and the pictures were taken.

3) Recompression of the chamber followed, the entire cycle lasting for approximately 30 milliseconds.

During the course of the exposures, the chamber was in a magnetic field of 13.4 kilogauss.

2·2. *12 in.* H_2 *chamber.*

2·2.1. Geometrical arrangement, vacuum tank and optics.

The mounting of the vaccum tank in the magnet, the suspension of the chamber in the tank, and the optical arrangement, are shown in Fig. 2. The tank is

F. Eisler, R. Plano, A. Prodell, N. Samios, M. Schwartz, J. Steinberger, P. Bassi, V. Borelli, G. Puppi, H. Tanaka, P. Waloschek, V. Zoboli, M. Conversi, P. Franzini, I. Mannelli, R. Santangelo and V. Silvestrini.

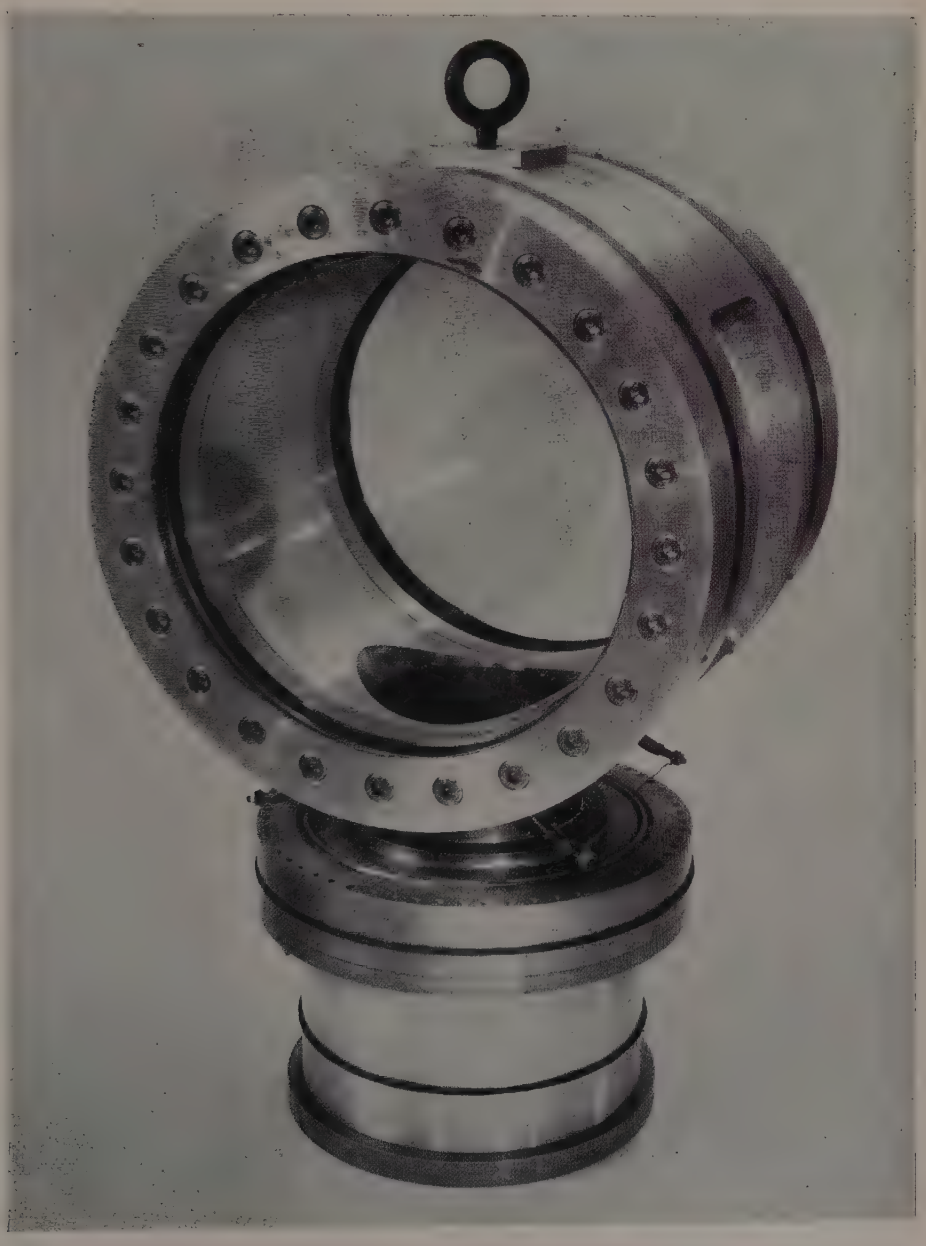

Fig. 1. – Photograph of 12 in. diameter propane chamber.

in the form of a cross. The vertical member accomodates the chamber and H_2 reservoir assembly, as well as the major part of the radiation shield and its liquid nitrogen reservoir. The horizontal extensions are tubes $12\frac{5}{8}$ in. ID, extending for 24 in. on either side and house radiation shields at liquid N_2 temperature, each with its own small reservoir (not shown in Fig. 2 for the camera arm). They are designed in order to keep the solid angle of room temperature radiation seen by the chamber to a sufficiently small value.

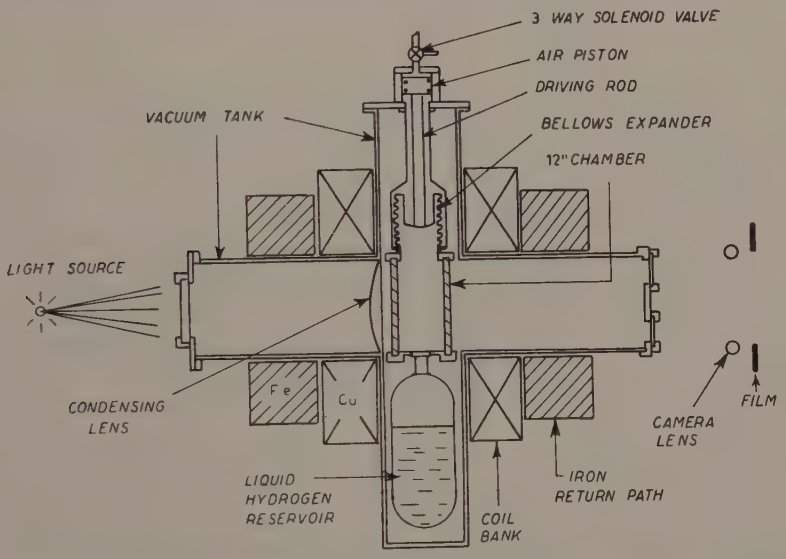

Fig. 2. – Schematic drawing showing the mounting of the chamber and the vacuum tank in the magnet and the arrangement of the light source and cameras.

The optical system is in its basic elements and dimensions the same for the two 12 in. chambers. The light source is a high speed flash lamp (G.E. FT-220), masked to an aperture of $1\frac{1}{2}$ in. diameter, at a distance on ~ 60 in. from the chamber. A $12\frac{1}{2}$ in. diameter 30 in. focal length lens is mounted on the radiation shield immediately behind the chamber. This illuminates a truncated conical region in the chamber, $11\frac{3}{4}$ in. diameter at the back surface, and $11\frac{1}{4}$ in. diameter at the front surface. The three lenses (Goerz-Artar 100 mm F.L.) are located 120° apart on a $11\frac{1}{2}$ in. circle, 40 in. from the inside surface of the front glass. The film, 35 mm Linagraph-Ortho, is contained in interchangeable magazines (Beattie Varitron) with film plane parallel to chamber plane. The magnification is 1/10, and the stereo angle to the center of the chamber is .23 radians for each of the three pairs of views. The triangular optical system has the advantage, considerable from the point of view of

rapid, routine analysis, that the measurement accuracy is nearly independent of track orientation.

2·2.2. Expansion system. – The chamber is closed at the top by means of a bellows, 7 in. high, $6\frac{1}{4}$ in. O.D., $4\frac{1}{2}$ in. I.D., of welded construction using .050 in. thick stainless steel plate. Together, chamber and bellows form a closed system filled entirely with liquid hydrogen. The bellows is driven by means of a $3\frac{1}{2}$ in. diameter air piston at the end of an 18 in. long, 2 in. diameter (1/16 in. wall thickness) hollow stainless steel piston rod (See Fig. 3).

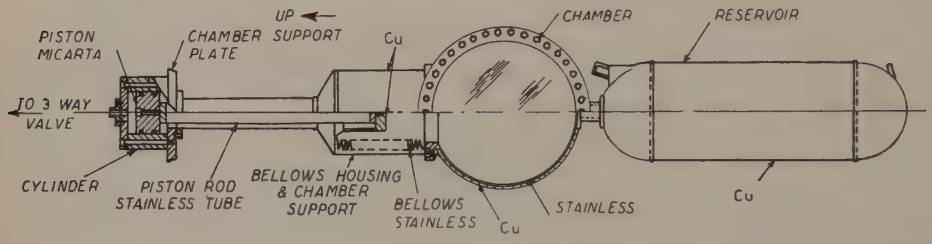

Fig. 3. – Schematic drawing of the hydrogen chamber, hydrogen reservoir and bellows expansion system.

Before expansion the bellows is compressed by means of air pressure (300 psi.) on the air piston. The expansion and recompression are achieved by release of the air and subsequent reintroduction, controlled by means of a 3 way valve in the same way as for the propane chamber. The speed of the expansion is controlled by an orifice between valve and piston, so that the speed does not exceed the capability of the bellows. The expansion cycle consists of a 10 ms expansion stroke, a 15 ms expanded phase, and a 10 ms recompression. The first bellows failed at this mounting after $\sim 75\,000$ strokes. The second (present) bellows, with some improvements in the mounting, has withstood $\sim 120\,000$ cycles without failure. Under normal operating conditions, the H_2 vapor pressure is 80 p.s.i.g. and the pre-expansion pressure is 85 p.s.i.g. We do not know the expanded pressure. The expansion stroke is $\sim \frac{3}{4}$ cm; this corresponds to a volume expansion of $1\frac{1}{2}\%$.

2·2.3. Temperature control. – The chamber is supported by a housing surrounding the bellows and expansion rod. The lower part of this housing is a copper tube 7 in. high, and the upper part is a stainless steel tube, $2\frac{1}{2}$ in. diameter $\times 14$ in. high. The region between the bellows and the chamber support, called the « bellows chamber », is connected externally to the hydrogen exhaust system through a needle valve. Below the chamber, the 15 liter H_2 reservoir is suspended (see Fig. 3). The chamber is cooled by the evaporation

of a small stream of liquid hydrogen directed from the reservoir on to the top of the bellows, in the bellows chamber. The amount of this cooling is determined by the fixed pressure head of about 1 psi. which impels the coolant flow, and the resistance of the needle valve at room temperature in the exhaust flow. Thermal control is by means of manual adjustment of the needle valve. Hydrogen consumption is $\frac{3}{4}$ liter/h for the uncycled chamber, $2\frac{1}{2}$ liter/h at 17 cycles per minute, and 4 liters/h at 30 cycles per minute.

The chamber construction is of stainless steel, plated with $\frac{1}{8}$ in. of copper. We feel however that the thermal uniformity of the liquid is achieved not by conduction in the copper but by convection in the liquid.

2·3. *Magnet.* – A cross-section of the magnet is shown in Fig. 2. It consists of two sets of coils, each 14 in. I.D. $\times$ 37 in. O.D. $\times$ 7 in. deep, surrounded by an iron return path. There are no poles. The iron end pieces are bored 14 in. in diameter to permit illumination and photography. The weight of the magnet is 10 tons. The gap between coils is $11\frac{3}{4}$ in. Each set consists of 14 pancakes electrically in series with the cooling water in parallel. The water connections are brought in on the inner diameters of the coil and leave at the outer. During its operation at the Cosmotron it was energized with 3 000 amperes at 210 volts, giving an average field of 13.4 kilogauss. The field fell off by 4% from the center to the edges. Current in the magnet was stabilized to $\pm 2\%$.

3. – Arrangement of beam and exposure.

The experimental arrangement at the Cosmotron is shown in Fig. 4. The circulating proton beam in the Cosmotron was permitted to impinge on a 6 in. long beryllium target in a straight section. Negative pions produced in the forward direction, were then bent out of the machine by the Cosmotron's magnetic field. They passed in succession through a collimator, the shielding wall, another collimator, a steering magnet and

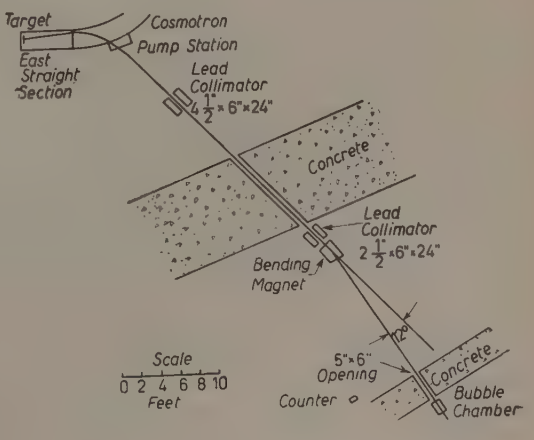

Fig. 4. – Experimental arrangement at the Cosmotron, showing target, collimators, shielding, bending magnet and bubble chamber.

two additional collimators. The collimation served to limit the energy spread of the beam to $\pm 1\%$ and to keep the beam at least $1\frac{1}{2}$ in. from the nearest chamber window.

To change the energy of the emerging pions, it was only necessary to change the steering magnet current and the time in the Cosmotron cycle at which the beam is ejected. The number of pion tracks per picture varied from ~ 30 to ~ 10.

4. – Scanning and analysis.

The pictures were scanned twice, once by a physicist and once by a technician. For measurement, the three views were independently projected on a screen to $1\frac{1}{2}$ times actual size, and the projected angles and radii of curvature were used to compute the direction cosines and momenta. On an average track, the error is $\pm .2°$ in the determination of the azimuthal angle, and $\pm 1°$ in the determination of the dip angle. The error in the momentum measurement is chiefly due to multiple Coulomb scattering. For the propane the fractional momentum error for a track with no dip is $.12/\beta\sqrt{l}$ and for the hydrogen $.04/\beta\sqrt{l}$, where l is the track length in decimeters. For such minimum ionizing tracks of ~ 12 cm length, the errors are 11% and 3.7% in the propane and hydrogen chambers respectively.

5. – Criteria for selection of events.

5·1. *Reaction* 1) $\pi^- + p \to \Lambda^0 + \theta^0$. – This reaction appears in the chamber as a stopping of the incident pion with either one or two V's having the stopping as possible origin (see Fig. 5). The event is accepted if either one or both V's are observed, and if all measured momenta and directions are consistent with the kinematics of the production reaction 1, and the decay reactions $\Lambda^0 \to \pi^- + p$ and $\theta^0 \to \pi^+ + \pi^-$.

5·2. *Reaction* 2) $\pi^- + p \to \Sigma^0 + \theta^0$. – Again the reaction will appear as a stopping with one or two V's having the stopping as origin, since the Σ^0 decays into Λ^0 and γ with a path length too short to be observed here, and the γ materializes only rarely. The kinematical conditions on the θ^0 are the same as those for 1): that is, given the direction of motion of the θ^0, its momentum is determined. The momentum is usually sufficiently different from that of the Λ^0 process to serve as a means of identification. On the other hand, the correlation between direction of motion and momentum of the Λ^0 is broadened by the recoil momentum (~ 70 MeV/c) in the Σ^0 decay. In the analysis of

F. Eisler, R. Plano, A. Prodell, N. Samios, M. Schwartz, J. Steinberger, P. Bassi, V. Borelli, G. Puppi, H. Tanaka, P. Waloschek, V. Zoboli, M. Conversi, P. Franzini, I. Mannelli, R. Santangelo, and V. Silvestrini.

Fig. 5. – An example of the reaction $\pi^- + p \to \Lambda^0 + \theta^0$ at 960 MeV in the hydrogen chamber.

F. Eisler, R. Plano, A. Prodell, N. Samios, M. Schwartz, J. Steinberger, P. Bassi, V. Borelli, G. Puppi, H. Tanaka, P. Waloschek, V. Zoboli, M. Conversi, P. Franzini, I. Mannelli, R. Santangelo, and V. Silvestrini.

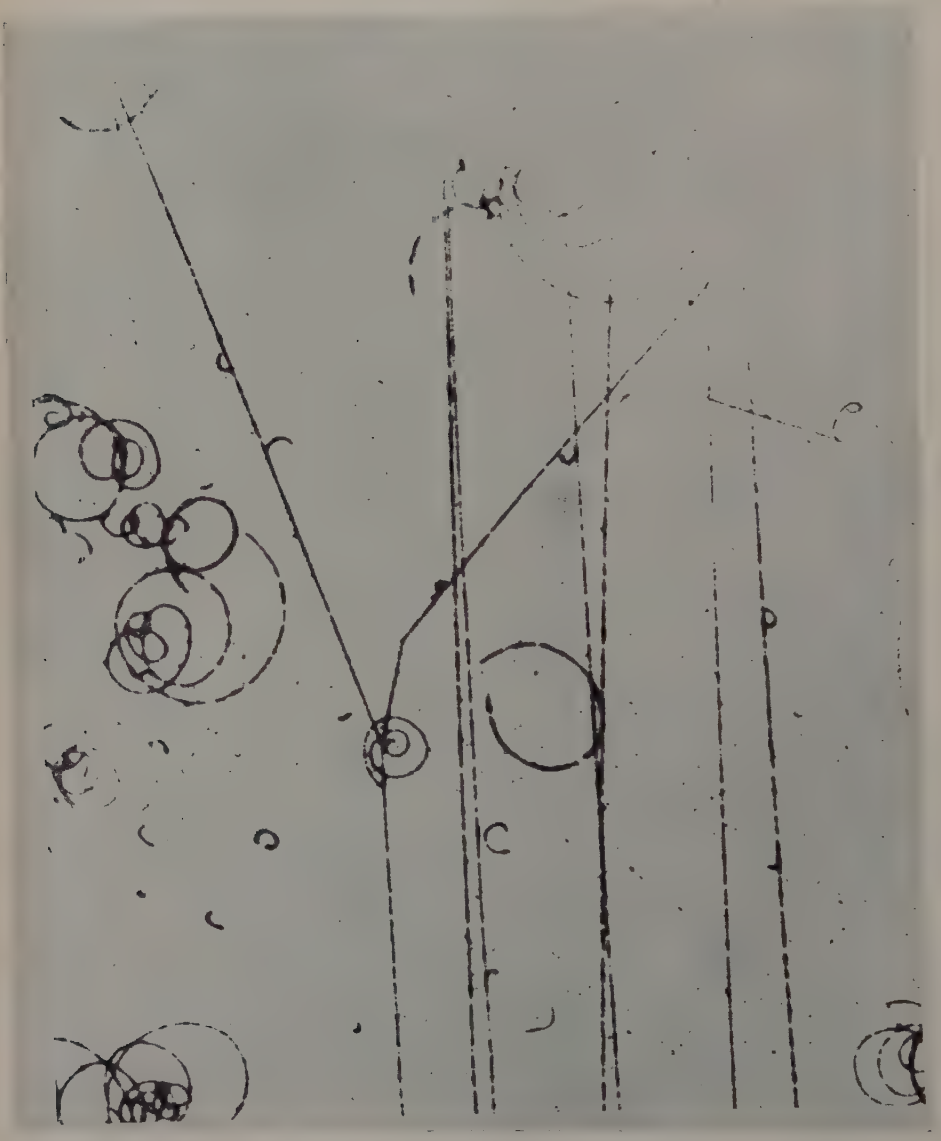

Fig. 6. – An example of the reaction $\pi^- + p \to \Sigma^- + K^+$ at 960 MeV in the hydrogen chamber.

the H_2 chamber photographs single Λ^0 events were accepted if compatible with reaction 2). In the case of the propane pictures it was found impossible to separate such events from the carbon background. (See following section).

5·3. *Reaction* 3) $\pi^- + p \to \Sigma^- + K^+$. – Here one sees a two pronged star produced by an incident pion. In order to avoid measuring all other two pronged stars, for instance, the very common π-p elastic scattering events, we require evidence of a possible Σ^- decay (a break in this track) (see Fig. 6). Both production and decay angles and momenta must be consistent with the kinematics.

6. – Contaminations in the propane data.

The selection criteria of the preceding section in principle select not only a well defined fraction (that fraction in which the particles decay within the chamber) of the free proton events, but in addition a certain fraction of bound proton events. The bound proton events are rejected only when the disturbance in the kinematical relationships due to the Fermi momentum in carbon exceeds the measurement error. In principle, if the measurement can be made arbitrarily precise, the rejection of carbon events can be made arbitrarily complete. We concern ourselves here with an empirical determination of the size of the remaining carbon contamination. Consider the three reactions in turn:

6·1. $\pi^- + p \to \Lambda^0 + \theta^0$. – In the case of this reaction we need worry about contamination only in the event that just one V particle is observed to decay in the chamber. In the event that both V's are seen the contribution of carbon and Σ^0-θ^0 which satisfy all kynematical relationships for Λ^0-θ^0 is negligible. These double events can now be used to estimate the contamination among the singles. The procedure used will be illustrated by using the data at 1300 MeV in the large chamber. (See Table II for details at all energies).

At this energy 57 doubles were observed. Of these, 15 had charged prongs emerging from the production vertex and were immediately classed as carbon events. In addition there were 44 events without prongs, of which 17 were classed as Λ^0-θ^0 events in hydrogen, 11 as Σ^0-θ^0 events in hydrogen and 16 as carbon events. This gives a total of 31 carbon doubles. For 29 of these carbon events we have measured the production angles and momenta of the Λ^0 and θ^0.

TABLE II. – *Determination of contamination in large propane chamber data for the reactions* $\pi^- + p \rightarrow {}^{\Lambda^0+\theta^0}_{\Sigma^0+\theta^0}$.

ENERGY	1300 MeV	1200 MeV	910 MeV
No. of Λ^0-θ^0 doubles	17	16	21
No. of Σ^0-θ^0 doubles	11	7	2
No. of carbon doubles without prongs	16	25	17
No. of carbon doubles with prongs	15	26	2
No. of single Λ^0's which fit Λ^0-θ^0	31	30	36
No. of single θ^0's which fit Λ^0-θ^0	7	20	12
No. of single θ^0's which fit Σ^0-θ^0	8	9	10
% of Λ^0's from sure carbon events which fall on Λ^0-θ^0 kinematics	22%	14%	21%
% of θ^0's from sure carbon events which fall on Λ^0-θ^0 kinematics	30%	25%	26%
% of Λ^0's from sure Σ^0-θ^0 on Λ^0-θ^0 kinematics	45% (combined)		—
% of θ^0 from sure Σ^0-θ^0 on Λ^0-θ^0 kinematics	18% (combined)		—
% of θ^0's from sure Λ^0-θ^0 on Σ^0-θ^0 kinematics	18% (combined)		—
% contamination of single Λ^0's from Λ^0-θ^0	33%	30%	15%
Corrected number of single Λ^0's from Λ^0-θ^0	20.8	21.0	30.8
% Contamination of single θ^0's from Λ^0-θ^0	13%	23%	17%
Corrected number of single θ^0's from Λ^0-θ^0	6.1	15.4	9.9
% contamination of all Λ^0-θ^0 events	20%	21%	11%
Corrected total of Λ^0-θ^0 events	43.9	52.4	61.7
% contamination of single θ^0's from Σ^0-θ^0	23%	44%	—
Corrected number of single θ^0's from Σ^0-θ^0	6.2	5.1	—
% contamination of all Σ^0-θ^0 events	10%	24%	—
Corrected total of Σ^0-θ^0 events	17.2	12.1	—

Consider the Λ^0 contamination first. A plot is made of p_Λ versus θ_Λ with each event represented as a rectangle whose width is equal to the error in θ_Λ and whose height is equal to the error in p_Λ (see Fig. 7). In addition to the Λ's from the double events above we plot 8 single Λ's whose carbon origin is manifest by a star at the production vertex. The kinematical curve for $\pi^- + p \to \Lambda^0 + \theta^0$ is also drawn. We find here that 22% of all sure carbon Λ^0's fall on the hydrogen kinematics. This means that 22% of the 16 sure carbon double events without prongs would have been classed as hydrogen events if the θ^0 had not been seen. In addition 5, of the sure Σ^0-θ^0 events would have been classed as Λ^0-θ^0 if the θ^0 had not been seen. Consequently the percentage contamination of the single Λ^0's is

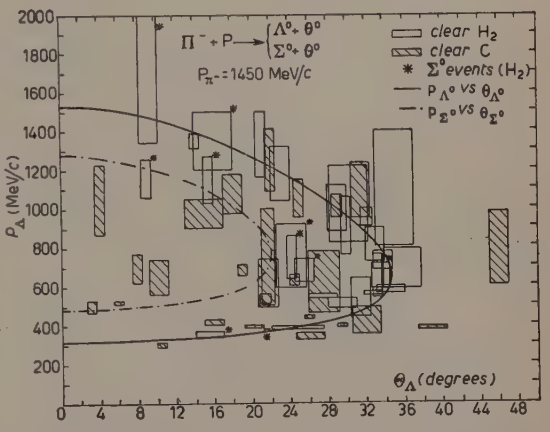

Fig. 7. – A plot of p_{Λ^0} versus θ_{Λ^0} for Λ^0's from hydrogen doubles and sure carbon events. Of the 37 sure carbon Λ^0's measured, 11 fell off scale on the above plot and are not shown. The limiting curve for Λ^0's from Σ^--θ^0 events falls very close to the Λ^0-θ^0 curve and is not shown.

$$\frac{(.22)(16)+5}{17+(.22)(16)+5}\cdot 100\% = 33\%\,.$$

The analysis of single θ^0 contamination proceeds along similar lines. Here we find that 3.6 carbon events and 2.0 Σ^0-θ^0 events would have been added to the 17 Λ-θ events if the Λ were not seen. However, 3 of the 17 Λ-θ events would have been interpreted as Σ-θ events if it were not for the Λ^0. Hence, for the purpose of estimating the total cross-section we have a percentage contamination among the single θ^0's of

$$\frac{2.6}{17+2.6}\cdot 100\% = 13\%\,.$$

A total of 55 hydrogen candidates were observed of which 17 were doubles, 31 single Λ^0's and 7 were single θ^0's. Of these $31\times.33 = 10.2$ single Λ^0's and $7\times.13 = 0.9$ single θ^0's must be subtracted leaving us with 43.9 events for the purpose of estimating the total cross section. The net contamination was $11.1/55\cdot 100\% = 20\%$.

Similar procedures were used at 910 MeV and 1 200 MeV yielding contaminations of 11% and 21% respectively.

6·2. *The reaction* $\pi^- + p \to \Sigma^0 + \theta^0$. – In the analysis of the propane pictures for this reaction we use only those events in which the θ^0 is seen to decay, as explained in Sect. 6. The contamination, arising in this case only from the data on the single θ^0's, is estimated in the same way as before to be 10% at 1300 MeV, and 24% at 1200 MeV. The difference between the two energies is a result of a statistical fluctation in the relative number of singles and doubles found.

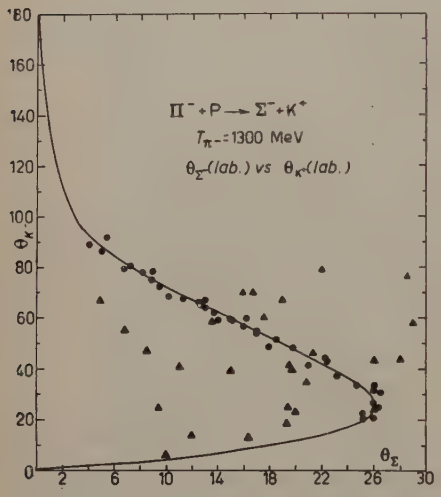

Fig. 8. – Plot for the angular correlation of all likely candidates for the reaction $\pi^- + p \to \Sigma^- + K^+$. Accepted events are indicated as circles and rejected events as triangles.

6·3. $\pi^- + p \to \Sigma^- + K^+$. – Here we estimate the contamination by plotting for all observed events the laboratory production angle of the Σ^- ($\theta_{\Sigma^-_{lab}}$) versus the laboratory production angle of the K^+ ($\theta_{K^+_{lab}}$). Ideally, the events which occur in hydrogen should fall on a curve corresponding to the known energy of the incoming π^- and those which occur in carbon should fall off the curve by an amount dependent on the Fermi momentum involved in the collision. A typical plot is shown in Fig. 8 (1300 MeV). For each event plotted, the shortest distance to the kinematical curve is measured. The distribution in these distances is plotted in Fig. 9. If the background is extended into the region of the peak, we find that 5.4 carbon events are likely to have angular correlations consistent with the hydrogen kinematics.

Now the 43 events which fell into this peak were further examined to determine if all other kinematical criteria are satisfied and 4 such events were rejected by this means. This leaves a net likely contamination of 1.4 events out of the 39 events finally used, or $3.5^{+5}_{-3.5}$%.

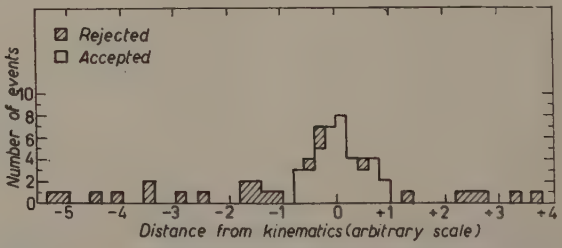

Fig. 9. – Plot of the shortest distance to the Σ^--K^+ angular correlation curve for all Σ^--K^+ candidates.

This result is also taken to hold at 1200 MeV since the kinematical problem is practically identical.

7. – « Contamination » in the hydrogen chamber data.

In the hydrogen chamber the only problem to be considered is the cross contamination between the Λ^0 and Σ^0 production reactions. At 950 MeV the kinematical separation between these two reactions is quite good. In Fig. 10 and 11 we have plotted the momentum versus production angle for all Λ^0's and all θ^0's respectively. In each case the curve corresponding to (Λ-θ) production at 950 MeV was drawn in. (The beam energy was subsequently determined to be 960 MeV from a study of the events themselves and is referred to as such everywhere else in this paper). In the Λ^0 case an additional curve was included which represented the closest that a Λ^0 from a Σ^0 decay could come to the Λ^0-θ^0 kinematics. In the θ^0 case the additional curve is that which correspond to $\Sigma^0 + \theta^0$ production. It can be seen that the separation in both cases is excellent so that one can neglect the cross contamination.

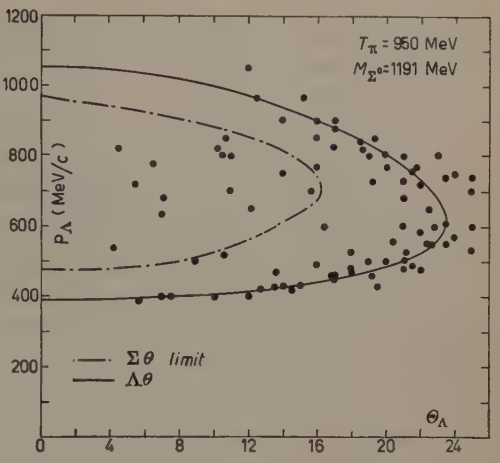

Fig. 10. – Momentum versus production angle, plotted for all Λ^0's seen in the hydrogen chamber at 960 MeV. The broken curve indicates the closest that a Λ^0 from a Σ^0-θ^0 event can get to the Λ^0-θ^0 curve.

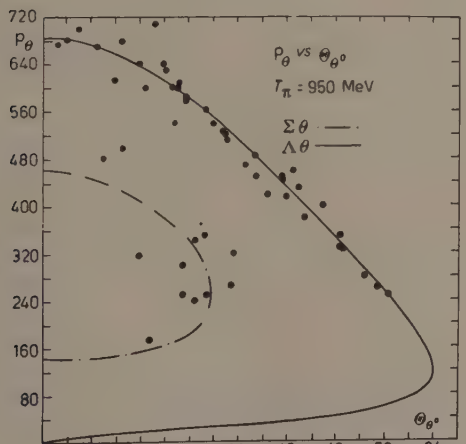

Fig. 11. – Momentum versus production angle, plotted for all θ^0's at 960 MeV in the hydrogen chamber.

8. – Results.

8·1. *Angular distributions.* – Before enumerating the results, it is necessary to discuss in some detail the geometrical corrections which must be applied to the measured angular distribution, to account for these events in

which the required strange particle decays occur outside the chamber. Since the chamber is large compared to the mean free path of Λ^0, θ^0, and Σ^-, these corrections will be small.

Consider first the case of the reaction $\pi^- + p \to \Sigma^- + K^+$. Since the Σ^- production angle in the laboratory is limited to a narrow cone ($\sim 30°$) and the incoming beam is well collimated, the Σ^- trajectory will leave the chamber through the cylindrical wall. Those leaving through the windows can be neglected. Again, because of the narrowness of the cone, the curvature of the chamber wall can be neglected in a calculation of the fraction which decay within the chamber. If the effective chamber length is L, the probability $P(\omega)$ that the Σ decay inside the chamber averaged over the distribution in points of production of the Σ^- in the chamber, is:

$$P(\omega) = 1 - \frac{\beta\gamma\tau}{L}\left(\exp\left[-L/\beta\gamma\tau\right] - 1\right),$$

where τ is the lifetime of the Σ^- and $\gamma = 1/\sqrt{1-\beta^2}$. In this, β is a function of the center of mass production angle ω. The angular distribution $d\sigma/d\Omega$ is then corrected by this amount:

$$\left(\frac{d(\omega)}{d\Omega}\right)_{corr} = \left(\frac{d\sigma}{d\Omega}\right)_{obs} \Big/ P(\omega).$$

For this calculation we have taken $L = 22$ cm and $\tau_{\Sigma^-} = 1.6 \cdot 10^{-10}$ s [8]

The situation is handled in essentially the same manner in the case of the reaction $\pi^- + p \to \Lambda^0 + \theta^0$. Here an event will be missed if neither of the two V's decays visibly in the chamber. Now both the Λ^0 and the θ^0 each have decay modes which are usually unobservable. In addition, they will occasionally leave the chamber before decaying by the usual, observable, modes. The differential (and total) cross-sections have to be corrected for both of these effects.

Let $P_{\Lambda^0}(\omega)$ and $P_{\theta^0}(\omega)$ be the respective probabilities that a Λ^0 or a θ_1^0 decay inside the chamber. These functions are evaluated just as in the case of the Σ^- (*).

---

[8] The lifetimes used here are preliminary values obtained from our data. The final values are at present being computed and will be published shortly.

(*) The assumption of production in a narrow cone is not valid for the θ. On the other hand, θ's produced at larger angles have small momenta. Since the incident beam passes only through a central region of the chamber, the particles always have a minimum distance of 3 cm to the windows. Since the maximum transverse momentum of θ^0 in these experiments is $\sim \frac{3}{4} m_\theta c$, the « transverse mean free path » is at most ~ 2.5 cm so that in the most unfavorable case no more than 30% could leave the chamber through the windows. The average transverse path before reaching the window is ~ 12 cm, corresponding to a negligible probability for loss through the window. We therefore make the same approximation also in the case of the θ^0.

If we now let W_{θ^0} and W_{Λ^0} be respectively the probabilities that a θ^0 decay into $\pi^- + \pi^+$ and a Λ^0 decay into $\pi^- + p$, then the probability that a Λ^0 or θ^0 or both decay inside the chamber is equal to

$$P_T = 1 - \{(1 - W_\Lambda P_\Lambda(\omega))(1 - W_\theta P_\theta(\omega))\}.$$

The angular distribution must be correspondingly corrected. We use $W_\Lambda = .65 \pm .05$ and $W_\theta = .42 \pm .07$ as previously reported [5], as well as $\tau_{\Lambda^0} = 2.4 \cdot 10^{-10}$ s, $\tau_{\theta^0} = 1.07 \cdot 10^{-10}$ s [8].

In the case of Σ^0-θ^0 production in the propane chamber only those events in which a θ^0 was observed were used. Therefore the probability that the θ^0 decay visibly inside the chamber is $W_\theta P_\theta(\omega)$. The value for $P_\theta(\omega)$ is computed just as before, but using the Σ^0-θ^0 kinematics.

The observed numbers of events as a function of production angle for the various reactions have been listed in Table III. Included in this tabulation

TABLE III. — *Tabulation of events for angular distribution of production.*

Energy (MeV)	910	960	1200	1300	910	960	1200	1300	960	1200	1300*
Reaction ($\pi^- + p \to$)	Λ^0-θ^0	Λ^0-θ^0	Λ^0-θ^0	Λ^0-θ^0	$\Sigma^- + K^+$	$\Sigma^- + K^+$	$\Sigma^- + K^+$	$\Sigma^- + K^+$	$\Sigma^0 + \theta^0$	$\Sigma^0 + \theta^0$	$\Sigma^0 + \theta^0$
Cos ω_Y											
−1.0 to − .9	10	13	14	19	0	2	0	4	0	1	4
− .9 to − .8	8	10	9	12	0	3	1	1	0	0	1
− .8 to − .7	4	9	7	7	1	2	0	1	2	1	1
− .7 to − .6	10	7	1	4	0	2	1	2	1	0	2
− .6 to − .5	0	4	4	6	0	3	1	2	1	1	1
− .5 to − .4	4	1	5	2	0	1	0	0	0	1	2
− .4 to − .3	4	3	6	8	0	3	0	2	0	0	1
− .3 to − .2	7	5	0	5	0	1	0	3	1	1	0
− .2 to − .1	1	2	0	2	1	2	0	0	0	1	0
− .1 to 0	0	4	2	2	1	2	1	1	0	1	0
0 to + .1	1	5	2	3	0	0	2	3	3	2	0
+ .1 to + .2	2	3	3	0	1	0	1	0	0	1	0
+ .2 to + .3	1	5	3	1	1	1	3	3	1	1	0
+ .3 to + .4	1	3	1	5	0	3	2	2	0	1	0
+ .4 to + .5	4	3	3	2	1	1	2	1	0	0	2
+ .5 to + .6	3	3	2	0	2	2	1	6	0	2	2
+ .6 to + .7	5	3	0	3	0	0	2	9	2	0	1
+ .7 to + .8	3	0	2	4	0	1	5	9	0	2	2
+ .8 to + .9	0	0	2	3	1	3	6	9	0	0	0
+ .9 to +1.0	0	0	0	2	0	1	4	5	1	0	0
Total	68	83	66	90	9	33	32	63	12	16	19

(*) Only large chamber used.

are also 9 examples of the reaction $\pi^- + p \to \Sigma^- + K^+$ at 910 MeV, just slightly above threshold where one would expect an isotropic distribution.

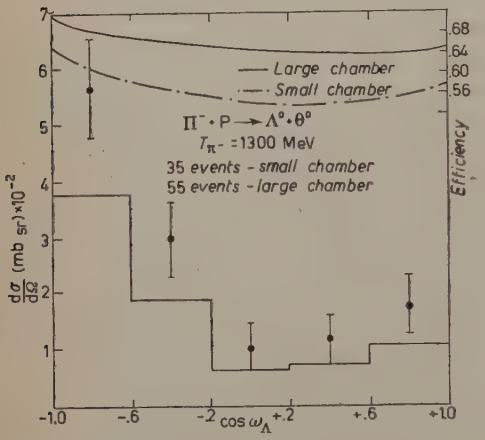

Fig. 12. – Differential cross section for $\pi^- + p \to \Lambda^0 + \theta^0$ at 1300 MeV.

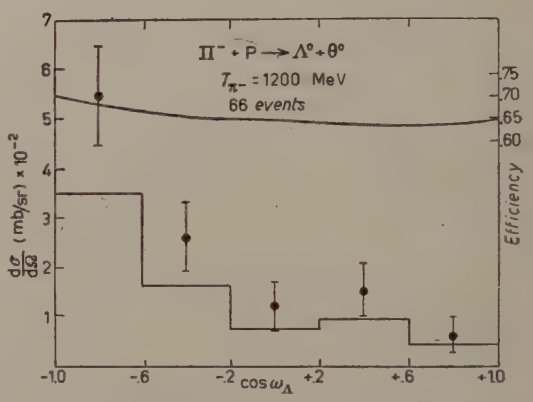

Fig. 13. – Differential cross section for $\pi^- + p \to \Lambda^0 + \theta^0$ at 1200 MeV.

The observed as well as the corrected differential cross-sections are plotted in Figs. 12-21. Also plotted is the detection efficiency as a function of angle.

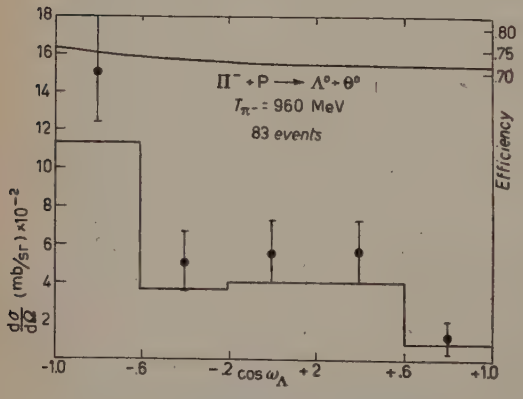

Fig. 14. – Differential cross section for $\pi^- + p \to \Lambda^0 + \theta^0$ at 960 MeV.

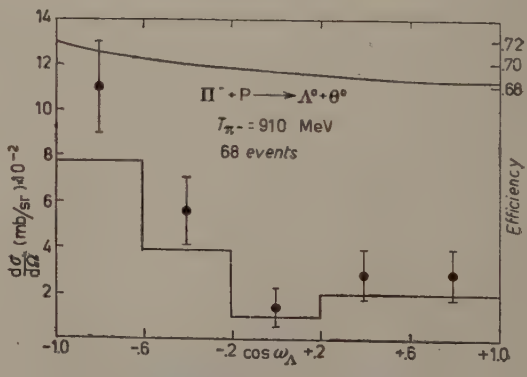

Fig. 15. – Differential cross section for $\pi^- + p \to \Lambda^0 + \theta^0$ at 910 MeV.

The errors on the corrected differential cross-sections are statistical. The scale is made to conform to the total cross-sections computed from a somewhat smaller sample of events chosen to minimize the possibility of systematic error. (See 8·2).

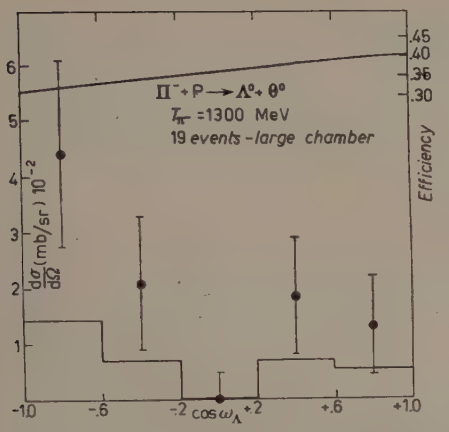

Fig. 16. – Differential cross section for $\pi^- + p \to \Sigma^0 + \theta^0$ at 1300 MeV.

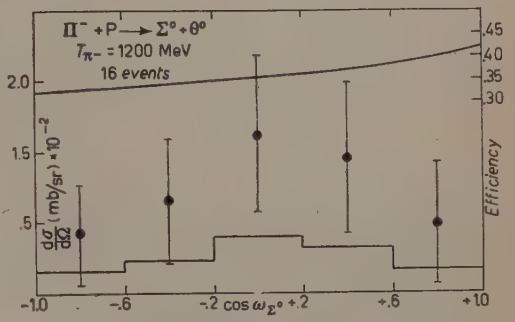

Fig. 17. – Differential cross section for $\pi^- + p \to \Sigma^0 + \theta^0$ at 1200 MeV.

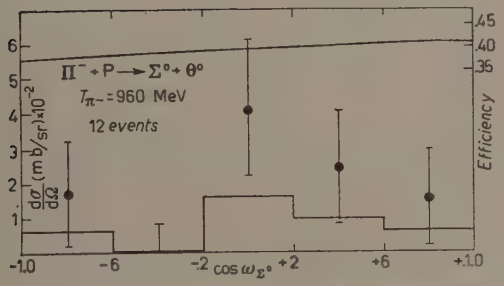

Fig. 18. – Differential cross section for $\pi^- + p \to \Sigma^0 + \theta^0$ at 960 MeV.

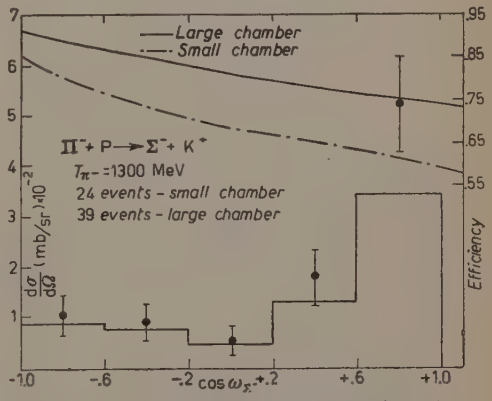

Fig. 19. – Differential cross section for $\pi^- + p \to \Sigma^- + K^+$ at 1300 MeV.

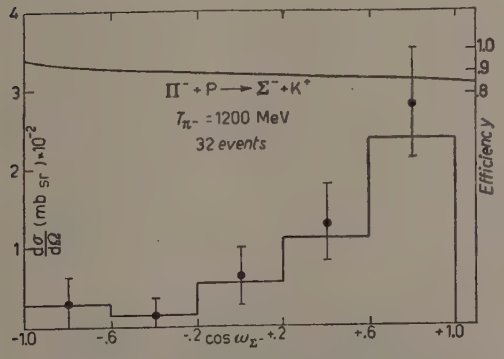

Fig. 20. – Differential cross section for $\pi^- + p \to \Sigma^- + K^+$ at 1200 MeV.

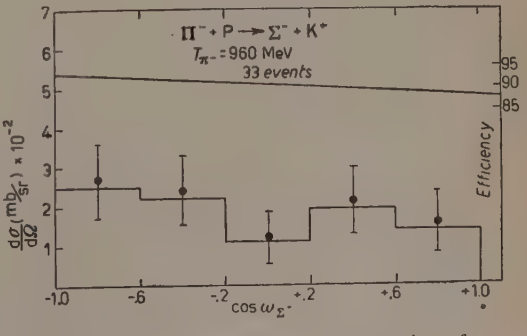

Fig. 21. – Differential cross section for $\pi^- + p \to \Sigma^- + K^+$ at 960 MeV.

8·2. *Total cross-sections.* – The preceding sections have explained how the event count for each reaction at each energy is corrected for geometrical inefficiency, normally unobservably decay modes and contamination. In computing the cross-sections the detailed procedures for estimating the incident pion flux differed somewhat from exposure to exposure although in all cases they had the following points in common.

1) A fiducial region was chosen in the chamber. Only those events in which the production point and one of the decay points fell inside the region were chosen and only that portion of the pion track length which fell inside the region was counted. For simplicity the region was always chosen to correspond to a certain prescribed plane figure in one of the projected views and consequently had a somewhat larger cross sectional area at the far side of the chamber than at the near side. All track counting was done on this view only.

2) Pictures of quality so poor as to offer some difficulty in finding the events were not used in computing the cross-sections. They were however used for the angular distributions inasmuch as the scanning bias introduced in favoring one angle of production as against another seemed to be small.

3) Tracks were not counted if their projected angle upon entering the fiducial region in the view on which the counting was done differed from the mean by more than $\sim 3°$.

4) In each case only a sample fraction of the film was flux counted and the average number of tracks per picture was multiplied by the total number of good pictures.

5) Those tracks which produced an interaction in the fiducial region were counted separately and their number was divided by two and added to the total number of non-interacting tracks.

The data from the small propane chamber were not used in computing total cross-sections. The procedures differed essentially only in the choice of fiducial region. At 960, 1200 and 1300 MeV the prescribed area on the view used to establish the fiducial region extended from the edge of the illuminated region on the incoming side of the chamber to 2 cm short of the edge of the illuminated region, in the beam direction, on the outgoing side of the chamber. At 910 MeV, the fiducial region was given by a trapezoid, 20 cm long in the beam direction, 15 cm wide at the beam entrance and 16 cm wide at the beam exit.

In computing the cross-sections, we used the values for muon and electron beam contamination measured by Cool, Piccioni and Clark [9]. Scanning

---

[9] R. Cool, O. Piccioni and D. Clark: *Phys. Rev.*, **103**, 1082 (1956).

efficiency was estimated by comparing the two independent scannings of the same film. In Table IV we have tabulated all of the relevent data needed to compute the cross-sections, as well as the final cross-sections themselves.

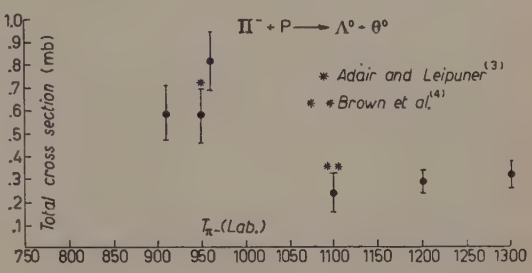

Fig. 22. – Plot of total cross section versus incident pion kinetic energy for the reaction $\pi^- + p \to \Lambda^0 + \theta^0$.

TABLE IV. – *Tabulation of data for computing total cross sections.*

Beam energy	910 MeV	960 MeV	1200 MeV	1300 MeV
A) $\pi^- + p \to \Lambda^0 + \theta^0$				
N	73.5±19%	59.4±15.3%	101.2±12.5%	81.94±15%
ϱ_l (g/cm²)	$2.04 \cdot 10^5 \pm$ 5%	$1.34 \cdot 10^5 \pm$ 5 %	$5.11 \cdot 10^5 \pm$10 %	$3.94 \cdot 10^5 \pm$ 5%
η	8%± 3%	7.5%± 3 %	5%± 4 %	7.5%± 3%
C	11%± 5%	—	21%± 8.4%	20%± 8%
E	98%± 3%	97%± 3 %	95%± 3 %	95%± 3%
σ (mb)	.59±.12 mb	.82±.13 mb	.29±.05 mb	.32±.06 mb
B) $\pi^- + p \to \Sigma^0 + \theta^0$				
N	—	17.5±41%	45±25 %	54.7±24 %
ϱ_l (g/cm²)	—	$1.34 \cdot 10^5 \pm$ 5%	$5.11 \cdot 10^5 \pm$10 %	$3.94 \cdot 10^5 \pm$ 5 %
η	—	7.5%± 3%	5%± 4 %	7.5%± 3 %
C	—	—	24.4%±15.7%	9.5%± 8.7%
E	—	97%± 3%	95%± 3 %	9.6%± 3 %
σ (mb)	—	.25±.10 mb	.12±.04 mb	.24±.06 mb
C) $\pi^- + p \to \Sigma^- + K^+$				
N	—	17.6±26%	37.4±18%	51.27±16%
ϱ_l (g/cm²)	—	$1.34 \cdot 10^5 \pm$ 5%	$5.11 \cdot 10^5 \pm$10%	$3.94 \cdot 10^5 \pm$ 5%
η	—	7.52± 3%	5%± 4%	7.5%± 3%
C	—	—	5%± 3%	5%± 3%
E	—	97%± 3%	95%± 3%	95%± 3%
σ (mb)	—	.25±.07 mb	.13±.03 mb	.23±.04 mb

N = number of events corrected for detection efficiency;
ϱ_l = track length in g/cm²;
η = percentage of muon-electron beam contamination;
C = percentage contamination of events;
E = scanning efficiency.

In Figs. 22-24 the total cross-sections as a function of pion laboratory energy for the three reactions are presented. The measurements of LEIPUNER and ADAIR ([3]), BROWN *et al.* ([4]), have been included.

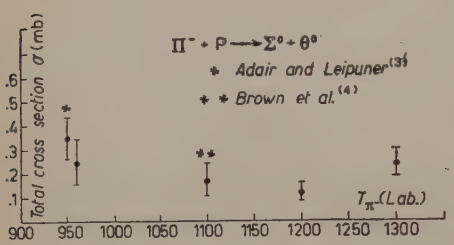

Fig. 23. – Plot of total cross section versus incident pion kinetic energy for the reaction $\pi^- + p \to \Sigma^0 + \theta^0$.

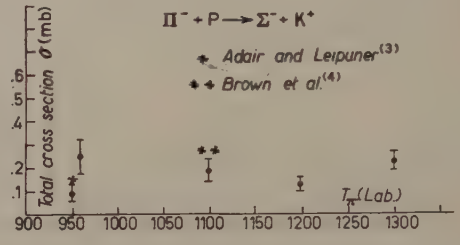

Fig. 24. – Plot of total cross section versus incident pion kinetic energy for the reaction $\pi^- + p \to \Sigma^- + K^+$.

9. – Discussion of results.

Before attempting to study the angular and energy dependence of the cross-sections, it is possible to make the following general remarks about the production processes observed.

1) It is possible to set some limit on the possible violation of the Gell-Mann, Nishijima scheme ([10,11]) in the production of strange particles.

Firstly, the reaction $\pi^- + p \to \Sigma^+ + K^-$, forbidden by the scheme, has not been observed to occur. This is to be compared to 113 examples of $\pi^- + p \to \Sigma^- + K^+$, observed in the magnetic chambers.

Secondly, no examples have been observed where two Λ^0's are produced in a carbon collision. This is to be compared to ~ 110 Λ^0-0 doubles in carbon.

2) It has been suggested ([12]) that the cross-sections for $\pi^- + p \to \frac{\Sigma^- + K^-}{\Sigma^0 + K^0}$ along with the cross-section for $\pi^+ + p \to \Sigma^+ + K^+$ can be used as a weak check on charge independence in strange particle producing reactions. In particular, charge independence implies that the three relations

$$a) \qquad \sqrt{2\sigma(\Sigma^0)} \leqslant \sqrt{\sigma(\Sigma^-)} + \sqrt{\sigma(\Sigma^+)},$$

$$b) \qquad \sqrt{\sigma(\Sigma^-)} \leqslant \sqrt{2\sigma(\Sigma^0)} + \sqrt{\sigma(\Sigma^+)},$$

$$c) \qquad \sqrt{\sigma(\Sigma^+)} \leqslant \sqrt{2\sigma(\Sigma^0)} + \sqrt{\sigma(\Sigma^-)},$$

([10]) M. GELL-MANN and A. PAIS: *Proc. of the Fifth Annual Rochester Conference on High Energy Physics* (New York, 1955).

([11]) T. NAKANO and K. NISHIJIMA: *Progr. Theor. Phys. Japan*, **10**, 581 (1953).

([12]) J. J. SAKURAI: *Phys. Rev.*, **107**, 908 (1957).

should hold for the differential cross-sections at any angle as well as for the total cross-section. The Michigan group ([13]) has found that a portion of its data at 1100 MeV seems to violate inequality (*a*). In addition, LEIPUNER and ADAIR ([3]) have found total π^- cross-sections at 950 MeV which when compared to a reasonable extrapolation of the 1100 MeV π^+ cross-section would indicate a violation of the same inequality. The latter result comes about because of a Σ^0 cross-section of $(.35 \pm .09)$ mb, a Σ^- cross-section of $(.09 \pm .04)$ mb and a Σ^+ cross-section of .15 mb. In the present experiment at 960 MeV we have found Σ^0 and Σ^- cross-sections consistent with charge independence $(\sigma(\Sigma^0) = .25 \pm .10)$ and $(\sigma(\Sigma^-) = .25 \pm .07)$. This discrepancy may perhaps be attributed in part to a reduction in the possibility of systematic error in the present experiment by the use of a larger chamber and magnetic field.

As far as the cross-sections themselves are concerned, increased statistical accuracy has borne out the early observations that Λ^0's tend to be produced backward and Σ^+'s tend to be produced forward in the center of mass. There is no significant indication in the present data about structure in the Σ^0 differential cross-section.

We have attempted to analyze the available $(900 \div 1000)$ MeV data on Λ^0-θ^0 production in terms of *s* and *p* waves in order to see to what extent limits can be placed on the relative sizes of the $s_{\frac{1}{2}}$, $p_{\frac{1}{2}}$ and $p_{\frac{3}{2}}$ amplitudes for the outgoing particles. Data from LEIPUNER and ADAIR ([3]) at 950 MeV and from the Berkeley bubble chamber group ([14,15]) at 990 MeV have also been included.

In addition to the differential cross-sections, we have used the measurements on the parity violating up-down asymmetry in the decay of the Λ^0 ([7,15]). Let the Λ^0's be produced with polarization *P* along the normal to the production plane in the sense of $P_{\pi^-{}_{\text{in}}} \cdot p_{\Lambda^0}$. Then the decay pions from the Λ^0 will be emitted with the distribution $1 + P\alpha \cos\theta$, where θ is the angle between the pion and the normal and $|\alpha| \leq 1$. This distribution yields information about the magnitude of *P*.

Now, if we take the $s_{\frac{1}{2}}$ amplitude $A_{s_{\frac{1}{2}}}$ to be real and positive, then we have 6 parameters which will completely describe the production and decay. These are $A_{s_{\frac{1}{2}}}$, Re $A_{p_{\frac{1}{2}}}$, Im $A_{p_{\frac{1}{2}}}$, Re $A_{p_{\frac{3}{2}}}$, Im $A_{p_{\frac{3}{2}}}$, and α. The angular distribution in the outgoing Λ^0 is of the form

$$\frac{\mathrm{d}\sigma}{\mathrm{d}\Omega} = |A_{s_{\frac{1}{2}}} + (2A_{p_{\frac{3}{2}}} + A_{p_{\frac{1}{2}}}) \cos\theta|^2 + \sin^2\theta \left| A_{p_{\frac{1}{2}}} - \frac{1}{\sqrt{2}} A_{p_{\frac{3}{2}}} \right|^2 .$$

([13]) L. BROWN, D. A. GLASER, D. I. MEYER, M. L. PERL and J. VAN DER VELDE: *Phys. Rev.*, **107**, 906 (1957).

([14]) F. S. CRAWFORD, M. CRESTI, M. L. GOOD, K. GOTTSTEIN, E. M. LYMAN, F. T. SOLMITZ, M. L. STEVENSON and H. K. TICHO: *Bull. Am. Phys. Soc.*, II, 3, no. 1 (1958).

([15]) F. S. CRAWFORD, M. CRESTI, M. L. GOOD, K. GOTTSTEIN, E. M. LYMAN, F. T. SOLMITZ, M. L. STEVENSON and H. K. TICHO: *Phys. Rev.*, **108**, 1102 (1957).

We can have however only 5 independent pieces of data—three from the angular distribution of production, and two from the asymmetry as a function of production angle. In carrying out the analysis, these were taken to be

$$(1) \qquad N(-1 \leqslant \cos\omega_\Lambda \leqslant -.3) = 257.9 \pm 17.0$$

$$(2) \qquad N(-.3 \leqslant \cos\omega_\Lambda \leqslant +.3) = 108.1 \pm 11.0$$

$$(3) \qquad N(+.3 \leqslant \cos\omega_\Lambda \leqslant 1) = 73.1 \pm 9.3$$

$$(4) \qquad \alpha P(-1 \leqslant \cos\omega_\Lambda \leqslant 0) = 0.52 \pm .11$$

$$(5) \qquad \alpha P(\ 0 \leqslant \cos\omega_\Lambda \leqslant 1) = 0.45 \pm .19$$

In the absence of an independent determination of α, solutions were found for the s and p wave amplitudes for various values of α and are listed in Table V.

TABLE V. – *Solutions for the* $s_{\frac{1}{2}}$, $p_{\frac{1}{2}}$ *and* $p_{\frac{3}{2}}$ *amplitudes for the reaction* $\pi^- + p \to \Lambda^0 + \theta^0$ *for several values of the decay parameter* α. *The data used are from the energy region* (900÷1000) MeV. *The total cross section is taken as* $0.6 \cdot 10^{-27}$ cm^2.

α	$A_{s_{\frac{1}{2}}}(\cdot 10^{-15}$ cm)	$A_{p_{\frac{3}{2}}}(\cdot 10^{-15}$ cm)	$A_{p_{\frac{1}{2}}}(\cdot 10^{-15}$ cm)
1	3.4	$-1.8-3.8i$	$-3.9-1.7i$
0.9	3.6	$-2.0-4.1i$	$-3.3-1.7i$
0.88	3.7	$-2.0-4.2i$	$-3.1-1.7i$

It was found that no solutions existed for $|\alpha| < \sim .78$. There is some indication in the MIT multiplate cloud chamber data ([16]) that the emitted protons are polarized opposite to their direction of motion, indicating that α is positive. Hence the solutions listed are for positive α. To obtain the solutions for negative α (and hence negative P) one need only change the signs of Im $A_{p_{\frac{1}{2}}}$ and Im $A_{p_{\frac{3}{2}}}$.

We have investigated the solutions to see to what extent the fractional contributions to the total cross section of the $s_{\frac{1}{2}}$, $p_{\frac{1}{2}}$ and $p_{\frac{3}{2}}$ states can vary and still fall within the experimental errors. In doing this we have taken the total number of events as fixed with no error. It is possible to obtain reasonable fits to the data with $.15 \leqslant f_{s_{\frac{1}{2}}} \leqslant .5$ where $f_{s_{\frac{1}{2}}}$ is the fractional contribution to the total cross-section due to the $s_{\frac{1}{2}}$ state. For various possible values of $f_{s_{\frac{1}{2}}}$ we have explored the possible range of $f_{p_{\frac{1}{2}}}/f_{p_{\frac{3}{2}}}$. These regions of fit are listed in Table VI. One thing which might be noted is that none of the possible outgoing states needs to be especially weak or especially strong to give a fit to the data.

([16]) E. BOLDT, H. BRIDGE, D. O. CALDWELL and YASH PAL: *Bull. Am. Phys. Soc.*, II, **3**, 163 (1958).

TABLE VI. – *Range of solutions for* $f_{p_{\frac{1}{2}}}/f_{p_{\frac{3}{2}}}$ *for various values of* $f_{s_{\frac{1}{2}}}$. *f is the fractional contribution to the total cross section made by a particular state. Reasonable agreement with the data can be obtained for* $.15 \leqslant f_{s_{\frac{1}{2}}} \leqslant .5$.

$f_{s_{\frac{1}{2}}}$	$(f_{p_{\frac{1}{2}}}/f_{p_{\frac{3}{2}}})_{\min}$	$(f_{p_{\frac{1}{2}}}/f_{p_{\frac{3}{2}}})_{\max}$
.15	.92	.92
.165	.48	2.3
.225	.25	3.8
.39	.57	2.6
.45	.76	1.9

A similar type of analysis on the Σ^--K^+ data has not been carried out because nothing is known about the polarization of the Σ^- in production. No significant up-down asymmetry has been observed in the Σ^- decay ([7,15]).

* * *

We would like to acknowledge our indebtedness to the many colleagues who have helped us in this work.

We wish to thank Drs. R. ADAIR, R. GARWIN, D. GLASER, and R. SHUTT for many helpful discussions during the development of the chambers, and Messrs. J. WOODS and E. HOYLE for much of the machine shop work involved in the construction of the chamber and magnet.

In addition we would like to thank Drs. W. MORRE, G. COLLINS, L. LEIPUNER, Messrs. E. DEXTER and A. SCHLAFKE and all of the other members of the Cosmotron Staff for their help in obtaining the exposures. Many thanks go to Dr. D. TYCKO and to the I. B. M. Watson Laboratory for making the computation possible and to Mrs. D. GOURSKY for her patient work in scanning the film.

Finally we wish to acknowledge the help of Drs. R. BUDDE, M. CHRETIEN and J. LEITNER who collaborated with us in the early phases of this experiment.

RIASSUNTO

Sono presentati i risultati sulle sezioni d'urto totali e differenziale nelle reazioni $\pi^- + p \to \begin{matrix}\Lambda^0 + 0' \\ \Sigma^0 + 0' \\ \Sigma^- + K^-\end{matrix}$ a 910, 960, 1200 e 1300 MeV, ottenuti usando camere a bolle ad idrogeno ed a propano in un campo magnetico di 13.4 kG. Viene fatta una descrizione dettagliata sia delle camere e del loro funzionamento che del metodo di analisi.

IL NUOVO CIMENTO Vol. X, N. 3 1° Novembre 1958

Evaluation of γ_0' from the Angular Distribution of Jet Particles in LS Using certain Suppositions about their Angular Distribution in the CMS.

V. Petržílka

Physical Institute of the Czechoslovak Academy of Sciences
Faculty of Technical and Nuclear Physics of the Charles University - Praha

(ricevuto il 25 Luglio 1958)

Summary. — In this paper is made an attempt for finding the procedure for the evaluation of γ_0' using for the integral angular distribution of shower particles in a jet three different suppositions. The derived expressions for the evaluation of γ_0' in these three cases are proved on eight jets with γ_0' from 1 to 300.

For the determination of the energy of the primary particle in a nucleon-nucleon collision, in which secondary particles are produced, some authors have used the method of the median angle, others tried to correlate the angles containing the percentages of F and $(1 - F)$ of the total numbers of particles, whereas C. C. Dilworth *et al.* [1] on one hand and C. Castagnoli *et al.* [2] on the other hand developed methods using for the determination of γ_0' the angle measurements of shower particles in a jet.

In our case there is made an attempt for finding the procedure for the evaluation of γ_0' by using for the integral angular distribution of shower par-

[1] C. C. Dilworth, S. J. Goldsack, T. F. Hoang and L. Scarsi: *Nuovo Cimento*, **10**, 1261 (1953).

[2] C. Castagnoli, G. Cortini, C. Franzinetti, A. Manfredini and D. Moreno: *Nuovo Cimento*, **10**, 1539 (1953).

ticles in a jet an expression $F_i(u)$, giving its theoretical dependence on $u = \gamma_0' \Theta$ or $u = \sqrt{\gamma_0'^2 - 1} \sin \Theta$, where $\gamma_0' = (1 - \beta_0'^2)^{-\frac{1}{2}}$ represents the primary energy of one nucleon in rest mass units and Θ the angle of emission of a shower particle, with respect to the primary observed in L.S.

In Fig. 1, as an example only, two distributions $F_2(u)$ and $F_3(u)$ given by L. VON LINDERN [3] are plotted as a function of u. In the same figure for the jet $(0+14)\alpha$ (Nr. 8 in the Table I) the histogram H_1, beginning at the angle Θ_1 and ending at the angle Θ_{13}, and the histogram H_2 from Θ_{13} to Θ_1 for 13 shower particles are drawn, supposing the value of $\gamma_0' = 309$ to be known.

The areas of P_{H_1} and P_{H_2} formed by the histograms H_1 and H_2 can be calculated from the expressions

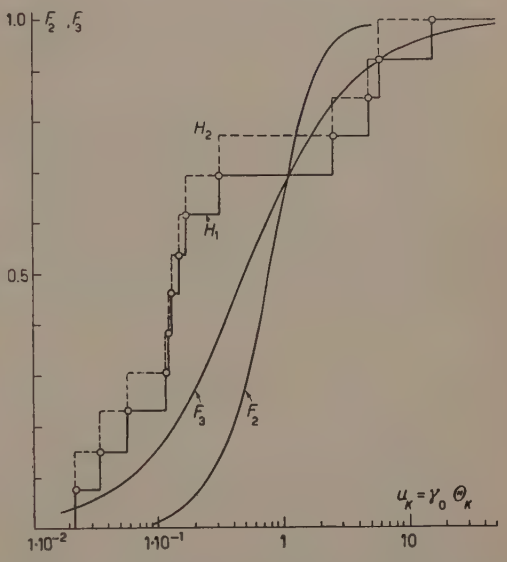

Fig. 1. – Histograms H_1 and H_2 for the jet Nr. 8 from the Table I. The functions F_2 and F_3 are represented by equations (10) and (11).

$$(1)\quad P_{H_1} = \gamma_0' \sum_{k=1}^{n_s-1} y_k(\Theta_{k+1} - \Theta_k) \quad \text{or} \quad P_{H_1} = \sqrt{\gamma_0'^2 - 1} \sum_{k=1}^{n_s-1} y_k(\sin\Theta_{k+1} - \sin\Theta_k)\,,$$

$$(2)\quad P_{H_2} = \gamma_0' \sum_{k=1}^{n_s-1} y_{k+1}(\Theta_{k+1} - \Theta_k) \quad \text{or} \quad P_{H_2} = \sqrt{\gamma_0'^2 - 1} \sum_{k=1}^{n_s-1} y_{k+1}(\sin\Theta_{k+1} - \sin\Theta_k)\,,$$

where n_s denotes the number of shower particles, $u_k = \gamma_0' \Theta_k$ or $u_k = \sqrt{\gamma_0'^2 - 1} \sin\Theta_k$ the value of u corresponding to the track of the k-th shower particle in the jet and $y_k = ky_1$ is the k-th value of the co-ordinate corresponding to Θ_k. Then the mean value of both these surfaces is equal to

$$(3)\quad P_M = \frac{1}{2}(P_{H_1} + P_{H_2}) = \gamma_0' S_1 \qquad \text{or} \qquad P_M = \frac{1}{2}(P_{H_1} + P_{H_2}) = \sqrt{\gamma_0'^2 - 1}\, S_2\,,$$

if we denote by S_1 and S_2 the expressions

$$(4)\qquad S_1 = \frac{1}{2}\sum_{k=1}^{n_s-1} y_k(\Theta_{k+1} - \Theta_k) + \frac{1}{2}\sum_{k=1}^{n_s-1} y_{k+1}(\Theta_{k+1} - \Theta_k)\,,$$

---

[3] L. v. LINDERN: *Nuovo Cimento*, **5**, 491 (1957).

or

$$S_2 = \frac{1}{2}\sum_{k=1}^{n_s-1} y_k(\sin\Theta_{k+1} - \sin\Theta_k) + \frac{1}{2}\sum_{k=1}^{n_s-1} y_{k+1}(\sin\Theta_{k+1} - \sin\Theta_k)\,. \tag{5}$$

The surface P_T formed by the theoretical curve $F_i(u)$ is given by the expression

$$P_T = \int_{u_1}^{u_{n_s}} F_i(u)\,\mathrm{d}u\,. \tag{6}$$

If we apply the claim of the equality of the mean surface P_M and the theoretical surface P_T, we obtain the relation

$$P_M = \frac{1}{2}(P_{H_1} + P_{H_2}) = \int_{u_1}^{u_{n_s}} F_i(u)\,\mathrm{d}u = P_T\,, \tag{7}$$

from which we can determine the value of γ_0', supposing the theoretical function for $F_i(u)$ is given.

Using for $F_i(u)$ the relations given by K. SYMANZIK [4] and L. VON LINDERN [3] on the basis of Heisenberg's theory [5], we obtain for the evaluation of γ_0' three equations in the following way.

For the isotropic emission of shower particles in the CMS and under the assumption $\beta_k'/\beta_0' = 1$, where β_k' is the velocity of one shower particle in the CMS, we can obtain according to L. VON LINDERN for the integral distribution of $F_i(u)$ the expression ([4], p. 495):

$$F_1 = \frac{\gamma_0'^2 \sin^2\Theta}{1 + (\gamma_0'^2 - 1)\sin^2\Theta} = \frac{\gamma_0'^2}{\gamma_0'^2 - 1}\,\frac{u^2}{1+u^2}\,, \tag{8}$$

if we put $u = \sqrt{\gamma_0'^2 - 1}\,\sin\Theta$.

For higher values of the primary energy, *i.e.* for higher values of γ_0' it is possible to use for F_1 the approximated relation

$$F_1 = \frac{u^2}{1+u^2}\,, \tag{9}$$

where $\mu = \gamma_0'\Theta$.

---

[4] K. SYMANZIK, in W. HEISENBERG: *Kosmische Strahlung* (Berlin-Göttingen-Heidelberg, 1953), Anhang VII*a*, p. 563.

[5] W. HEISENBERG: *Zeits. f. Phys.*, **133**, 65 (1952); *Kosmische Strahlung* (Berlin-Göttingen-Heidelberg, 1953).

For the isotropic emission of shower particles and in the case of Heisenberg spectrum ([5,3]) L. VON LINDERN gives for $F_i(u)$ the formula ([4], p. 496)).

$$F_2 = 1 - \frac{1}{(1+u^2)^{\frac{3}{2}}}, \tag{10}$$

in which for u either the relation $u = \sqrt{\gamma_0'^2 - 1}\sin\Theta$ or $u = \gamma_0'\Theta$ is to be used, with respect to the value of γ_0'.

For a strong anisotropic emission in the CMS and in the case of Heisenberg spectrum it is possible to use according to K. SYMANZIK ([4]) and L. v. LINDERN ([4], p. 496) for $F_i(u)$ the expression

$$F_3 = 1 - \frac{1}{1+2u} = \frac{2u}{1+2u}, \tag{11}$$

which should be valid for $\gamma_0' > 20$ with $u \doteq \gamma_0'\Theta$.

Hence using for $F_i(u)$ the expression (8) for F_1, we get from (7), (3) and (5)

$$\sqrt{\gamma_0'^2-1}\,S_2 = \frac{\gamma_0'^2}{\gamma_0'^2-1}\cdot \tag{12}$$
$$\cdot\left\{\sqrt{\gamma_0'^2-1}\,(\sin\Theta_{n_s} - \sin\Theta_1) - \operatorname{arctg}\left(\sqrt{\gamma_0'^2-1}\sin\Theta_{n_s}\right) + \operatorname{arctg}\left(\sqrt{\gamma_0'^2-1}\sin\Theta_1\right)\right\},$$

which for higher values of γ_0' can be written in accordance with the expressions (9), (7), (3) and (4) in the form

$$(\Theta_{n_s} - \Theta) - S_1 = \frac{1}{\gamma_0'}\left\{\operatorname{arctg}(\gamma_0'\Theta_{n_s}) - \operatorname{arctg}(\gamma_0'\Theta_1)\right\}. \tag{13}$$

The left hand side of the equation (13) being constant, we can put different expected values for γ_0' into the right hand side of this equation and in this way find the value of γ_0' satisfying this equation. In the case of the equation (12) we have to perform this procedure on both sides.

In a similar way we obtain for F_2 given by the expression (10) from the equation (7) the equation

$$(\Theta_{n_s} - \Theta_1) - S_2 = \left\{\frac{\sin\Theta_{n_s}}{\sqrt{1+(\gamma_0'^2-1)\sin^2\Theta_{n_s}}} - \frac{\sin\Theta_1}{\sqrt{1+(\gamma_0'^2-1)\sin^2\Theta_1}}\right\}, \tag{14}$$

or for higher energies the equation

$$(\Theta_{n_s} - \Theta_1) - S_1 = \left\{\frac{\Theta_{n_s}}{\sqrt{1+\gamma_0'^2\Theta_{n_s}^2}} - \frac{\Theta_1}{\sqrt{1+\gamma_0'^2\Theta_1^2}}\right\}. \tag{15}$$

The last representation of $F_i(u)$ by the expression (11) gives for the evaluation of γ_0' with respect to (7), (3) and (4) the equation

$$(16) \qquad (\Theta_{n_s} - \Theta_1) - S_1 = \frac{1}{2\gamma_0'} \left[\ln \frac{1 + 2\gamma_0' \Theta_{n_s}}{1 + 2\gamma_0' \Theta_1} \right].$$

It is possible to use for $F_i(u)$ in the equation (7) also other integral angular distributions of shower particles in a jet, for example the distribution given recently by D. ČERNAVSKIJ ([6]) in his preprint.

In the described way the value of γ_0' was determined for 8 jets using the formulas (12), (14) and (16) and the obtained results are given in the following Table I.

TABLE I.

Jet Nr.	Denotation of the jet	Character of the jet	γ_0' calculated from the formula: $\gamma_0' = 1/(\mathrm{tg}\,\Theta)_{\frac{1}{2}}$	γ_0' calculated from the formula of Castagnoli *et al.* ([2])	γ_0' calculated from the formula (12)	γ_0' calculated from the formula (14)	γ_0' calculated from the formula (16)
1	P 4	(4+17) p	1.52	3.79	1.63	1.56	—
2	P 17	(4+ 6) p	5.16	5.21	6.68	5.09	—
3	P 1	(4+37) p	10.94	12.72	7.57	5.63	—
4	P 53	(1+19) α	20.6	15.2	15.4	10.6	—
5	P 27	(0+17) p	73.8	46.4	27.9	18.7	33.4
6	P 38	(5+10) p	88.5	103.9	—	80.0	116.6
7	P 26	(5+ 9) p	170.5	149.9	—	79.9	120.1
8	P 115	(0+14) α	2220.0	926.0	—	181.0	309.0

The values of γ_0' calculated from the equation (12) do not show in the region from $\gamma_0' \cong 1$ to $\gamma_0' \cong 15$ a disagreement with the values calculated by using the formula of CASTAGNOLI *et al.* ([2]); two of them are higher, two of them lower than the values calculated from Castagnoli's formula.

For higher energies there is possible to see that the values of γ_0' calculated from the equations (12), (14) or (16) are always lower than the values, which gives Castagnoli's formula in a first approximation, what can be considered as a reasonable result.

The value $\gamma_0' = 309$ for the jet Nr. 8 is in a satisfactory agreement with

---

([6]) D. ČERNAVSKIJ: *O množestvennom obrazovanii častic pri vysokych energijach*. Fizčeskij Institut im. Lebeděva ANSSSR. Preprint.

the value $\gamma_0' = 420$ obtained by P. Ciok *et al.* ([7,8]) using the $F/(1-F)$ plot against tg Θ.

From these eight examples there is not possible to draw any definite conclusion. A greater experimental material, *i.e.* a greater number of jets would be necessary to prove the usefulness of the described procedure; the evaluation of the error in each case is also desirable. Nevertheless the described way for the evaluation of γ_0' gives the further possibility for its determination.

* * *

I am indebted to thank Dr. J. Pernegr for the experimental data of jets.

(7) P. Ciok, M. Danysz, J. Gierula, A. Jurak, M. Mięsowicz, J. Pernegr, J. Vrána and W. Wolter: *Nuovo Cimento*, **6**, 1409 (1957).

(8) J. Pernegr, V. Petržílka and J. Vrána: *Czechosl. Journ. Phys.*, **8**, 137 (1958).

RIASSUNTO (*)

Nel presente lavoro si fa un tentativo di trovare il procedimento per la valutazione del γ_0' partendo da tre differenti supposizioni per la distribuzione angolare integrale delle particelle di uno sciame in un jet. Le espressioni derivate per la valutazione del γ_0' in questi tre casi si dimostrano esatte in otto jets con γ_0' da 1 a 300.

(*) *Traduzione a cura della Redazione.*

IL NUOVO CIMENTO Vol. X, N. 3 1° Novembre 1958

Gauge Invariance in the Theory of Superconductivity.

D. Pines (*) and J. R. Schrieffer (+)

Laboratoire de Physique, Ecole Normale Supérieure - Paris

(ricevuto il 26 Luglio 1958)

Summary. — It is shown that when due account is taken of the Coulomb interactions between electrons, a theory of superconductivity which gives a satisfactory account of the Meissner effect in the London gauge can be extended to give a satisfactory account in any other gauge. Calculations based on the Bardeen-Pines collective treatment of the electron-phonon system show that in the long wave length region ($k \lesssim k_c \cong r_s^{-1}$ where r_s is the interelectronic spacing) only the plasmons respond to a longitudinal vector potential. Their response is such as to maintain gauge invariance. The individual electrons are surrounded with a screening cloud of virtual plasmons in such a way that they carry no longitudinal current to order (k^2/k_c^2), and are hence unaffected by a longitudinal vector potential to this order. The introduction of the screening cloud is shown to correspond closely to the backflow introduced by Feynman and Cohen to guarantee longitudinal current conservation for the excitations in liquid helium. The calculations are carried out to order m/M and k^4/k_c^4, and involve the use of the random phase approximation for terms which couple plasmons and electrons. For the wave lengths of importance in the Meissner effect ($k \ll k_c$), these approximations are well-justified. An explicit prescription is given for extending the Bardeen, Cooper and Schrieffer derivation of the Meissner effect to an arbitrary gauge, and their results are shown to be essentially unaltered.

(*) National Science Foundation Senior Post-Doctoral Fellow, on leave of absence from Princeton University, 1957-58. Present address: Institute for Advanced Study, Princeton, N.J.

(+) National Science Foundation Post-Doctoral Fellow, on leave of absence from Institute for the Study of Metals and the Department of Physics, University of Chicago, Chicago, Ill., 1957-58.

1. – In order to establish a satisfactory theory of the Meissner effect in a superconductor, one must show that for any choice of gauge,

a) the transverse components of the Fourier transforms of the current density and the vector potential are related by

$$\boldsymbol{J}_{\perp}(\boldsymbol{q}) = -\alpha(q^2)\boldsymbol{A}_{\perp}(\boldsymbol{q}) , \tag{1}$$

where $\alpha(q^2) > 0$ as $q^2 \to 0$, and

b) the longitudinal current vanishes for time independent fields

$$\boldsymbol{J}_{\parallel}(\boldsymbol{q}) = 0 . \tag{2}$$

Considerations regarding the Meissner effect are generally carried out in the London gauge for which $\operatorname{div} \boldsymbol{A} = 0$ and the component of $\boldsymbol{A}$ perpendicular to the surface of the specimen vanishes. In this gauge (2) is automatically satisfied. It is the purpose of this paper to show that when due account is taken of the Coulomb interactions between electrons, a theory which gives a satisfactory account of the Meissner effect in the London gauge can be easily extended to give a satisfactory account in any gauge.

BARDEEN, COOPER, and SCHRIEFFER [1] have recently proposed a theory of the Meissner effect in the London gauge. Their derivation of the Meissner effect has been criticized because a straightforward application of their technique does not lead to gauge invariant results. This difficulty arises because the continuity equation is not satisfied by their states, a fact which is closely connected with the objection raised by BUCKINGHAM [2] to the earlier energy gap model of Bardeen. We give an explicit prescription for extending the BCS derivation of the Meissner effect to an arbitrary gauge, and show that their results are essentially unaltered.

Our approach takes advantage of the special simplicity introduced in the gauge problem by the Coulomb interactions between electrons. As a result of the Coulomb interaction, the dominant long wave length longitudinal excitations of the electron gas are the plasmons of frequency near ω_p, a property which any consistent theory must possess. In the collective description of BOHM and PINES [3], the plasmons are initially described by a set of co-ordinates and momenta (Q_k, π_k) representing a field of frequency ω_p. These plasmons are simply the quantized oscillations appropriate to the longitudinal

---

[1] J. BARDEEN, L. COOPER and J. R. SCHRIEFFER: *Phys. Rev.*, **108**, 1175 (1957), hereafter referred to as BCS.

[2] M. J. BUCKINGHAM: *Nuovo Cimento*, **5**, 1763 (1957).

[3] D. BOHM and D. PINES: *Phys. Rev.*, **92**, 609 (1953), hereafter referred to as BP.

vector potential and electric field. There is, furthermore, a coupling between the plasmons and the single particles, the strength of which is the ratio of the characteristic frequencies for individual particle and plasmon excitation. The coupling constant for a plasmon of wave vector k and a particle of momentum p is given by

$$g_k^2 = \frac{\omega_{n0}^2}{\omega_p^2}(\boldsymbol{p} \to \boldsymbol{p} + \boldsymbol{k}) = \frac{[(\boldsymbol{k}\cdot\boldsymbol{p}/m) + (k^2/2m)]^2}{\omega_p^2}, \tag{3}$$

and is very weak for long wave lengths ($k \ll r_s^{-1}$, if r_s is the interparticle spacing). However, this interaction plays the essential role of suppressing long wave length electron excitations and to obtain a consistent treatment it must be taken into account.

The BP collective description is well suited to our present purposes because in it a change in gauge corresponds to a simple displacement of the co-ordinates, Q_k. It is possible by means of a simple canonical transformation to decouple the plasmons from the electrons to order

$$g^2 = \langle g_k^2 \rangle_{\text{Av}} \cong \frac{1}{5}\frac{k^2 v_0^2}{\omega_p^2}, \tag{4}$$

where v_0 is the velocity of an electron at the Fermi surface and the average is carried out over all electronic momenta. This transformation guarantees the gauge invariance of the system properties to order g^4. Hence if one has, in the London gauge (as do BCS)

$$\lim_{q\to 0} \boldsymbol{J}_\perp(q) = -\frac{ne^2}{mc}\boldsymbol{A}_\perp(q), \tag{5}$$

by proper inclusion of plasmons and a simple canonical transformation one finds in any other gauge, at worst,

$$\lim_{q\to 0} \boldsymbol{J}_\perp(q) = -\frac{ne^2}{mc}(1 + g_q^4)\boldsymbol{A}_\perp(q), \tag{6a}$$

$$\lim_{q\to 0} \boldsymbol{J}_\parallel(q) = -\frac{ne^2}{mc} g_q^4 \boldsymbol{A}_\parallel(q). \tag{6b}$$

Since $g_q^2 \ll 1$ for the long wave lengths of importance in the Meissner effect, the Meissner effect is thereby established in an arbitrary gauge in essentially unaltered form.

The results (6a) and (6b) are based on the neglect of terms of order m/M and the assumption that the BP random phase approximation (RPA) may be applied to terms giving rise to electron plasmon interaction. The validity

of this approximation for the normal state has recently been discussed in some detail by NOZIÈRES and one of us (4); it is shown be valid for wave lengths such that $k \lesssim k_c = 0.47 r_s^{\frac{1}{2}}$. In the superconducting state, the RPA may be expected to be equally valid for terms involving plasmons explicitly, since these are but slightly altered on the transition from the normal to the superconducting state.

Our resolution of the difficulties with a gauge transformation represents a formal realization of the proposal made by BARDEEN (5) in response to the Buckingham objections. It is in some ways similar to the recent work of ANDERSON (6). Our approach is also closely related to a recent proposal of FEYNMAN (7) to the effect that a gauge invariant theory must include a « back-flow » around each electron as it moves through the metal. This « back-flow » is nothing but the plasmon cloud carried by each electron in consequence of the electron-plasmon interaction. The proof of the equivalence follows along the lines of a proof given earlier by one of us (8) in a discussion of the roton energy spectrum in liquid helium. We find that for long wave lengths, the longitudinal current carried by an electron plus its associated back-flow vanishes and therefore only the plasmons are coupled to the gauge potential. Since the plasmons satisfy the continuity equation to order g^4, we find a gauge invariant expression for the current density to this order, consistent with the arguments given above.

In Sect. 2 we give the formal justification of the above remarks. In Sect. 3 we discuss briefly certain remaining problems in the theory of superconductivity.

2. – A generalization of the BP formulation to the problem of interacting electrons, phonons, and plasmons has been carried out by BARDEEN and one of the authors (9). The Hamiltonian which describes the interaction of this system with an external vector potential may be represented schematically as

$$H = H_{\mathrm{el}} + H_{\mathrm{pl}} + H_{\mathrm{int}} - \frac{1}{c}\sum_q \tilde{\boldsymbol{j}}(q)\cdot\boldsymbol{A}(-q) + H_{\mathrm{ph}} + H_{\mathrm{el\text{-}ph}} + H_{\mathrm{sr}}\,, \tag{7}$$

(4) P. NOZIÈRES and D. PINES: *Phys. Rev.* (to appear in July 15th, 1958 issue).

(5) J. BARDEEN: *Nuovo Cimento*, **5**, 1766 (1957).

(6) P. W. ANDERSON: *Phys. Rev.*, **110**, 827 (1958).

(7) R. P. FEYNMAN: Discussion at *International Conference on Low Temperature Physics* (Leiden, 1958) and private communication.

(8) D. PINES: Discussion at the *International Congress on Theoretical Physics* (Seattle, 1956) and *Proc. of Stevens Institute, Conference on the Many-Body Problem* (Hoboken, N.J., 1957), to be published.

(9) J. BARDEEN and D. PINES: *Phys. Rev.*, **99**, 1140 (1955), hereafter referred to as I. We adopt the notation of I with the exception that we use Hermitian plasmon variables π_k, Q_k instead of the anti-Hermitian P_k, Q_k used there.

if terms of order (m/M) are neglected and if one makes the RPA for terms involving the interaction between plasmons and electrons. The first three terms describe the one electron energies, a collection of plasmons of frequency ω_p, and a linear coupling between electrons and plasmons. The fourth term describes the coupling to an external vector potential and the remaining terms describe the phonon field, its coupling to the electrons, and the short range part of the Coulomb interaction between the electrons. In this representation the current density contains both an individual electron and a plasmon part, and is

$$\tilde{\boldsymbol{j}}(q) = -\frac{e}{m}\sum_i \left(\boldsymbol{p}_i + \frac{\hbar \boldsymbol{q}}{2}\right) \exp\left[-i\boldsymbol{q}\cdot\boldsymbol{x}_i\right] - \frac{nei}{m}\sqrt{\frac{4\pi e^2}{q^2}}\,\boldsymbol{q}Q_q = \boldsymbol{j}(q) + \boldsymbol{j}_{\mathrm{pl}}(q)\,. \tag{8}$$

The plasmon contribution vanishes for $q > k_c$, the maximum wave-vector for which it is advantageous to introduce plasmons.

Because the plasmons are described explicitly by an auxiliary field in I, the system is over-described; in general one has to impose a subsidiary condition relating the electron, phonon and plasmon variables, corresponding to the fact that plasmons are composed of electrons and phonons. The subsidiary condition takes the form:

$$\left(\pi_k + \sqrt{\frac{4\pi e^2}{k^2}}\,\varrho_{-k} + u_k q_{-k}\right)\Psi = 0\,, \qquad (k < k_c)\,, \tag{9}$$

where q_k is the phonon co-ordinate and u_k gives the admixture of phonons in a plasmon of momentum π_k. The usefulness of the foregoing approach stems from fact that for the ground state and low-lying excited states which do not involve the simultaneous excitation of many electrons, the subsidiary conditions may be neglected ([10]).

The essential role that plasmons play in gauge invariance is brought out by the fact that a long wave length gauge transformation is equivalent to a displacement of the uncoupled plasmon co-ordinates, Q_k. To see this we remark that the first four terms in (7) arise from

$$\sum_i \left(\boldsymbol{p}_i + \frac{e}{c}\sum_k \boldsymbol{A}_k \exp\left[i\boldsymbol{k}\cdot\boldsymbol{x}_i\right] + i\sum_{k<k_c} \boldsymbol{k}\sqrt{\frac{4\pi e^2}{k^2}}\,Q_k \exp\left[i\boldsymbol{k}\cdot\boldsymbol{x}_i\right]\right)^2 \Big/ 2m\,.$$

Thus, a gauge transformation, $\boldsymbol{A}_k \to \boldsymbol{A}_k + i\boldsymbol{k}\varphi_k$ is equivalent to a displacement

$$Q_k \to Q_k + \sqrt{k^2/4\pi e^2}\,\varphi_k\,. \qquad \text{for } k < k_c.$$

([10]) D. Bohm, K. Huang and D. Pines: *Phys. Rev.*, **107**, 71 (1957).

In I, the coupling between electrons and phonons, $H_{\text{el-ph}}$, was considered in detail. A canonical transformation was carried out which eliminated this interaction in lowest order, and which simultaneously removed the phonon co-ordinates from the subsidiary condition (9). In the new Hamiltonian there appeared an effective interaction between the electrons due to virtual phonon exchange. This interaction, together with the screened Coulomb interaction, provided the basic interaction used in the BCS theory of superconductivity. BCS calculate the Meissner effect in the London gauge, for which the plasmon contribution to the current (8) will play no role. If the BCS calculation is repeated in a general gauge, one finds a plasmon response to the external longitudinal vector potential which cancels the direct gauge potential contribution to the longitudinal current. There will also be an individual electron response to the longitudinal vector potential, so that one finds a gauge dependent result in this approximation ([11]).

The apparent gauge dependence of the theory is simply removed by a further canonical transformation, namely that which eliminates the electron-plasmon coupling term, H_{int}, to order g^2 in the Hamiltonian. The transformation serves to clothe each electron with its appropriate cloud of virtual plasmons and thereby eliminates the coupling between the longitudinal vector potential and the « dressed » electrons to order g^2. The interaction term, H_{int}, is

$$H_{\text{int}} = i \sum_{ik<k_c} \sqrt{\frac{4\pi e^2}{k^2}} \left(\frac{\boldsymbol{k}\cdot\boldsymbol{p}_i}{m} - \frac{\hbar k^2}{2m} \right) Q_k \exp\left[i\boldsymbol{k}\cdot\boldsymbol{x}_i \right], \tag{10}$$

and the appropriate transformation may be generated by ([12])

$$S = i \sum_{ik<k_c} \sqrt{\frac{4\pi e^2}{k^2}} \left(\frac{(\boldsymbol{k}\cdot\boldsymbol{p}_i)/m - \hbar k^2/2m}{\omega_p^2} \right) \pi_k^* \exp\left[i\boldsymbol{k}\cdot\boldsymbol{x}_i \right]. \tag{11}$$

After the transformation generated by (11), the current density becomes, to order g^2,

$$\tilde{\tilde{\boldsymbol{j}}}(q) = \boldsymbol{j}_\perp(q) - \frac{ien}{m} \boldsymbol{q} \sqrt{\frac{4\pi e^2}{q^2}} Q_i, \tag{12}$$

([11]) This difficulty would exist even if the electronic wave-functions of BCS were sufficiently accurate to yield a longitudinal sum rule for the individual electrons. It arises because at this stage one has overdescribed the system in terms of both plasmons and electrons; the description of the density fluctuations in terms of plasmons has been carried out in the Hamiltonian, but the description of the longitudinal current in terms of plasmons has not yet been carried out.

([12]) This transformation is somewhat simpler than that used in BP. The present transformation may easily be seen to give the results found there for all terms of order g^2.

where again we have made the RPA for terms involving the interaction between plasmons and electrons. Thus in the new representation the longitudinal current is carried entirely by the plasmons; the « dressed » electrons make no contribution to the longitudinal current (to order g^2).

This is our desired result; it guarantees the gauge invariance of the theory to order g^4. To see this explicitly, we calculate the kernel $K_{\mu\nu}(q)$ defined by

$$J_\mu(q) = K_{\mu\nu}(q) A_\nu(q) , \tag{13}$$

where $J_\mu(q)$ represents the expectation value of the current density. For the system ground state, $K_{\mu\nu}(\boldsymbol{q})$ may be expressed as

$$K_{\mu\nu} = -\frac{1}{c}\left\langle 0 \left| j_\mu(q) \frac{P}{e} j_\nu(-q) + j_\nu(-q) \frac{P}{e} j_\mu(q) \right| 0 \right\rangle - \frac{ne^2}{mc}\delta_{\mu\nu} , \tag{14}$$

where $|0\rangle$ is the wave function for the ground state with energy E_0, the propagator e is defined by $e = E_0 - H$, and P is a projection operator which requires that principal parts be taken in intermediate state sums. The usual approximation of keeping only terms linear in A has been made. If we now calculate $K_{\mu\nu}$ with the aid of our expression (12) for the transformed current, and the Hamiltonian transformed by (11), we find a plasmon contribution which is

$$K^{pl}_{\mu\nu}(q) = \frac{q_\mu q_\nu}{q^2}\frac{ne^2}{mc} .$$

This is just the result suggested by BARDEEN [5]. The total kernel is given by

$$K_{\mu\nu}(q) = \frac{q_\mu q_\nu - q^2\delta_{\mu\nu}}{q^2}\frac{ne^2}{mc} - \frac{1}{c}\left\langle 0 \left| j_{\perp\mu}(q) \frac{P}{e} j_{\perp\nu}(-q) + j_{\perp\nu}(-q) \frac{P}{e} j_{\perp\mu}(q) \right| 0 \right\rangle ,$$

where the second term includes only transverse excitations. The kernel satisfies the conditions of gauge invariance ($K_{\mu\nu}(q) q_\nu = 0$) and current conservation ($q_\mu K_{\mu\nu}(q) = 0$). Since the transverse current is unaffected by our transformation, the BCS calculation of $K_{\mu\nu}$ in the London gauge is valid in a general gauge if their expression is generalized to

$$K_{\mu\nu}(q) = \frac{q_\mu q_\nu - q^2\delta_{\mu\nu}}{q^2} K(q)_{\mathrm{BCS}} .$$

This result is valid to terms of order g^4 and (m/M), and only requires the use of the RPA for terms involving plasmons explicitly. Such accuracy is certainly sufficient for the Meissner effect, since the wave lengths of importance there are such that $k \ll k_c$.

To see the connection between the above approach and the recent FEYNMAN proposal we first remark that the transformation (11) is equivalent to introducing a new set of wave-functions, Ψ, defined by:

$$\Psi = \exp\left[\sum_{ik<k_c}\left\{\frac{\sqrt{4\pi e^2/k^2}((\boldsymbol{k}\cdot\boldsymbol{p}_i)/m - \hbar k^2/2m)}{\hbar\omega_p^2}\pi_k^* \exp\left[+i\boldsymbol{k}\cdot\boldsymbol{x}_i\right]\right\}\right]\varphi\,, \tag{15}$$

if the φ were the system wave-functions before we took the electron-plasmon coupling into account. We next apply the subsidiary condition, (9), and so obtain ([13]):

$$\Psi = \exp\left[-\frac{1}{n}\sum_{ijk<k_c}\exp\left[+i\boldsymbol{k}\cdot(\boldsymbol{x}_i - \boldsymbol{x}_j)\right]\frac{\boldsymbol{k}\cdot\boldsymbol{p}_i + \hbar k^2/2}{\hbar k^2}\right]\varphi\,, \tag{16}$$

The wave-function (16) is just the appropriate generalization to the present case of the backflow wave-function proposed by FEYNMAN and COHEN ([14]) for liquid helium. It guarantees that the current carried by the states described by Ψ should have a divergence-free expectation value (to order g^2), which is the physical point of introducing the backflow. What we have done is to describe the backflow around an electron in terms of the virtual plasmon cloud which it carries along, a description which is physically equivalent but mathematically more convenient than that obtained with (16).

3. – There remains the problem that the single particle matrix elements of the electron density, ϱ_k, have not been properly screened. As a result, the longitudinal f sum rule

$$\sum_n \frac{2m}{\hbar k^2}|(\varrho_k)_{n0}|^2\omega_{n0} = n\,, \tag{17}$$

is not satisfied unless the subsidiary conditions are invoked. Our treatment screens the single particle current density and therefore provides a formulation sufficiently accurate to guarantee gauge invariance and satisfaction of the diagonal elements of the continuity equation. A more complete treatment in which the entire continuity equation is satisfied and the matrix elements of ϱ_k are appropriately screened may be possible on the basis of the minority carrier method introduced by Nozières and one of us for the normal metal ([15]). The

---

([13]) We assume the phonons have been decoupled from the electrons and the subsidiary conditions by the procedure described in I.

([14]) R. P. FEYNMAN and M. COHEN: *Phys. Rev.*, **102**, 1189 (1956).

([15]) P. NOZIÈRES and D. PINES: *Phys. Rev.*, **109**, 761 (1958).

minority carrier technique makes possible the explicit satisfaction of the longitudinal f sum rule and gives a satisfactory account of longitudinal phenomena (such as ultrasonic attenuation) in the normal state. It is our hope that this method can be successfully extended to the superconducting state. We intend to return to this problem in the future.

* * *

We should like to thank Professors JOHN BARDEEN and RICHARD FEYNMAN for stimulating discussions on the subject matter of this paper. We should also like to thank Professor YVES ROCARD for the hospitality extended to us by the Laboratoire de Physique de l'Ecole Normale Supérieure.

RIASSUNTO (*)

Si dimostra che, tenendo il dovuto conto delle interazioni coulombiane tra gli elettroni, qualsiasi teoria della superconduttività che renda conto in modo soddisfacente dell'effetto Meissner nel gauge di London può essere estesa a renderne conto altrettanto soddisfacente in qualsiasi altro gauge. Calcoli basati sul trattamento collettivo di Bardeen-Pines del sistema elettrone-fonone mostrano che nella regione delle onde lunghe ($k \lesssim k_c \cong r_s^{-1}$, dove r_s è la distanza fra gli elettroni) solo i plasmoni reagiscono in risposta a un potenziale vettore longitudinale. La loro risposta è tale da conservare l'invarianza di gauge. Gli elettroni individuali sono circondati da una nube schermante di plasmoni virtuali in modo tale da non portare correnti longitudinali fino ad intensità dell'ordine k^2/k_c^2 e non sono quindi influenzati da potenziali vettori longitudinali fino a tale ordine. Si dimostra che l'introduzione della nube schermo corrisponde strettamente al flusso retrogrado introdotto da FEYNMAN e COHEN per garantire la conservazione della corrente longitudinale per le eccitazioni nell'elio liquido. I calcoli sono proseguiti fino all'ordine m/M e k^4/k_c^4, e richiedono l'uso dell'approssimazione di random phase pei termini che accoppiano plasmoni ed elettroni. Per le lunghezze d'onda aventi importanza nell'effetto Meissner ($k \ll k_c$), queste approssimazioni sono ampiamente giustificate. Si dà una prescrizione esplicita per l'estensione della derivazione di Bardeen, Cooper e Schrieffer dell'effetto Meissner ad un gauge arbitrario e si mostra che i loro risultati restano in essenza inalterati.

(*) *Traduzione a cura della Redazione.*

IL NUOVO CIMENTO Vol. X, N. 3 1° Novembre 1958

On the Optical Model for Nuclear Reactions.

L. Verlet and J. Gavoret

Laboratoire de Physique, Ecole Normale Supérieure - Paris

(ricevuto il 30 Luglio 1958)

Résumé. — La matrice de diffusion au sein de la matière nucléaire indéfinie a été calculée exactement dans le modèle où seules les corrélations statistiques sont prises en considération et grâce à l'emploi d'une interaction nucléon-nucléon séparable. On en déduit un potentiel complexe pour la diffusion des nucléons par les noyaux. On discute la convergence des séries de perturbation et la validité du modèle classique de Lane et Wandell. Enfin, en faisant l'approximation de Thomas-Fermi, on montre qu'à basse énergie l'absorption a principalement lieu à la surface du noyau.

1. – Introduction.

In the last few years, great progresses have been made in our understanding of the gross properties of nuclei, mainly due to the work of Brueckner, Bethe and others ([1-6]). They have shown that when the so-called cluster terms may be neglected, one can derive the properties of the infinite nuclear matter in its ground state from an integral equation involving explicitly only two particles. The effect of the other particles is taken into account both by the average field they produce and by their presence which, due to the Pauli principle, forbids a number of intermediate states. Though historically the problem of describing the interactions of a particle propagating in the nuclear

(1) K. A. Brueckner, C. Levinson and H. Mahmoud: *Phys. Rev.*, **95**, 217 (1954).
(2) K. A. Brueckner and C. A. Levinson: *Phys. Rev.*, **97**, 1344 (1955).
(3) K. A. Brueckner and J. L. Gammel: *Phys. Rev.*, **109**, 1023 (1958).
(4) L. C. Gomes, J. D. Walecka and V. F. Weisskopf: *Ann. Phys.*, **3**, 241 (1958).
(5) H. A. Bethe: *Phys. Rev.*, **103**, 1353 (1956).
(6) C. de Dominicis and P. C. Martin: *Phys. Rev.*, **105**, 1417 (1957).

medium through a complex potential was examined by WATSON and his co-workers before BRUECKNER's work ([7,8])—see also Ref. ([9]) and ([10])—explicit calculations related to this problem have not been pushed very far ([11-15]). There appear in fact, when one goes from the ground state of nuclear matter to the scattering problem, a number of new difficulties which make this problem rather formidable.

1) The decoupling operation of the various particles, which enables to establish a two-body integral equation cannot be accomplished in one step. One has first to decouple the incident particle from the target nucleus. The integral equation for the scattering amplitude of the incoming particle inside the target still involves the real nuclear states. A second operation must be done to disentangle the particles of the target nucleus. We shall make the assumption that the nucleus may be correctly described by a Fermi gas, so that we shall escape this problem as well as the difficulties ([9]) connected with the fact that the real nuclear ground state has, in the general case, momentum components onto the incoming wave function.

2) If the optical potential is calculated according to WATSON's work ([7-10]), one has to solve a scattering integral equation which involves a Green's function in which the complex potential to be calculated appears. This particular form of the Green's function makes the self-consistency problem quite awkward to solve when the imaginary part of the potential is not negligible. In the present work we shall suppose that all particles move in a real well whose momentum dependence will be treated, rather empirically in the effective mass approximation.

3) When the two colliding particles are in the Fermi sea the scattering matrix depends very weakly on the absolute momentum of the particles involved. It can then be shown ([2,3,6]) that it is legitimate to replace by a sphere the complicated bispherical domain (Fig. 2) on which the integration over the intermediate relative momentum must be made. This approximation renders feasible the numerical calculation of the t-matrix, even when a complicated nucleon-nucleon interaction is used ([2,3]). The situation in the scattering problem is quite different: the t-matrix depends strongly on the absolute momentum so that its evaluation is in general quite complicated even in the case where the target nucleus is taken as a Fermi gas and where the self-consistency problem is left out or treated in the effective-mass approximation.

([7]) K. M. WATSON: *Phys. Rev.*, **89**, 575 (1953).
([8]) N. C. FRANCIS and K. M. WATSON: *Phys. Rev.*, **97**, 1336 (1955).
([9]) G. TAKEDA and K. M. WATSON: *Phys. Rev.*, **94**, 1087 (1954).
([10]) K. M. WATSON: *Phys. Rev.*, **105**, 1388 (1957).

In fact, calculations done up to now have resorted in some way to perturbation theory ([11-13,15]) or to the extension to low energy of the classical model of GOLDBERGER ([16]) an extension which has still to be justified ([17-21]).

This paper will be developed around a calculation of the t-matrix (Sect. **2**). We used separable nucleon-nucleon interactions ([22]) which have the advantage of permitting an exact calculation ([6]) within the framework of approximations sketched above, but the inconvenient of their unphysical nature which renders rather futile an attempt to give a precise fit to the experimental data. We can hope, however, to be able to draw some general conclusions about the optical model. It will appear (Sect. **3**) that at low and intermediate energies, the complex potential thus derived is fairly independent of the precise shape of the separable potential that is used. The rate of convergence of the perturbation series depends very strongly on the « singularity » of the nucleon-nucleon interaction. It will be shown that this convergence is much better for the real part of the optical potential than for the imaginary part where it is, in fact, quite bad. The main effect of the introduction of an effective mass of $0.8\ M$ is to decrease very much the imaginary part of the potential especially at low energy (the reduction factor is around 3 at zero energy).

The following Section (Sect. **4**) will be devoted to the study of the classical approximation. We shall give a formulation of the classical model in which the imaginary part of the potential is more directly related than usually to the experimentally measured cross-sections. We shall show that the anisotropic part of the nucleon-nucleon potential contributes little, even at high energy. The results for the isotropic part are in qualitative agreement with those obtained recently by VAN DER VEGT and JONKER ([21]).

The validity of the classical model will then be tested by comparing the absorption potential obtained from the classical model in which the free nucleon-nucleon cross-sections are calculated with a separable potential, with the more exact result obtained from the t-matrix calculation (Sect. **3**) using the same nucleon-nucleon interaction. It will be seen that the agreement

---

([11]) M. CINI and S. FUBINI: *Nuovo Cimento*, **2**, 443 (1955).
([12]) K. A. BRUECKNER, R. J. EDEN and N. C. FRANCIS: *Phys. Rev.*, **100**, 891 (1955).
([13]) K. A. BRUECKNER: *Phys. Rev.*, **103**, 172 (1956).
([14]) W. B. RIESENFELD and K. M. WATSON: *Phys. Rev.*, **102**, 1157 (1957).
([15]) L. VERLET: *Nuovo Cimento*, **7**, 821 (1958) and *Thesis* to appear in *Ann. Phys.*
([16]) M. L. GOLDBERGER: *Phys. Rev.*, **74**, 1269 (1948).
([17]) A. M. LANE and C. F. WANDEL: *Phys. Rev.*, **98**, 693 (1955).
([18]) E. CLEMENTEL and C. VILLI: *Nuovo Cimento*, **10**, 176 (1955).
([19]) S. HAYAKAWA, M. KAWAI and K. KIKUCHI: *Progr. Theor. Phys.*, **13**, 415 (1955).
([20]) G. C. MORRISON, H. MUIRHEAD and P. A. B. MURDOCH: *Phil. Mag.*, **46**, 795 (1955).
([21]) A. VAN DER VEGT and C. C. JONKER: *Physica*, **33**, 359 (1957).
([22]) Y. YAMAGUCHI: *Phys. Rev.*, **95**, 1628 (1954).

between the two methods is not very good: below 100 MeV the classical approximation underestimates the imaginary potential by about 50%.

In the last section, we shall try to get an insight in the behaviour of the imaginary part of the potential in the surface region which will be treated in the Thomas-Fermi approximation. It will appear that the absorption is, at low energy, much bigger in the surface region than in the center of the nucleus and that this result is not due to our use of separable potentials although it may be completely altered in a more precise treatment of the problem. As it stands, this surface absorption has the advantage of compensating the too small volume absorption obtained when an appreciable effective mass effect is taken into account; this surface absorption is made plausible by some recent phenomenological analysis ([23-25]).

2. – Calculation of the optical potential from the t-matrix.

In the calculation of the optical potential from the t-matrix, the approximations stated in Sect. **1** have been made.

The target nucleus is represented by a Fermi gas with $N = Z$ and no Coulomb forces. In this section and the two following ones the density will correspond to a value for r_0 of 1.27 fermis and the absolute energy $-\Delta E$ of the top of the Fermi sea is -10 MeV. The effect of varying the density will be studied in Sect. **5**.

We take for the separable potentials the simplest possible form which in momentum space is written ([22]):

$$(\boldsymbol{p}\,|\,V\,|\,\boldsymbol{p}') = -\frac{\lambda}{M}\, g(p)\, g(p')\,. \tag{1}$$

Such a potential acts only in S-states.

The normalization of (1) is such that the forward part of the scattering amplitude for free nucleons takes the form:

$$f(p) = 2\pi^2 \lambda g^2(p) \Big/ \left[1 + \lambda \int \frac{\mathrm{d}\boldsymbol{q}\, g^2(q)}{p^2 - q^2 + i\varepsilon}\right]. \tag{2}$$

The t-matrix for the two nucleon system is equal to $4\pi f(p)$.

([23]) F. E. Bjorklund, S. Fernbach and N. Sherman *Phys. Rev.*, **101**, 1832 (1956).
([24]) H. Amster: *Phys. Rev.*, **104**, 1606 (1956).
([25]) F. E. Bjorklund and S. Fernbach: *Phys. Rev.*, **109**, 1295 (1958).

We used two kinds of separable potentials:

1) The Yamaguchi potential ([22]) for which:

$$g(p) = \frac{1}{p^2 + \beta^2}. \qquad \text{(Y. potential).}$$

We fit all the four low energy scattering constants by using two different potentials for the singlet and triplet states.

2) A more « singular » potential which fits exactly the effective range formula ([6,26]). For this potential one has:

$$g(p) = \frac{1}{\sqrt{p^2 + \beta^2}}. \qquad \text{(E.R. potential).}$$

We have again chosen two different interactions in the singlet and in the triplet states.

The average total cross-section $(\sigma_{nn}+\sigma_{np})/2$ obtained with those two potentials is shown in Fig. 1. The experimental data ([27]) are also given for comparison. For σ_{nn} we took $2\pi\,(\mathrm{d}\sigma_{pp}/\mathrm{d}\Omega)_{90°}$ supposing charge independence and the isotropy of the proton-proton cross-sections at all energies. We see that both potentials fit fairly well the total cross-section up to 80 MeV. Then they lead to cross-sections which are substantially smaller than the experimental ones, especially so in the case of the Y-potential. To obtain the t-matrix in the nuclear medium, one has still:

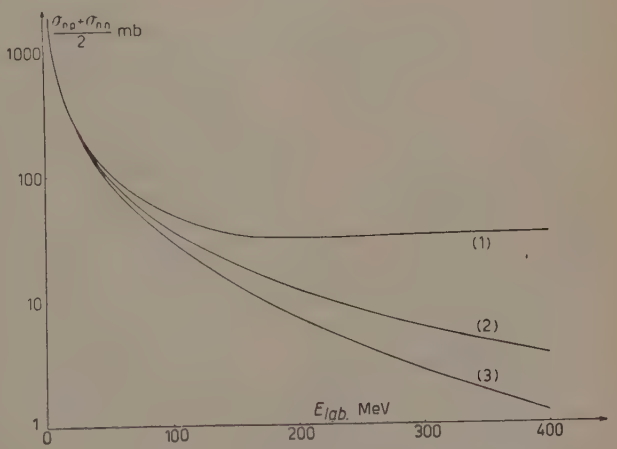

Fig. 1. – The average cross section $(\sigma_{np}+\sigma_{nn})/2$ as a function of the energy in the laboratory. Curve 1: experimental curve ([27]) with $\sigma_{nn} = 2\pi(\mathrm{d}\sigma_{pp}/\mathrm{d}\Omega)_{90°}$. Curves 2 and 3: cross sections obtained with the E.R. and Y potentials respectively.

1) To take into

([25]) A. Martin and M. Gourdin: *Nuovo Cimento*, **6**, 757 (1957).
([27]) L. Beretta, C. Villi and F. Ferrari: *Suppl. Nuovo Cimento*, **12**, 499 (1954).

account the antisymmetrization between the incident nucleon and the target nucleons. In the case of an S-state separable potential the direct and the exchange parts are equal, and we get from this a factor 2.

2) To sum over the spins and isotopic spins of the target nucleons and to average over the spin of the incident nucleon. This leads to a factor $\frac{3}{4}$ both for the triplet and singlet spin states.

3) To sum over the $A/4$ different states of the Fermi-gas and multiply by a factor $1/\Omega$, where Ω is the volume of the nucleus, which comes from the normalization of the incident particle wave function. This gives:

$$\frac{1}{\Omega}\sum_{i=1}^{A/4} = \frac{1}{(2\pi)^3}\int \mathrm{d}\boldsymbol{k} = \frac{2}{\pi^2}\int u\,\mathrm{d}u p\,\mathrm{d}p\,, \qquad \text{where} \qquad u = \left|\frac{\boldsymbol{k}_N + \boldsymbol{k}}{2}\right|.$$

The triplet state contribution to the optical potential is then found to be:

$$\mathcal{V}_t = \frac{-48\pi\lambda_t}{Mk_N}\int \frac{p\,\mathrm{d}p\,u\,\mathrm{d}u\,g_t^2(p)}{1+\lambda_t(M^*/M)\int \mathrm{d}\boldsymbol{q} g_t^2(q)/(p^2-q^2+i\varepsilon)}\,. \tag{3}$$

To this term must be added the singlet contribution which has a similar form. In this formula M^* is the effective mass. The integration domains are as follows (Fig. 2). $\boldsymbol{q}$ must lie outside two Fermi spheres whose centers are $2u$ apart. The fact that $\boldsymbol{k}$ must lie inside the left Fermi sphere imposes on p and u the following limits: u varies from $k_N - p$ to $\sqrt{(k_N^2/2)+(k_F^2/2)-p^2}$ and p varies from $(k_N - k_F)/2$ to $(k_N + k_F)/2$. For the potentials that we have used, the integration on $\boldsymbol{q}$ is immediate and leads for (3) to a denominator of the form $1-(J_1+iJ_2)$. The expression for the real part of the denominator is too long to be given here; its analytical form depends on the form of the potential that is used. For J_2 one has generally:

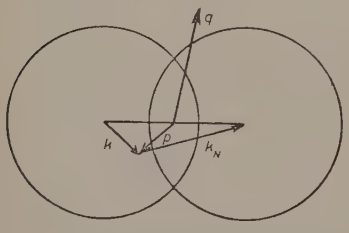

Fig. 2. – Integration domain for Eq. (3).

$$J_2 = \pi^2\lambda g^2(p)(p^2+u^2-k_F^2)/u\,,$$

when $(p^2+u^2-k_F^2)$ is positive. Whenever this last expression is negative, which may happen when $k_N < \sqrt{2}k_F$, J_2 is equal to zero. As in (3) the integrations on u and p cannot be done analytically, the results we give below for the optical potential have been computed numerically.

3. – Results.

Some of the results have been summarized in Table I. We have computed for 4 incident particle energies (— 10 MeV ($k_N = k_F$), 27 MeV, 80 MeV, 230 MeV) and generally, for both the Y potential and the ER potential, the real part of the optical potential given by the two first Born approximations and its exact value; the real part when the Pauli principle is not taken into account; the imaginary part given in the second Born approximation and exactly; the imaginary part when the Pauli principle is neglected and when the classical model is used.

TABLE I.

E_N	— 10 MeV		+ 30 MeV		80 MeV		230 MeV	
k_N	k_F		$1.5k_F$		$2k_F$		$3k_F$	
	Y	ER	Y	ER	Y	ER	Y	ER
$\mathcal{V}_R^{(1)}$	46.5	32.2	35.0	26.4	24.1	19.6	10.5	11.1
$\mathcal{V}_R^{(2)}$	13.7	17.1	13.7	15.1	4.8	8.9	— 0.6	2.8
$\mathcal{V}_R$	66.7	69.8	48.7	51.5	23.1	25.7	8.7	13.7
$\mathcal{V}_{RWP}$	21.5	21.7	21.45	21.2	16.6	17.4	8.1	10.6
$\mathcal{V}_I^{(2)}$	0	0	8.5	4.8	10.0	6.5	4.0	4.2
$\mathcal{V}_I$	0	0	20.6	23.9	12.1	16.1	3.1	6.0
$\mathcal{V}_{I\,WP}$	31.9	34.2	27.6	30.4	13.6	17.2	3.4	6.4
$\mathcal{V}_{I\,C}$	0	0	9.7	11.05	8.5	8.8	2.8	5.35

The consideration of this table leads us to the first conclusion that at low and intermediate energies the optical potential is, to a good approximation, independent of the shape of the separable potential. This independence was already shown in the saturation problem by DE DOMINICIS and MARTIN [6]. At higher energy, the differences are especially apparent in the results for the imaginary part of the potential. But it appears also that the values of the imaginary potential calculated with the Pauli principle are proportional to those calculated without it when one goes from one potential to the other;

so that the differences in the imaginary part of the potential at high energy are directly related to the differences in the free nucleon-nucleon cross-sections as can be expected on the basis of the classical model.

The convergence of the series which gives the real part of the potential is seen to be rather good in the case of the Yamaguchi potential. For instance, for $k_N = k_F$, the rate of convergence as measured by the ratio of the second Born approximation to the first is of the order of 30% and the sum of the two first terms is only 10% lower than the exact result. It may be noted that the rate of convergence of the perturbation series with a nucleon-nucleon local gaussian potential with which a fit for the real part of the optical potential may be obtained ([15]) is also of the order of 30%. On the other hand, the convergence, for the imaginary part of the potential, is quite bad. For $k_N = 1.5\,k_F$ the exact result is more than twice the result given by the first non vanishing term in the perturbation series, *i.e.* the second Born approximation. We may expect that in the case of a regular local interaction the perturbation series has not a structure very different from the one obtained with a « regular » separable potential, so that the value for the imaginary potential that we got in ([15]) with the second Born approximation may be substantially below the exact value.

The E.R. potential being more « singular », the convergence of the corresponding perturbation series is worse, especially for the imaginary part of the potential; for $k_N = 1.5\,k_F$, the contribution of the second Born approximation is only 20% of the exact value.

The effect of the velocity dependence of the average potentials is illustrated by Fig. 3 and 4. We have plotted the curves for $M^*/M = 1$ and $M^*/M = 0.8$. When an effective mass different from M is used the energy scale for the incident neutron must be modified so as to keep constant the product $M^*(V - E_N)$. The energy of the incident neutron is then:

$$E_N = \frac{M}{M^*}\,\frac{k_N^2 - k_F^2}{2} + \Delta E\,.$$

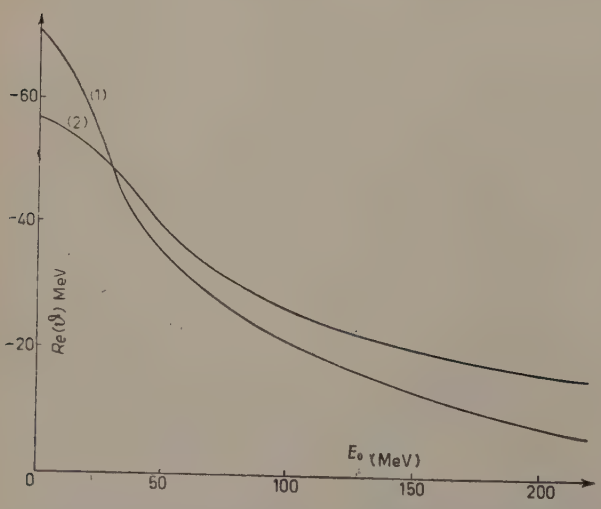

Fig. 3. – The real part of the optical potential calculated with the E.R. separable potential with $M^* = M$ (curve 1) and $M^* = 0.8M$ (curve 2).

Self consistency for neutrons near the top of the Fermi gas is obtained for

$M^*/M = 0.7$. We took the value $0.8\,M$ for the effective mass as a compromise since a lower value would tend to overestimate the velocity dependence for high momenta. The role of the effective mass is especially striking at zero energy for the imaginary potential; as has been already noted [12] its second Born approximation is then divided by a factor $(M/M^*)^3 \simeq 2$. The effect on the exact value is still bigger: the reduction factor is for the E.R. potential of the order of 3. It would be a little smaller for the Y potential for which the convergence is better.

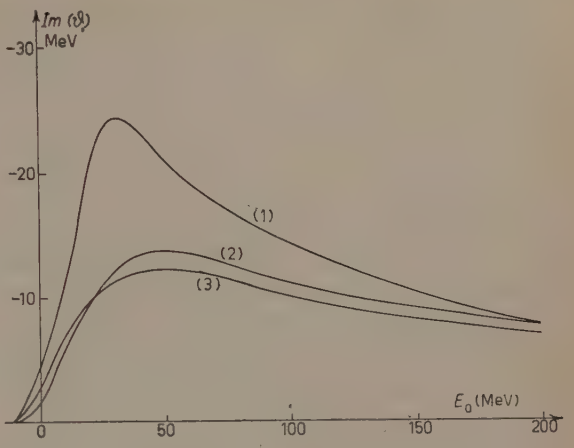

Fig. 4. – The imaginary part of the optical potential calculated with the E.R. potential. Curve 1 and 2: result of the t-matrix calculation with $M^* = M$ and $M^* = 0.8\,M$ respectively. Curve 3: result of the classical model calculation.

4. – The classical model.

We shall make now a further approximation which leads to the classical model: supposing that the wave length of the incident particle is small compared with the interparticle distance, the absorption potential is proportional to the sum of the cross-sections with the restriction that the possible final states should be permitted by the Pauli principle. One sees easily, using the same method and notations as in Sect. 2, that the imaginary potential is then:

$$\mathcal{V}_{IC} = -\frac{8}{\pi^2 M k_N}\int \mathrm{d}p\,\mathrm{d}u\,\mathrm{d}\boldsymbol{q}\,u\sigma(p, \boldsymbol{p}\cdot\boldsymbol{q})\,\delta(p-q)\,. \tag{4}$$

$\sigma(p, \boldsymbol{p}\cdot\boldsymbol{q})$ is the average of the differential cross-sections for neutron proton and proton proton collisions. The integration domains are the same than in Sect. 2, and there is also the restriction $p^2 + u^2 - k_F^2 > 0$. We approximate the differential cross-section by the expression:

$$\sigma(p, \boldsymbol{p}\cdot\boldsymbol{q}) = \sigma_0(p) + \sigma_1(p)P_1(\cos\theta) + \sigma_2(p)P_2(\cos\theta)\,. \tag{5}$$

The quantities $\sigma_0(p)$, $\sigma_1(p)$, $\sigma_2(p)$ are directly related to experiment.

The imaginary part of the potential corresponding to the isotropic term in the cross-section is easily calculated. For the integration on $\boldsymbol{q}$, one has:

$$\int \mathrm{d}\boldsymbol{q}\,\delta(p-q) = \frac{2\pi p}{u}\,(u^2 + p^2 - k_F^2)\,. \tag{6}$$

After an immediate integration on u, one has an expression for the imaginary part of the potential where the only integration to be done involves quantities directly related to experiment (*).

The results are shown in Fig. 5. They are qualitatively similar to those obtained by VAN DER VEGT and JONKER ([21]). The differences arise mainly from the fact that we did not make the assumption $\sigma_{nn} = \frac{1}{4}\sigma_{np}$.

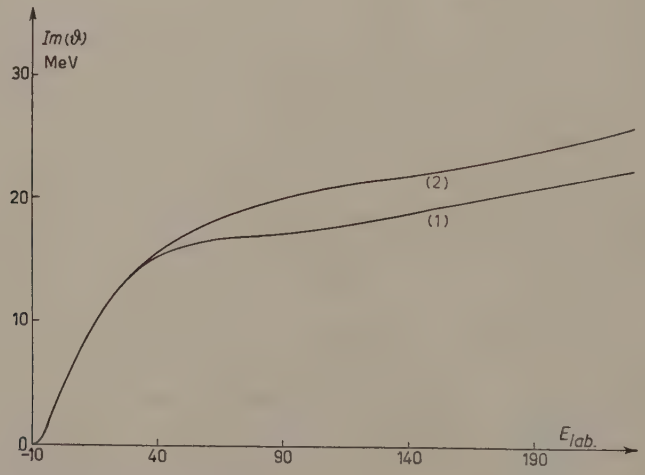

Fig. 5. – Imaginary potential obtained with the classical model using the experimental cross sections of Fig. 1 when only the isotropic part is included (curve 1) and when the anisotropy is taken into account (curve 2).

The contribution to the imaginary potential due to the P_1 term in (5) cancels out. The P_2 contribution has been calculated using the experimental values ([27]) of $\sigma_2(p)$; it is found to be fairly small. The imaginary potential with the P_2 correction included is shown in Fig. 5. The smallness of the anisotropy correction leads us to think that the addition of anisotropic terms to the separable potentials would not essentially change the results of the t-matrix calculation for the imaginary potential.

(*) Similar expressions will be derived for π and K-mesons in a forthcoming paper.

We shall now introduce in the classical expression (4) the free nucleon-nucleon cross-sections calculated with the separable potentials of Sect. 2 (curves 2 and 3, Fig. 1) and compare it with the imaginary part of the potential obtained from the t-matrix. We thus single out the effect of the classical approximation with the restriction that we have still to show that the results obtained do not depend essentially on the fact that the potentials which were used are separable. The results are tabulated for both potentials in Table I and they are shown, for the ER potential in Fig. 4. It is seen that below 100 MeV the « exact » and the classical calculations differ by a factor of the order of 2. The failure of the classical model to lead to more than semi-quantitative results is of course not unexpected. From these results one is also tempted to conclude that above 100 MeV, the classical model still underestimates the absorption and that it is altogether better to neglect the Pauli principle than to take it into account through the Goldberger approximation. We shall see, however, that this last point rests on the special form of the potentials that we have used. To see this, we have calculated the ratio between the second Born approximation for the t-matrix with and without the exclusion principle, both for local and separable potentials. In Table II we have given

TABLE II. – *Ratios of various approximations of the t-matrix calculated with the Pauli principle taken into account to the same quantities when the exclusion principle is left out.*

E_N (MeV)	k_N/k_F	Gaussian		Yukawa		ER potential			Y potential		
		Dir.	Exch.	Dir.	Exch.	2[d]Born	Exact	Class.	2[d]Born	Exact	Class.
1	2	3	4	5	6	7	8	9	10	11	12
27	1.5	0.32	0.37	0.31	0.34	0.42	0.79	0.36	0.34	0.75	0.35
80	2	0.47	0.65	0.45	0.58	0.61	0.94	0.51	0.60	0.89	0.63
230	3	0.47	0.71	0.53	0.58	0.82	0.94	0.83	0.75	0.91	0.82

these ratios for the direct and exchange terms of the Gaussian and Yukawa potentials ([15]) which fit the low energy-data (columns 3-6 of Table II) and for the ER and Y separable potentials (columns 7 and 10 of the same table). We see that at fairly low energies these ratios are much the same whatever the potential is. On the opposite, at high energy the reduction due to the Pauli principle is much bigger for a local regular potential than for a separable potential. The reduction factor for the classical model, calculated with separable potentials (columns 9 and 12), is much the same than the one given by the second Born approximation of the « exact » t-matrix calculated with the same potentials. The exact result is much less affected by the Pauli

principle than the second Born approximation. This obvious fact is illustrated by the figures of columns 8 and 11. The unsensivity of the second Born result to the nucleon-nucleon interaction, added to the fact that the reduction factor is almost the same in the classical model and in the second order calculation, seems to point to the safe conclusion that the classical model overestimates badly the role of the Pauli principle at low and intermediate energies. As at high energy the effect of the Pauli principle depends strongly on the kind of interaction that is used, one cannot draw any conclusions from these arguments as to the validity of the Goldberger approximation at high energy.

5. – Behaviour of the imaginary potential in the surface region.

We shall now try to get an insight on the behaviour of the optical potential in the region of the nuclear surface. We shall make the Thomas-Fermi approximation, *i.e.* we define in each point a local Fermi gas whose momentum k_F depends on the local density ϱ:

$$k_F = (3\pi^2\varrho/2)^{\frac{1}{3}} .$$

We shall assume that the matter distribution is identical with the charge distribution given by Hofstadter's experiments ([28]). As we are only interested in the surface region, we can choose any heavy nucleus. For instance, for gold, one has:

$$\varrho(r) = \frac{169}{1 + \exp\left[(r - 6.38)/0.535\right]} , \tag{7}$$

in which r is expressed in fermis. In each point, we can define a local t-matrix in the same way as in Sect. 3, and thus a local complex potential. In this section we shall take $\Delta E = 7$ MeV, which, taking (7) into account, gives, for the auxiliary well, the value of 45 MeV when $M^*/M = 1$.

We cannot expect, with this method, to obtain anything of interest for the real part of the well, whose radial behaviour on the other hand is rather well explained to day ([29]). The potential lies about 1 fermi outside the matter distribution for two reasons:

1) The saturating character of the nuclear forces makes the relation between the potential and the density non-linear so that the potential lies outside the density by about $\frac{1}{2}$ Fe due to this effect; as we used, for the sake

([28]) B. HAHN, D. G. RAVENHALL and R. HOFSTADTER: *Phys. Rev.*, **101**, 1131 (1956).
([29]) L. WILETS: *Phys. Rev.*, **101**, 1805 (1956).

of simplicity forces which are not saturating (although they give at normal density the right order of magnitude for the binding energy ([6])), we cannot take this effect into account.

2) The finite range of the force, which is manifested especially by the direct part of the first Born approximation ([30]); this effect, when properly treated yields another $\frac{1}{2}$ Fe for the potential extension. Due to the unrealistic character of the separable potential, we cannot hope to reproduce correctly this effect either.

On the other hand, we can hope to have some insight on the imaginary potential at low energy because we properly take into account the Pauli principle which is very important in this case, and because the finite range effect should be smaller than for the real potential as only Born approximations higher than the first one are non-vanishing. We plotted in Fig. 6 and 7 the

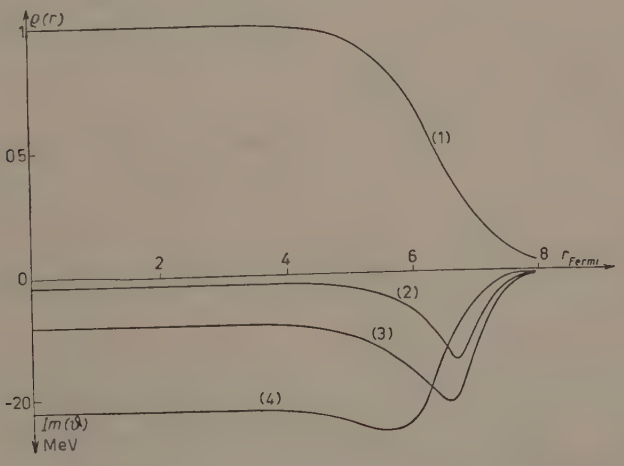

Fig. 6. – Radial density (curve 1) and radial behaviour of the imaginary potential in the Thomas-Fermi approximation for $E_n = 0$ (curve 2), $E_n = 10$ MeV (curve 3) and $E_n = 30$ MeV (curve 4) with $M^*/M = 1$.

imaginary potential for $M^*/M = 1$ and $M^*/M = 0.8$ respectively for severa values of the incident particle energy. We see that the absorption takes place mainly on the surface at low energy. This is due to the fact that in the surface region there is a competition between two effects: a decrease in the density which finally, as the value of r increases, makes the absorption go to zero, and the action of the Pauli principle which becomes less and less im-

([30]) S. D. DRELL: *Phys. Rev.*, **100**, 97 (1955).

portant when one goes towards the surface of the nucleus. The predominance of this second effect at low energy explains the surface absorption. When the energy rises, the Pauli principle plays a smaller role so that the decrease of the density when one goes towards the outside tends to be the main effect.

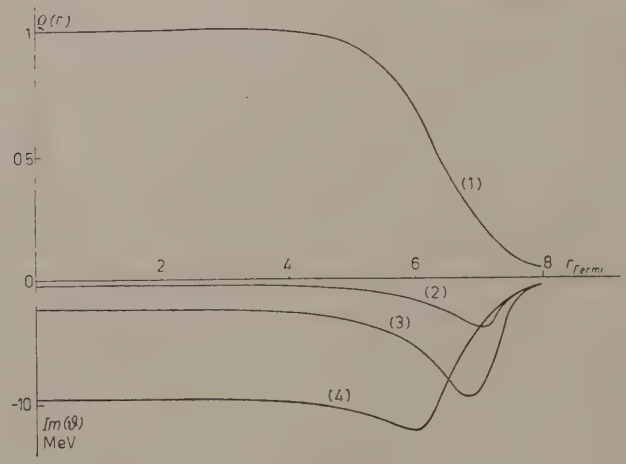

Fig. 7. – Same as Fig. 6 except that $M^*/M = 0.8$.

About these results, we wish to make the following remarks:

1) The surface absorption does not seem to be due to our use of the separable potential, although it may be exaggerated by it. We have made the same treatment of the surface behaviour of the imaginary potential with a local gaussian potential treated in second Born approximation. At zero energy of the incoming particle it gives an absorption on the surface which, at its maximum, is twice as big as it is in the center. On the other hand, the ratio of the second Born approximation to the exact value, as given with the ER separable potential with $M^*/M = 1$, goes from 0.25 at the center to 0.1 in the region of maximum absorption, always at zero energy. This shows that we may expect a bigger contribution of higher Born approximations in the surface region than in the center, so that an exact calculation of the t-matrix with a local regular potential would give a surface absorption still more pronounced than when only the second Born approximation is considered. At zero energy the classical model gives also a surface absorption whose maximum is 3 times what it is at the center of the nucleus.

2) The experimental situation, although it is still not completely clear, is not in contradiction with a surface absorption ([23-25]). In reference ([25]) ex-

perimental neutron elastic cross-sections are analyzed in terms of a real Saxon-type potential and of an imaginary potential of the form ([31]):

$$V_I \exp\left[-\left(\frac{r-R_0}{b}\right)^2\right],$$

where $R_0 = r_0 A^{\frac{1}{3}}$. The constants are: $b = 0.98$ Fe, $r_0 = 1.25$ Fe, V_I is equal to 7 MeV, 9.5 MeV and 11 MeV when the incident neutron energy is equal to 4.1 MeV, 7 MeV and 14 MeV respectively. It may be seen that the results of this experimental analysis are in agreement, as far as orders of magnitude are concerned, with those that we deduced theoretically.

3) Apart from the Thomas-Fermi approximation, some other approximations which have been made in this work may have an important influence on the shape of the absorption potential:

— The velocity dependence has been assumed to be the same throughout the surface. It is obviously not the case as the velocity dependence tends to disappear when one goes towards the outside of the nucleus. It would seem naively that this effect tends to give a bigger surface absorption than the one which is calculated when the same velocity dependence as in the center of the nucleus is extended throughout.

— We have neglected cluster terms which are probably important in the surface region ([32]) but we did not find any easy way to appreciate their influence.

([31]) There is also an $\boldsymbol{l}\cdot\boldsymbol{s}$ force, which is irrelevant for the present discussion.

([32]) We are indebted to Dr. DE DOMINICIS for having pointed out this fact to us.

RIASSUNTO (*)

La matrice di diffusione dentro la materia nucleare indefinita è stata calcolata esattamente nel modello in cui si prendono in considerazione solo le correlazioni statistiche e con l'impiego di un'interazione nucleone nucleone separabile. Se ne deduce un potenziale complesso per la diffusione dei nucleoni da parte dei nuclei. Si discute la convergenza delle serie di perturbazione e la validità del modello classico di Lane e Wandell. Infine, applicando l'approssimazione di Thomas-Fermi, si dimostra che alle basse energie l'assorbimento avviene principalmente alla superficie del nucleo.

(*) *Traduzione a cura della Redazione.*

IL NUOVO CIMENTO Vol. X, N. 3 1° Novembre 1958

Two-Stage Model of Fermi Interactions.

N. Byers (*) and R. E. Peierls

Department of Mathematical Physics, University of Birmingham - England

(ricevuto il 31 Luglio 1958)

Summary. — The model of Fermi interactions which involves an intermediate charged boson of spin one is formulated and found to be capable of reproducing all the results of the direct interaction theory with *A* and *V* coupling provided the mass of the intermediate particle is sufficiently large. The only apparent difficulty for the model is the predicted radiative decay of the muon.

We have considered the possibility of an intermediate charged vector boson in β decay. Experimental evidence at present indicates that the weak interactions can be reasonably well described by four-fermion interactions of the ***V-A*** type [1]. As has been pointed out by many authors, this strongly suggests the presence of a charged spin-one intermediate particle. We have considered the possibility of such an intermediate vector field, χ_μ. It would interact with fermion fields by Yukawa coupling terms of the type

$$ig\bar{\psi}_A\gamma_\mu\psi_B\chi_\mu \qquad \text{or} \qquad ig'\bar{\psi}_A\gamma_\mu\gamma_5\psi_B\chi_\mu\,, \tag{1}$$

where A, B are, for instance, proton and neutron, neutrino and electron, or neutrino and muon. (As has been pointed out by Schwinger [2], the strange particle decays may also be accounted for by postulating that this field also couples with pairs such as proton and Λ^0, or Σ^0, neutron and Σ^-, etc.) If one

---

(*) Present address: Department of Physics, Stanford University, Stanford, California, U.S.A.

(1) E. D. G. Sudarshan and R. E. Marshak: *Phys. Rev.*, **109**, 1860 (1958).

(2) J. Schwinger: *Ann. of Phys.*, **2**, 407 (1947).

takes $g = g'$ and equal for all fermion pairs, one obtains the two-component neutrino theory and, in the limit as the mass M of the intermediate particle becomes infinitely large, the Feynman–Gell-Mann ([3]) scheme, which is in reasonably close agreement with experiment.

We use a vector meson theory that consistently describes the interactions of a spin-one particle of mass M formulated in a relativistically covariant way without the introduction of a subsidiary condition ([4]). A Hamiltonian formulation of such a theory is well known ([5]) but is not convenient for the study of processes of second and higher order in the coupling constant. A formulation which does not contain a supplementary condition and is manifestly covariant greatly facilitates such considerations.

In this framework, it is easily seen that in the limit of large M, the effective β interaction is uniquely a mixture of vector and axial vector coupling. For large but finite values of M, the effective β interaction is somewhat non-local. The form of this interaction is practically that discussed by LEE and YANG ([6]) and, as they have shown, the non-locality tends to increase the value of the Michel parameter above .75. This mechanism thus does not remove the discrepancy with the measured value of the Michel parameter, but any explanation for this discrepancy may well leave a little more room for a slight increase so that the present evidence (*) in this respect need not rule out a charged vector boson intermediate particle (+).

To describe such particles, we take a free-field Lagrangian of the form

$$\mathcal{L} = -(M^2 \chi_\mu \chi_\mu^* + \partial_\mu \chi_\nu \partial_\mu \chi_\nu^* - \partial_\mu \chi_\nu \partial_\nu \chi_\mu^*) . \tag{2}$$

The equations of motion are then

$$-\Box^2 \chi_\mu + \partial_{\mu\nu}^2 \chi_\nu + M^2 \chi_\mu = 0 . \tag{3}$$

It follows from (3) that $\partial_\mu \chi_\mu = 0$, and therefore that there are just three solutions of (2) of given energy and momentum. To describe the interactions,

---

([3]) R. FEYNMAN and M. GELL-MAMM: *Phys. Rev.*, **109**, 193 (1958).

([4]) W. PAULI: *Rev. Mod. Phys.*, **13**, 203 (1941).

([5]) G. WENTZEL: *Quantum theory of fields*, (New York, 1949).

([6]) T. D. LEE and C. N. YANG: *Phys. Rev.*, **108**, 1611 (1957).

(*) A redetermination of the Michel parameter in progress at present was reported at the 1958 Annual International Conference on High Energy Physics at CERN. The preliminary result reported was $\varrho = .736 \pm .022$.

(+) It has recently been pointed out by G. FEINBERG (preprint) that a charged intermediate particle in μ-decay would also predict the decay mode $\mu \to e + \gamma$ with a frequency of about five times the experimental upper limit. As the calculation of this branching ratio involves a divergent integral, this result though indicating a real difficulty for this theory, is not unambiguous.

we add to (3) $\mathcal{L}^{\text{free}}(\psi_A, \psi_B, \ldots) + \mathcal{L}^{\text{int.}}$, where

$$\mathcal{L}^{\text{int.}} = j_\mu \chi_\mu + j_\mu^* \chi_\mu^* \tag{4}$$

and j_μ is a sum of terms of the type given by (1) (*). It then follows that $M^2 \partial_\mu \chi_\mu = \partial_\mu j_\mu$. The fact that $\partial_\mu \chi_\mu$ no longer vanishes identically means that in the vicinity of the source-currents there appear virtual spinless bosons These are the analogue of the scalar photons in electrodynamics which produce the Coulomb interactions. In β decay, they give rise to the 0-0 transitions. The fact that $\partial_\mu \chi_\mu = 0$ in source-free regions is sufficient to ensure that the real particles described by the theory are spin-one particles.

Such a theory can be quantized in the standard way (5). One can postulate canonical commutation relations for three of the four field variables, the space-like $\boldsymbol{\chi}$ and their conjugate momenta $\boldsymbol{\pi}$. The fourth component, χ_0, can be eliminated and one obtains the Hamiltonian formulation of vector meson theory (5). The interaction Hamiltonian is given by

$$H_{\text{int.}} = \boldsymbol{j} \cdot \boldsymbol{\chi} + \boldsymbol{j}^* \cdot \boldsymbol{\chi}^* - M^{-2}(j_0 \boldsymbol{\nabla} \cdot \boldsymbol{\pi} + j_0^* \boldsymbol{\nabla} \cdot \boldsymbol{\pi}^* - j_0 j_0^*) ,$$

in which the role of the scalar mesons is seen to be quite similar to that of the scalar photons in electrodynamics.

However, a more convenient formalism for the present purpose is that of YANG and FELDMAN (7). Here only the commutation relations for the free fields are needed and these can be formulated in a completely covariant way (8). One has

$$i[\chi_\mu(x), \chi_\nu^*(x')] = (\delta_{\mu\nu} - M^{-2} \partial_{\mu\nu}^2) D(x - x') .$$

Then using the Heisenberg representation, one solves the field equations directly. The Green's function for equation (3) has the form

$$\mathcal{D}_{\mu\nu}(x - x') = -i \int \frac{\mathrm{d}^4 k}{(2\pi)^4} \frac{\delta_{\mu\nu} + k_\mu k_\nu M^{-2}}{k^2 + M^2} .$$

The fermion fields satisfy equations of the type

$$\psi_A(x) = \psi_A^{\text{in}}(x) + i \int \mathrm{d}^4 x' S^{\text{ret}}(x - x') \gamma_\mu (g + g' \gamma_5) \psi_B(x') \chi_\mu(x') , \tag{5}$$

(*) We use the summation convention $j_\mu \chi_\mu = \sum_1^3 j_i \chi_i - j_0 \chi_0$.

(7) C. N. YANG and G. FELDMAN: *Phys. Rev.*, **79**, 927 (1950). The treatment of vector mesons with vector coupling given in this paper is not applicable to the β-decay problem. For β-decay, the vector field must interact with a current which is not conserved. If $\partial_\mu j_\mu \neq 0$, equations (34) of YANG and FELDMAN are not consistent.

(8) R. E. PEIERLS: *Proc. Roy. Soc.*, A **214**, 143 (1952).

and the χ_μ satisfy

$$\chi_\mu(x) = \chi_\mu^{\text{in}}(x) - \int \mathrm{d}^4x' \mathcal{D}_{\mu\nu}^{\text{ret}}(x - x') j_\nu^*(x') , \tag{6}$$

where $S^{\text{ret}}(x - x')$ is the retarded Green's function for the Dirac equation and ψ_A^{in} and χ_μ^{in} satisfy the free field equations. If one solves equation (5) by an iteration procedure, it is clear that ψ_A will contain terms of the form

$$\int \mathrm{d}^4y \, \mathrm{d}^4z \, S(x - y)\gamma_\mu(g_{AB} + g'_{AB}\gamma_5)\psi_B(y)\mathcal{D}_{\mu\nu}(y - z)\bar{\psi}_D(z)\gamma_\nu(g_{CD} + g'_{CD}\gamma_5)\psi_C(z) . \tag{7}$$

From this it is clear that the propagator for, *e. g.*, the process $\mathrm{n} \to \mathrm{p} + \mathrm{e} + \bar{\nu}$, which is

$$\langle 0 \,|\, T(\psi_\mathrm{p}\psi_\mathrm{e}\psi_\nu\psi_\mathrm{n}) \,|\, 0 \rangle , \tag{8}$$

to second order in g will give a transition matrix element which is identical to that obtained from an effective Hamiltonian of the form

$$H_{\text{eff}} = \int \mathrm{d}^4x \, \mathrm{d}^4y \bar{\psi}_\mathrm{p}(x)\gamma_\mu(g + g'\gamma_5)\psi_\mathrm{n}(x)\mathcal{D}_{\mu\lambda}(x - y)\bar{\psi}_\mathrm{e}(y)\gamma_\lambda(g_\mathrm{e} + g'_\mathrm{e}\gamma_5)\psi_\nu(y) . \tag{9}$$

(Matrix elements of (9) are found to be identical to those obtained using H_{int} in the Hamiltonian formulation and perturbation theory up to second order).

If one takes $g_\mathrm{e} = g'_\mathrm{e}$ (*i.e.* two-component neutrinos) and $\gamma_5\psi_\nu = \psi_\nu$, the matrix element of (9) is

$$2\,\frac{\delta_{\mu\lambda} + k_\mu k_\lambda M^{-2}}{k^2 + M^2}\,(\bar{u}_\mathrm{p}(p')\gamma_\mu(g + g'\gamma_5)u_\mathrm{n}(p))(\bar{u}_\mathrm{e}(q')\gamma_\lambda u_\nu(q)) , \tag{10}$$

where $k = p - p' = q + q'$ and the $u(p)$ are Dirac spinors. Except for the factor $(k^2 + M^2)^{-1}$, one easily sees using the Dirac equation $(i\gamma \cdot p + m_A)u_A(p) = 0$ for the various spinors that (10) is equivalent to the usual four-fermion coupling in the scheme

$$\boldsymbol{V} - (g'/g)\boldsymbol{A} + (m_\mathrm{n} - m_\mathrm{p})m_\mathrm{e}M^{-2}\boldsymbol{S} - (g'/g)(m_\mathrm{n} + m_\mathrm{p})m_\mathrm{e}M^{-2}\boldsymbol{P} .$$

Similarly for μ-decay a scalar coupling term appears multiplied by the factor $m_\mu m_\mathrm{e}/M^2$. Apart from these extremely small contributions the non-local effects are all contained in the factor $(k^2 + M^2)^{-1}$ and such effects have been analyzed by LEE and YANG [5]. We have examined the additional radiative corrections to the Michel parameter which are due to the presence

of the intermediate particle, and find that they are negligible. Therefore assuming lepton conservation and the two-component neutrino theory, this model cannot account for the fact that the experimental value of the Michel parameter is somewhat smaller than .75. If another explanation is found for this effect, it seems unlikely that it will allow for the mass of the γ particle to be much less than five or ten times the muon mass. So far we have not found any specific effects due to such a particle that can be observed with present techniques.

RIASSUNTO (*)

Si da una formula per il modello delle interazioni di Fermi che coinvolge un bosone carico intermedio di spin uno e la si trova capace di riprodurre tutti i risultati della teoria dell'interazione diretta con accoppiamento A e V purchè la massa della particella intermedia sia sufficientemente grande. La sola difficoltà apparente presentata dal modello è il decadimento radiativo del muone.

(*) *Traduzione a cura della Redazione.*

NOTE TECNICHE

Graphical Method for the Analysis of Bubble Chamber Pictures.

V. Borelli, P. Franzini, I. Mannelli, A. Minguzzi-Ranzi,
R. Santangelo (*), F. Saporetti, V. Silvestrini,
P. Waloschek and V. Zoboli

Istituto di Fisica dell'Università - Bologna
Istituto di Fisica dell'Università - Pisa
Istituto Nazionale di Fisica Nucleare - Sezioni di Bologna e Pisa

(ricevuto il 25 Luglio 1958)

Summary. — A simple method for the analysis of bubble chamber pictures is described. It is sufficiently precise for most works and has been succesfully used during the last year. Some details of practical interest are included.

1. - Introduction.

Efforts have been made in many laboratories to analyse accurately stereoscopic photographs of bubble chamber events. Though it can be realized with very primitive technical means, the method described hereafter is enough precise for most of the bubble chamber works performed so far. For work involving high statistics more automatic methods, making use of digitizers and computers, will be preferred. Nevertheless we think that our « by hand method » is useful for routine checks and analysis of special events, for which a computer program is not convenient.

For the reconstruction of the events following the present method, it is necessary to know:

a) the relative position of the front side fiducial marks;

b) the relative position of the photocameras and their position with respect to the central axis of the chamber;

c) the depth of the chamber;

d) the magnetic field.

(*) At present at the Istituto di Fisica dell'Università, Padova.

It is not necessary to know the distance from the chamber to the photocameras. Also a « turning » of the photographic system or of the front glass (when changed) can be ignored and will be found out later from the pictures. Refraction indexes and glass thicknesses are not needed. Naturally, if all these things are known, one can check the correctness of the approximations used, especially if the stereoscopic angles are big.

In practice, to obtain the reconstruction in space, we draw on a big sheet of paper, (« drawing plane »), all the relevant points of a picture, repeat this for each stereoscopic view and get graphically the projected and depth co-ordinates. With slide rules and Wulff-nets we get the angles and lengths in space.

2. - Description of the method.

If we imagine the photographic system as free from any refraction effects, the geometry becomes very simple, as shown in Fig. 1. If the fiducial marks of the front glasses are coincident in both views, then the same geometry is valid for the analysis.

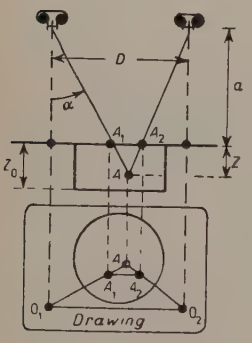

Fig. 1.

As one deduces from Fig. 1, the z co-ordinate of a point will be given by:

$$z = \frac{\overline{A_1A_2}\cdot a}{D - \overline{A_1A_2}}, \tag{1}$$

and the co-ordinates in the « drawing plane » are obtained just by projection of the image points A_1 and A_2 from the optic axes O_1 and O_2 (*).

It can be shown that, if refraction effects are taken into account, in a good approximation all remains unchanged in Eq. (1), except the parameter a (exact formulae are given by P. Bassi *et al.* (1)). The latter is related to the distance, a', between the photocameras and the front glass of the bubble chamber by the formula

$$a = a'\cdot n\cdot(1-\varepsilon), \tag{2}$$

when n is the refraction index of the liquid and ε depends essentially on the angle α (see Fig. 1). α is small enough to neglect the variation of a, and use a mean value, empirically determined from the separation of the images B_1,B_2 of points (B) of the bottom of the chamber (+)

$$a = \frac{z_0(D - \overline{B_1B_2})}{\overline{B_1B_2}}. \tag{3}$$

(*) We suppose that the optic axes are normal to the front glass of the chamber.

(1) P. Bassi, A. Loria, J. A. Meyer, P. Mittner and I. Scotoni: *Nuovo Cimento*, **5**, 1729 (1957).

(+) As bottom points, the fiducial marks scretched on the bottom of the bubble chamber may be used, or the end points of tracks leaving the chamber at bottom.

Within our approximation the segment $\overline{A_1A_2}$ is parallel to the line $\overline{O_1O_2}$ going through the traces of the optic axes on the « drawing plane ». From formula (3), it is clear that the knowledge of all the refraction indexes and glass thicknesses is not necessary, provided one knows z_0, the depth of the chamber.

The parameter a is also independent of the distance from where the pictures are actually projected. The essential fact in the reprojection system is that the figures formed by the fiducial marks are similar to the original ones and equal in all views. Distortion-free objectives in general will satisfy these conditions.

3. - Some remarks.

The exact superposition of the different views may be obtained by displacement of the drawing paper. This avoids the use of complicated adjustment systems of the film. Also completely independent projectors could be used. Nevertheless, a rough superposition of the different views is very useful during the scanning work.

If one measures the co-ordinates of well defined points, like individual bubbles (true stereoscopy), the finding of the corresponding images is in general easy. For faster work it is convenient to look for corresponding points on portions of tracks without reference to the bubbles. In this case (near stereoscopy) one starts selecting a point in one view, draws from the same a parallel to O_1O_2, and then, in the other view, the intersection of this line with the track will give the « corresponding » point. The rest of the geometry is now very easy, and in Fig 2. is sketched how it works with three views (*).

Points A and B in Fig. 2 represent two point of a track. The « dip-angle » (defined as in emulsion technique) is given by:

$$\text{tg}\,\delta = \frac{\Delta z}{L_0}, \tag{4}$$

and the « projected angle » can be measured on the drawing.

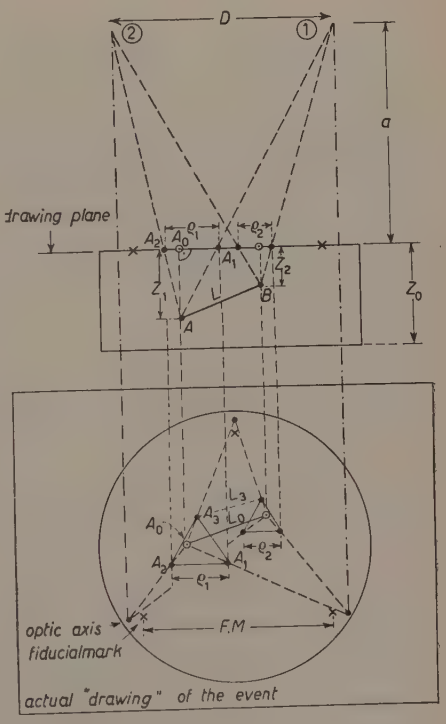

Fig. 2.

(*) As is well known, for « near stereoscopy » at least three photographs are necessary to get uniform precision in the measurement of dip angles. In our case we use for each point three projections. Each point corresponds to a « triangle » that must be similar and parallel to the one formed by the traces of the optical axes. This gives a good mean value for the z-coordinate of the point and allows to check for possible errors.

For curved tracks one may draw tangents in the different views, with the help of « templates » (curves of defined radii) attached to a drafting machine. One can then obtain the orthogonaly projected tangent with two points, like it has been done with a track. But one can easily show that this two points do not allow to calculate with enough precision the dip angle (formula (4)) and it is convenient to select points « on the track » or even better defined bubbles to compute δ.

If the highest precision in the projected angles is not required (always the dip angles have far larger errors), one may use three points of each track and get the tangent using the sagitta. This method is very fast and simple; the errors involved are estimated in the following paragraph.

The angles used here are given in a polar system with axis normal to the front glass of the bubble chamber. The transformation to any other system and the computation of angular parameters (*i.e.* co-planarity) can be conveniently done on stereographic projection nets (Wulff-spheres) of adequate precision.

4. - Precision of the measurements.

The approximations done in the reconstruction of the events will affect especially the depth-co-ordinate z. The depths will depend on how well the « corresponding » points have been found, how well the paper has been adjusted to make the fiducial marks coincident and on the correctness of the formula giving z. One can compute all these errors analytically but many sources of error remain uncertain. We have collected enough material to show on an example what errors are done in routine work.

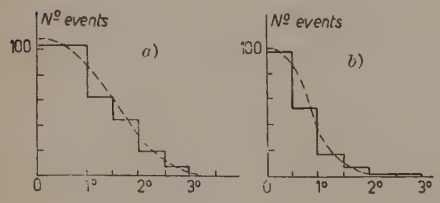

Fig. 3.

More than 1000 elastic $\pi^- + p$ collisions were measured in a 30 cm propane bubble chamber (+) (see ref. (2) and (3)). The co-planarity of these events illustrates the precision of the measurements. A small background of inelastic events do not affect the present discussion. We define as « angle of co-planarity » the angle between the plane of the two emerging particles and the incident track.

« Flat events » (azimuth less than 30°) are suitable to see how well are measured dip angles. Fig. 3*a* shows the co-planarity for 343 such flat events.

(+) A magnetic field of 13400 G was applied to the chamber; three phopographs were taken and used for the analysis of each event.

(2) S. Bergia, V. Borelli, L. Lavatelli, A. Minguzzi-Ranzi, P. Waloschek, V. Zoboli, G. Brautti, L. Chersovani, and R. Tosi: *Geneva Conference*, June 1948,

(3) F. Eisler, R. Plano, A. Prodell, N. Samios, M. Schwartz, J. Steinberger. P. Bassi, V. Borelli, G. Puppi, H. Tanaka, P. Waloschek, V. Zoboli, M. Conversi, P. Franzini, I. Mannelli, R. Santangelo and V. Silvestrini: *Nuovo Cimento*, in press.

The mean « non-co-planarity » is of about 1.5°; this means that the average error on the dip angles was even smaller.

Likevise, very steep events are suitable to see how well are measured the projected angles. In Fig. 3*b*, 177 such events are plotted (azimut between 60° and 90°), and the mean « non-co-planarity » is nearly 0.8°. Three points were taken on each track: the dip was computed with the two extreme points, the tangent was drawn using the sagitta at the central point in the orthogonal projection.

In cases of special interest (like V-events) it was in general possible to get the projected angle of a track of 10 cm lenght with a precision of about $\pm 0.2°$, and the dip angle with $\pm 1°$.

With the « fast » method described before, an average observer can analyse about 10 two-prong events per day, spending two hours at the projector and 3 to 4 h for slide-rule computations. About one half of the calculation time can be saved by the use of an electronic computer, without any change in the measurement method. If momenta are measured, the velocity is reduced to one third.

5. - Momentum measurements.

If a magnetic field, normal to the front glass of the chamber is applied, the projected radius of curvature will give the (horizontal) momentum of the particle. The following formula has proved to be useful and in general precise enough:

$$R_{p_\perp} = k_{(z)} \cdot L_0^2 \cdot (1/n) \cdot \sum_1^n R_i / L_i^2 , \tag{5}$$

where:

n is the number of views used;
R_i are the radii of curvature measured with templates on each view;
L_i are the cords of the used portions of the tracks (the same portion AB must be used in each view);
L_0 is the same cord in orthogonal projection, and
$k_{(z)}$ depends only on the depth of the central point of the portion of track used and is given by:

$$k_{(z)} = (D - \bar{\varrho})/D , \tag{6}$$

where $\bar{\varrho} = (\overline{A_1A_2} + \overline{B_1B_2})/2$.

R_i must be measured on the projector while L_i and L_0, as well as the segments $\overline{A_1A_2}$ and $\overline{B_1B_2}$ can be obtained from the drawings.

This procedure is equivalent to compute the mean of the sagittas for the different views, supposed to be equal. This is correct for flat tracks, and it can be shown to be enough approximate for the dipping ones.

The precision of the momentum measurements is very poor, especially in propane. The errors are mainly due to multiple Coulomb scattering; for low energetic particles the curvature changes along the track and a correction for ionization loss must also be applied. The uncertainty introduced by these and other effects justifies the use of the approximative method described before.

* * *

We are very grateful to Prof. G. PUPPI and to Prof. P. BASSI, who suggested to us the use of a graphical measurement method, and continuously encouraged us in our work. Prof. J. STEINBERGER contributed substantially to make the method reliable and accurate. For many discussions and help we thank Prof. M. CONVERSI.

Many other persons have contributed with suggestions and discussions. Part of the events shown in Fig. 3 have been measured by Drs. G. BRAUTTI, L. CHERSOVANI and R. TOSI at the Istituto di Fisica dell'Università, Trieste.

RIASSUNTO

Si descrive un metodo semplice per l'analisi delle fotografie di una camera a bolle. Questo metodo è sufficientemente preciso per la maggior parte dei casi ed è stato adoperato con successo durante lo scorso anno. Sono inclusi alcuni dettagli di interesse pratico.

LETTERE ALLA REDAZIONE

(La responsabilità scientifica degli scritti inseriti in questa rubrica è completamente lasciata dalla Direzione del periodico ai singoli autori)

Momentum Transfer Cross-Section in the Thomas-Fermi Theory,

T. Tietz

Department of Theoretical Physics - University of Łódź - Łódź

(ricevuto il 25 Giugno 1958)

In this paper we calculate the momentum transfer (diffusion) cross-section in the first Born approximation for the Thomas-Fermi field. The elastic collisions of electrons with molecules are defined as those encounters which leave unperturbed the initial internal state of the molecule, in our case the molecule is left in its normal state. In fact, one may easily show from the laws of conservation of momentum and energy that, if the angle of deflection of the electron is θ and if the molecule is initially at rest, the fraction $\Delta E/E$ of the original electron energy E imparted to the molecule is $\Delta E/E = (2m/M)(1 - \cos\theta)$. In the last formula m and M are the masses of the electron and molecule, respectively. This formula respects only the first order in m/M. As known the mean fraction energy loss per collision becomes $2(m/M)Q_d/Q_0$ where Q_d is the momentum transfer cross-section.

Q_d is often referred to as the diffusion cross-section on account of its importance in the discussion of diffusion phenomena. Q_0 is the total elastic cross-section. The momentum transfer cross-section is given by [1]

$$(1) \qquad Q_d = 2\pi\int_0^\pi I_0(\theta)(1-\cos\theta)\sin\theta\,\mathrm{d}\theta = Q_0 - 2\pi\int_0^\pi I_0(\theta)\cos\theta\sin\theta\,\mathrm{d}\theta\ ,$$

where $I_0(\theta)$ is the elastic differential cross-section.

Using the Rozental [2] approximate solution for the Thomas-Fermi function for free neutral atom $\varphi(x)$

$$(2) \qquad \varphi(x) = \sum_{i=1}^{3} c_i \exp[-a_i x]\ ,$$

where the constants c_i and a_i are given by $c_1 = 0.255$; $c_2 = 0.581$; $c_3 = 0.164$; $a_1 = 0.246$;

---

[1] H. S. W. Massey and B. H. S. Burhop: *Electronic and Ionic Impact Phenomena* (Oxford, 1952), p. 15.

[2] S. Rozental: *Zeits. Phys.*, **98**, 742 (1935).

$a_2 = 0.947$; $a_3 = 4.356$ one can calculate as it was shown by the author [3] analytically the elastic differential cross-section $I_0(\theta)$ in the first Born approximation. The mentioned paper of the author shows that our numerical values for $I_0(\theta)$ agree well with the exact numerical values for $I_0(\theta)$. Using the well known formula for the differential cross-section $I_0(\theta)$ in the first Born approximation we obtain according to equations (2) and (1) the following approximate formula for the momentum transfer cross-section Q_d.

$$(3)\quad Q_d = Q_0 + 4\pi g^2 \left[\frac{c_1^2}{\varkappa^2}\left(\frac{2}{\varkappa^2}\ln\frac{a_1^2+\varkappa^2}{a_1^2} - \frac{2a_1^2+\varkappa^2}{a_1^2(a_1^2+\varkappa^2)}\right) + \frac{c_2^2}{\varkappa^2}\left(\frac{2}{\varkappa^2}\ln\frac{a_2^2+\varkappa^2}{a_2^2} - \frac{2a_2^2+\varkappa^2}{a_2^2(a_2^2+\varkappa^2)}\right) + \right.$$

$$\left. + \frac{c_3^2}{\varkappa^2}\left(\frac{2}{\varkappa^2}\ln\frac{a_3^2+\varkappa^2}{a_3^2} - \frac{2a_3^2+\varkappa^2}{a_3^2(a_3^2+\varkappa^2)}\right)\right] + \frac{8\pi g^2 c_2 c_1}{\varkappa^2(a_2^2-a_1^2)}\left[\left(1+\frac{2a_2^2}{\varkappa^2}\right)\ln\frac{a_2^2+\varkappa^2}{a_2^2} - \right.$$

$$\left. - \left(1+\frac{2a_1^2}{\varkappa^2}\right)\ln\frac{a_1^2+\varkappa^2}{a_1^2}\right] + \frac{8\pi g^2 c_3 c_2}{\varkappa^2(a_3^2-a_2^2)}\left[\left(1+\frac{2a_3^2}{\varkappa^2}\right)\ln\frac{a_3^2+\varkappa^2}{a_3^2} - \left(1+\frac{2a_2^2}{\varkappa^2}\right)\ln\frac{a_2^2+\varkappa^2}{a_2^2}\right] +$$

$$+ \frac{8\pi g^2 c_3 c_1}{\varkappa^2(a_3^2-a_1^2)}\left[\left(1+\frac{2a_3^2}{\varkappa^2}\right)\ln\frac{a_3^2+\varkappa^2}{a_3^2} - \left(1+\frac{2a_1^2}{\varkappa^2}\right)\ln\frac{a_1^2+\varkappa^2}{a_1^2}\right],$$

and the total cross-section Q_0 is given by

$$(4)\quad Q_0 = 4\pi g^2\left[\frac{c_1^2}{a_1^2(a_1^2+\varkappa^2)} + \frac{c_2^2}{a_2^2(a_2^2+\varkappa^2)} + \frac{c_3^2}{a_3^2(a_3^2+\varkappa^2)} + \frac{2c_2c_1}{\varkappa^2(a_2^2-a_1^2)}\ln\frac{a_2^2(a_1^2+\varkappa^2)}{a_1^2(a_2^2+\varkappa^2)} + \right.$$

$$\left. + \frac{2c_3c_1}{\varkappa^2(a_3^2-a_1^2)}\ln\frac{a_3^2(a_1^2+\varkappa^2)}{a_1^2(a_3^2+\varkappa^2)} + \frac{2c_3c_2}{\varkappa^2(a_3^2-a_2^2)}\ln\frac{a_3^2(a_2^2+\varkappa^2)}{a_3^2(a_3^2+\varkappa^2)}\right].$$

In the last two formulas the symbols $\varkappa$ and g are given by (*) $\varkappa = (3^{\frac{3}{4}}hv)/(2^{\frac{7}{3}}\pi^{\frac{1}{3}}e^2Z^{\frac{1}{3}})$ and $g = (3^{\frac{1}{4}}h^2Z^{\frac{1}{3}})/(2^{17/3}\pi^{\frac{3}{4}}e^2m)$ respectively. In Table I we have several numerical

TABLE I. – *The numerical results for* $Q_0Z^{-\frac{2}{3}}/\pi a_0^2$ *and for* $Q_dZ^{-\frac{2}{3}}/\pi a_0^2$ *as the functions of* $V^{\frac{1}{2}}/Z^{\frac{1}{3}}$ (*vis given in* volt).

$V^{\frac{1}{2}}/Z^{\frac{1}{3}}$	$Q_0Z^{-\frac{2}{3}}/\pi a_0^2$ (in πa_0^2 units) Eq. (4)	$Q_dZ^{-\frac{2}{3}}/\pi a_0^2$ (in πa_0^2 units) Eq. (3)	$V^{\frac{1}{2}}/Z^{\frac{1}{3}}$	$Q_0Z^{-\frac{2}{3}}/\pi a_0^2$ (in πa_0^2 units) Eq. (4)	$Q_dZ^{-\frac{2}{3}}/\pi a_0^2$ (in πa_0^2 units) Eq. (3)
1	60.30	36.56	6	2.81	0.41
1.5	33.24	15.88	7	2.08	0.26
2	20.87	8.31	8	1.61	0.16
2.5	14.30	4.60	9	1.27	0.12
3	10.30	3.01	10	1.04	0.082
3.5	7.79	2.00	12	0.72	0.045
4	6.07	1.37	15	0.46	0.021
5	3.99	0.72	20	0.26	0.008 0

(3) M. MAJEWSKI and T. TIETZ: *Phys. Rev.*, **104**, 1298 (1957).

(*) The symbols appearing in $\varkappa$ and g have the following meanings: a_0 is the first radius of hydrogen, Z is the atomic number, e is the electronic charge, m is the electron rest mass, h is Planck's constant and v is the electron velocity of impact.

results for the total cross-section Q_0 as also the numerical results of the momentum transfer cross-section Q_d. In this Table I $Q_0 Z^{-\frac{2}{3}}$ and $Q_d Z^{-\frac{2}{3}}$ are given in πa_0^2 units as a function of $Z^{-\frac{1}{3}}\sqrt{V}$ where V is given in volt.

Since the exact numerical values for the momentum transfer cross-section Q_d calculated from the Thomas-Fermi theory as also the exact graph for Q_d are unknown, so we cannot compare our numerical results for Q_d with the above mentioned. As it is shown by the author (4) the numerical results for the total cross-section Q_0 agree well with the graph of Mott and Massey, so we may suppose that our results for the momentum transfer cross-section Q_d will too agree well with the exact numerical results.

(4) See reference (3).

IL NUOVO CIMENTO Vol. X, N. 3 1° Novembre 1958

Relativistic Electron-Neutron Scattering According to Meson-Theory.

L. K. Pandit

Seminar für Theoretische Physik der Universität Zürich - Zürich

(ricevuto il 29 Luglio 1958)

1. - Introduction.

Recently the present author [1,2] reported his calculations of the elastic scattering of high energy electrons by protons, using the charge-symmetrical pseudoscalar meson theory with both pseudoscalar and pseudovector couplings. In these calculations, which were carried to the lowest order in covariant perturbation theory, a relativistic cut-off due to Arnous and Heitler [3] was used. It was found that, for suitable choices of the coupling constant and the cut-off value, very good agreement with the experimental results of Hofstadter *et al.* [4] could be obtained. Thus, by adopting the coupling constant within reasonable limits, we could get agreement for the cut-off, K_0, ranging from a value of the order of the nucleon mass, M, up to ∞ (for pv-coupling $K_0 \simeq M$ is necessary as it diverges at ∞). Hofstadter and his coworkers [5] have now also measured the elastic scattering of electrons by deuterons. These measurements have actuated us to carry on the calculation of electron-neutron scattering in a manner exactly similar to that of electron-proton scattering. In the present paper, we shall report the results of these calculations and compare them with the experiments. In this comparison we take for the measured electron-neutron scattering cross-sections simply the difference of the experimental electron-deuteron and electron-proton cross-sections. At the high energies involved, this may be considered a plausible enough comparison.

---

[1] L. K. Pandit: *Nuovo Cimento*, **7**, 263 (1958).

[2] L. K. Pandit: *Helv. Phys. Acta*, **31**, 379 (1958).

[3] E. Arnous and W. Heitler: *Nuovo Cimento*, **2**, 1282 (1955).

[4] R. Hofstadter and R. McAllister: *Phys. Rev.*, **98**, 217 (1955); E. E. Chambers: *Ph. D. Thesis* (Stanford University, May 1956).

[5] M. R. Yearian and R. Hofstadter: *Phys. Rev.*, **110**, 552 (1958); R. Hofstadter, F. Bumiller and M. R. Yearian: to be published.

2. - Calculation results.

As the calculations are exactly similar to the case of scattering by protons, we shall not give any details of the calculations here — the interested reader is referred to the paper of ref. (2). In the terminology of that paper, the straightforward meson theoretical calculation (to order (e^2G^2)) leads to the Rosenbluth-formula (6) for the differential cross-section,

$$(1) \qquad \sigma(\theta) = \left(\frac{e^2}{2E}\right)^2 \frac{\cot^2(\theta/2)\cdot \operatorname{cosec}^2(\theta/2)}{1+(2E/M)\sin^2(\theta/2)} \cdot \left[F_{1n}^2 - \frac{1}{4}\frac{\boldsymbol{q}^2}{M^2}\left\{2(F_{1n}+\mu_n F_{2n})^2 \operatorname{tg}^2\frac{\theta}{2} + \mu_n^2 F_{2n}^2\right\}\right],$$

where θ is the angle of scattering, and E the energy of the incident electrons in the laboratory system, and the four-momentum transfer $\boldsymbol{q}$ is given by

$$(2) \qquad \boldsymbol{q}^2 = \frac{-4E^2\sin^2(\theta/2)}{1+(2E/M)\sin^2(\theta/2)} .$$

The rest mass of the electron has been neglected here. F_{1n} and F_{2n}, which are essentially functions of $\boldsymbol{q}^2$, are the so-called charge and magnetic moment form-factors of the neutron, respectively. μ_n is the anomalous magnetic moment of the neutron. What is now determined by meson-theory are the values of F_{1n}, F_{2n} as well as μ_n. The theoretical value of μ_n is (2), in nuclear magnetons:

$$(3) \qquad \mu_n = \frac{G^2}{4\pi^2}\gamma_n ,$$

where γ_n depends on the cut-off K_0. It is this value of the anomalous magnetic moment which we use (and must use if we wish to be consistent) in the cross-section formula, and not the experimental value as is done in the phenomenological fitting by HOFSTADTER *et al.* (5). In equation (3), G is the coupling constant for pseudoscalar coupling and is also used to represent $2MF/\mu$, F being the pseudovector coupling constant. Using this notation, μ_n is the same for both the couplings.

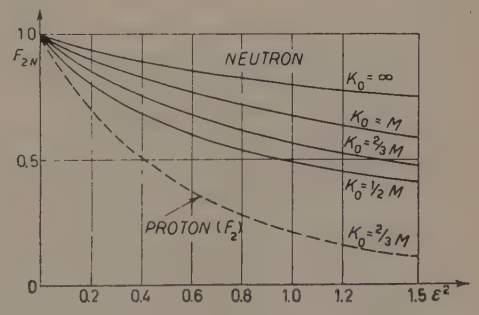

Fig. 1. – The magnetic moment form-factor of the neutron, F_{2n}, plotted as a function of ε^2 $(=-\boldsymbol{q}^2/M^2)$ for different values of K_0. For comparison a curve for the proton (shown dotted) is also given.

(6) M. N. ROSENBLUTH: *Phys. Rev.*, **79**, 615 (1950).

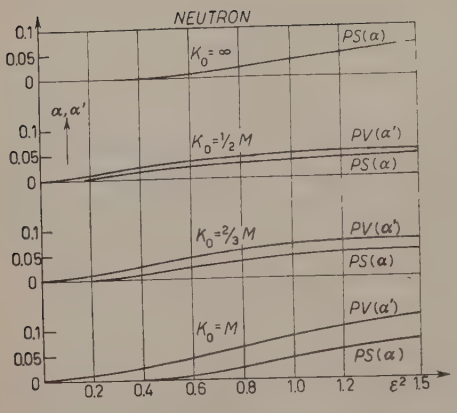

Fig. 2. – α (ps-coupling) and α' (pv-coupling) plotted as functions of ε^2 ($= -q^2/M^2$) for different values of K_0. α, α' multiplied by $-G^2/8\pi^2$ give the charge form-factor of the neutron, F_{1n}; for the two couplings.

The magnetic moment form factor, F_{2n}, is independent of the coupling constant, but is dependent on K_0 and is the same for both the couplings. Fig. 1 shows F_{2n} plotted as a function of the scattering parameter ε^2 ($= -q^2/M^2$) for various values of the cut-off. For comparison we also give in the figure one such curve for the proton.

F_{1n}, on the other hand, is different for the two couplings, the difference being very small for K_0 not much larger than M. For $K_0 = \infty$, however, the pseudovector coupling will give a divergent result. On the other hand, we find that F_{1n} is negligibly small for pseudoscalar coupling for all K_0 and for pseudovector coupling for K_0 not much larger than M. It therefore plays almost no part in the electron-neutron scattering. This is also the result found by HOFSTADTER and coworkers [5] experimentally. F_{1n}, which depends both on the coupling constant as well as the cut-off, can be expressed as:

$$F_{1n} = -\frac{G^2}{8\pi^2}\alpha, \qquad \text{for ps-coupling,} \tag{4}$$

$$= -\frac{G^2}{8\pi^2}\alpha', \qquad \text{for pv-coupling } G = \left(\frac{2MF}{\mu}\right).$$

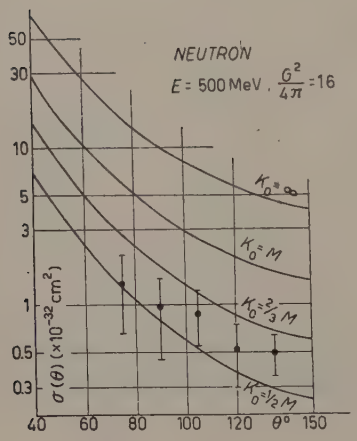

Fig. 3. – Differential cross-section for the scattering of 500 MeV electrons by neutrons plotted as a function of the laboratory angle of scattering. The values of K_0 and coupling constant are indicated in the figure. F_{1n} being negligible, the curves are the same for both the couplings excepting the curve for $K_0 = \infty$ which is for ps-coupling only.

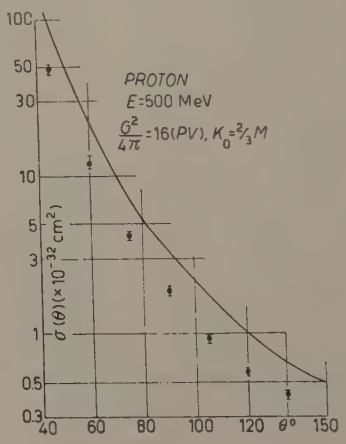

Fig. 4. – Differential cross-section for the scattering of 500 MeV electrons by protons plotted as a function of the laboratory angle of scattering, for $K_0 = \frac{2}{3}M$ and $G^2/4\pi = 16$ with pv-coupling.

where α and α' are functions of ε^2 and the cut-off. These are plotted in Fig. 2 and are seen to be very small.

Finally, in Fig. 3 we give the scattering cross-section, for 500 MeV electrons scattered by neutrons, as a function of the angle of scattering. For comparison with the proton case we also give similar results for electron-proton scattering in Fig. 4.

It will be noticed that the dependence of on K_0 has the opposite trend to that of the proton case, since for $K_0 \to 0$ the mesonic effects are eliminated. The meson cloud diminishes the scattering for the proton but is the only contibutor to the scattering for the neutron case.

3. - Discussion of the results - Conclusions.

For electron-proton scattering (2), we had found that excellent agreement with experiments could be obtained for many different suitable choices of the two parameters, K_0 and $G^2/4\pi$, involved. Thus, for $K_0 = \frac{3}{2}M$ and $G^2/4\pi = 31$ we had almost a perfect fit. Again for $G^2/4\pi = 16$ and $K_0 = \infty$ (only for ps-coupling, pv-coupling diverges in this case) the fit was very good. Therefore, what the best choice should be could not be determined by electron-proton scattering alone. But our results on electron-neutron scattering radically change this picture. We find that a theory without cut-off is completely ruled out by the data on electron-neutron scattering. It is absolutely essential to have a cut-off of the order of the nucleon mass, M, if we are to be able to come anywhere near the experimental values, for reasonable choices of the coupling constant. The situation is now very similar to the case of the anomalous magnetic moments of the neutron and the proton. Both of these cannot be simultaneously fitted to their experimental values in a second order perturbation calculation — though a cut-off of the order of the nucleon mass improves the situation a great deal (2). We find that if we wish to fit both the electron-neutron and the electron-proton scattering data simultaneously, the optimum values of the parameters involved are $K_0 = \frac{2}{3}M$ and $G^2/4\pi = 16$ ($F^2/4\pi \simeq 0.08$). The fit is, of course, then not perfect in either case — which is, naturally, to be expected in a lowest order perturbation calculation. But the agreement is then reasonable for both the data within a factor of 2. This is a very encouraging result, for the value of $K_0 = \frac{2}{3}M$ agrees very well with the cut-off required by the mass-difference of the charged and neutral π-mesons (3). At the same time the choice $G^2/4\pi = 16$, ($F^2/4\pi \simeq 0.08$) and $K_0 = \frac{2}{3}M$ is also the one required for fitting the data on pion-nucleon scattering (7).

This agreement between the values of K_0 required by three different phenomena indicates the universality of the cut-off. We may conclude, that meson-theory with this universal cut-off is in a position to explain the electron-nucleon scattering.

* * *

The author wishes to express his grateful thanks to Professor W. Heitler for his continued encouragement throughout this work. His sincere thanks are also due to the Swiss Atomic Energy Commission for financial aid.

(7) G. F. Chew: *Phys. Rev.*, **94**, 1748, 1755 (1957) and subsequent papers.

IL NUOVO CIMENTO Vol. X, N. 3 1° Novembre 1958

Preliminary Results on Nuclear Interactions of K^+-Mesons in the Energy Region (240÷300) MeV.

D. Keefe, A. Kernan and A. Montwill
University College - Dublin

(ricevuto l'11 Agosto 1958)

A total of 144 stars produced by K^+-mesons have been found during a track scan of 72 m of heavy meson track length in a stack (K_4) of photographic emulsion exposed to the separated 300 MeV K^+ beam at the Bevatron. The nominal beam momentum at entry to the stack was 625 MeV/c, the heavy mesons being produced in copper at 60° to the 6.2 GeV proton beam, and passed through a Beryllium degrader 26 in. thick. The actual energy at entry of the K-particles is 304 MeV.

The π to K ratio observed in the stack was about 2 : 1, but there was little trouble distinguishing between the two sorts of tracks since the blob density was about 30% higher in the K-meson tracks than the π-meson tracks, the latter having the minimum value. The K-meson tracks were chosen for following by line scanning 15 mm from the entry of the beam across the direction of motion, and selecting those tracks which, on the basis of counting 300 blobs, had a blob density within 10% of the expected value. (All plates were normalised by measuring the blob density in the π-meson tracks). As an additional check all tracks were blob-counted after ~ 8 cm, near their exit, to ensure that no error in following through had resulted in picking up a π-meson track in the process. Only 2% of the total track length followed was in fact due to π-mesons or protons.

A summary of the type of events found is shown in Table I. The angles of scattering in the CM system for the 4 K-H scatters found are 80°, 98°, 108°, and 136°.

Table I. – *Events found in* 72 m *of* K^+ *track.*

	Inelastic scatters	Charge exchange	K-H	Decay in flight
Number	94	46	4	16
Cross-section	280 mb	138 mb	17 mb	

The measured mean-free path in emulsion for nuclear interactions (including K-H) is 51 ± 5 cm and the fraction of charge exchange events among the *total* is 0.32. No event in which a charged π-meson was certainly created has been found.

Fig. 1 shows a plot of the fractional energy loss ΔE, versus the laboratory angle of scatter θ for the non-charge-exchange events. The full line shows

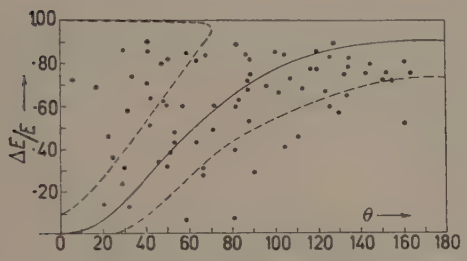

Fig. 1.

the variation expected for a K-meson striking a stationary nucleon. The region between the dashed curves is that allowed for collisions with nucleons of a Fermi gas with maximum momentum 215 MeV/c. From the scattering of the points outside this area it is clear that a large fraction of the events cannot be interpreted in terms of single scattering of the meson from just one nucleon within the nucleus. This is to be expected since an approximate calculation of the fraction of cases in which double scattering within a nucleus is expected to occur gives an answer of $\sim 30\%$ based on the formula of ref. (1).

The high proportion of events where the K-meson nucleus collision cannot be interpreted as an interaction with just one nucleon of the nucleon gas, makes an analysis of the events in the CM system of the meson and assumed target nucleon (such as for example was carried out in (2)), only very approximate.

In order to obtain some rough idea of the behaviour of the CM differential cross-section on an « average » nucleon, the very simple model of a stationary target nucleon was assumed. The angle of scattering of the K-meson in the Laboratory System, θ, and the inelasticity ΔE for each event were not in general in agreement with this hypothesis and so two angles in the CM frame, χ_{I} and χ_{II} could be computed. The better the approximation the more closely one expects χ_{I} and χ_{II} to approach each other. Fig. 2 shows the pairs of values (χ_{I}, χ_{II}) obtained for each event and the dashed lines show the limits of spread possible for collisions with a Fermi gas of nucleons ($P_{\max} = 215$ MeV/c). Again, one sees that about one third of the points do not conform with the picture of a single meson-nucleon collision. The most significant feature of the diagram is that of the points which *do lie within* the allowed region compatible with single scattering, the great majority correspond to strong backward scattering in the CM system, whether the CM angle is computed from the angle θ or the inelasticity ΔE in the Laboratory frame.

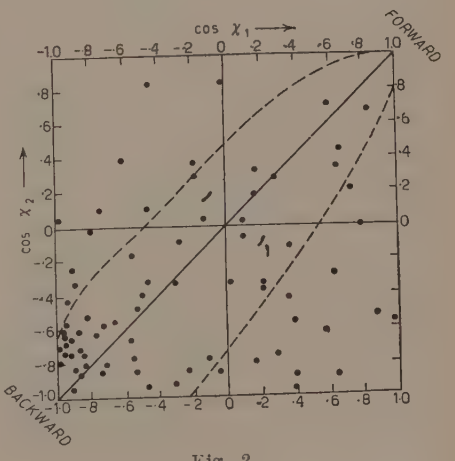

Fig. 2.

The data collected at the Geneva Conference on K-H interactions in this energy region (3) indicate a total cross-

(1) K. A. Brueckner, R. Serber and K. M. Watson: *Phys. Rev.*, **84**, 258 (1951).

(2) B. Bhowmik, D. Evans, S. Nilsson, D. Prowse, F. Anderson, D. Keefe, A. Kernan and J. Losty: *Nuovo Cimento*, **6**, 410 (1957).

(3) Reports of B.N.L., Bristol, Dublin U.C., Padua and U.C.L.A. groups; *Proc. Geneva Conference* (June 1958).

section of ~ 20 mb (to be compared with 14 mb at ~ 100 MeV), and a differential cross-section without any strong departures from isotropy. Thus apart from a slight increase in strength and a slight backward peaking there appears to be no serious change in the $T=1$ interaction. However, compared with the results on K^+ interactions at ~ 100 MeV, the rapid increase in nuclear absorption at the present energy, the high fraction, 0.32, of charge exchange events (if only single scattering had occurred in each nucleus this figure would have been 0.29), and the suggestion of strong backward scattering shown by a crude examination of conditions in the CM frame, are all most easily interpreted in terms of a change in the K-neutron interaction, in particular that part involving the $T=0$ state. The rapid change from the relatively small $T=0$ contribution at the lower energy to a significant one at ~ 270 MeV would support the evidence from the anisotropy (if confirmed) that this Isotopic Spin state was associated with an angular momentum state other than $l=0$.

* * *

We are greatly indebted to Dr. E. J. LOFGREN and the staff of his laboratory for the exposure of the stack and to Professor C. F. POWELL and his colleagues at Bristol for the processing of the plates, and to the groups at Padua, U.C.L.A. and Bristol for exchanges of information.

IL NUOVO CIMENTO Vol. X, N. 3 1° Novembre 1958

Some Features of the Electron Energy Spectrum in the K_{e3} Decay Process.

S. Furuichi (*), S. Sawada and M. Yonezawa

Department of Physics, Hiroshima University - Hiroshima

(ricevuto il 26 Agosto 1958)

In order to circumvent the difficulty that we have not detailed information of the effective coupling constants in the analysis of the K_{e3} decay process, it has been proposed to examine various physical quantities in correlation with the fixed pion energy (1). In this short note we will show that there exist some characteristic features in the theoretical energy spectrum of the electron in the K_{e3} decay process and the experimental analysis of these simple features seems to be easier than the investigation for the correlation with the pion energy.

For the benefit of the later discussions, we will at first give the electron-pion energy correlation function. Starting with the same transition matrices of the previous article, it is given by (2)

$$(1)\quad \mathcal{D}(p_0, l_0) \sim |F^S(l_0)|^2(W_\pi - l_0) + |F^V(l_0)|^2 m_K\{2p_0(m_K - l_0 - p_0) - m_K(W_\pi - l_0)\} +$$
$$+ |F^T(l_0)|^2 m_K^2(W_\pi - l_0)(m_K - l_0 - 2p_0)^2 + 2\,\mathrm{Re}\,[F^S(l_0)F^{T*}(l_0)]m_K(W_\pi - l_0)(m_K - l_0 - 2p_0),$$

and the available energy range of the electron for a fixed pion energy l_0 is

$$(2)\qquad p_{0_{\min}}^{\max} = (m_K - l_0 \pm l)/2\,,$$

$W_\pi = (m_K^2 + m_\pi^2)/2m_K$: available maximum energy of the pion;
m_K: K-meson mass;
p_0: electron energy;
l_0: pion energy;
l: pion momentum;

(*) Now at Department of Physics, Rikkyo University, Tokyo.

(1) Cf. for example A. Pais and S. B. Treiman: *Phys. Rev.*, **105**, 1616 (1957); S. Furuichi, S. Sawada and M. Yonezawa: *Nuovo Cimento*, **7**, 718 (1958).

(2) S. Furuichi, T. Kodama, S. Ogawa, Y. Sugahara, A. Wakasa and M. Yonezawa: *Progr. Theor. Phys.*, **17**, 89 (1957).

where the mass of the electron is neglected. As is seen in (1) the S-V and V-T interference terms do not appear. The general electron energy spectrum for the fixed pion energy is a polynomial of second degree in powers of the electron energy p_0. For an arbitrary pion energy, the pure scalar distribution is constant and the vector and the tensor give the spectra which are symmetric with respect to the middle point of the available energy range (2). $F^S(l_0)^2, \ldots$ can be given experimentally if the energy of the pion is given. However the experimental investigation of the pion energy spectrum is not an easy task and it will take time before the experimental data are sufficiently accumulated. In this note we will consider the expression (1) not assuming any particular assumptions about the effective coupling constants. We should like to note in connection with the present experimental indication that the actually meaningful bimodal distribution can be realized only with tensor interaction ([3]).

We propose here to investigate the quantity R which is the ratio of high energy secondary electrons to low energy electrons defined as

$$R = \frac{\text{number of electrons with energy} > W_e/2}{\text{number of electrons with energy} < W_e/2},$$

where W_e is the available maximum energy of the electron and is given by

$$W_e = (m_K^2 - m_\pi^2)/2m_K .$$

The theoretical lower limit of this ratio $R_{\min}$ can be given by

$$R_{\min} = \min \frac{\int_{m_\pi}^{W_\pi} \mathrm{d}l_0 \int_{W_e/2}^{p_0^{\max}} \mathrm{d}p_0 \, \mathcal{D}(p_0, l_0)}{\int_{m_\pi}^{W_\pi} \mathrm{d}l_0 \int_{p_{0\min}}^{W_e/2} \mathrm{d}p_0 \, \mathcal{D}(p_0, l_0)} = \min \frac{\int_{W_e/2}^{p_0^{\max}} \mathrm{d}p_0 \, \mathcal{D}(p_0, l_0)}{\int_{p_{0\min}}^{W_e/2} \mathrm{d}p_0 \, \mathcal{D}(p_0, l_0)},$$

where min means the minimum when all possibilities are granted for the energy dependence of the effective coupling constants. $R_{\min}$ can easily be calculated from the expression of the electron-pion energy correlation function (1). It gives

$$R_{\min} \sim 1 \quad \text{for any case when the } S\text{-}T \text{ interference does not exist},$$

$$\sim 0.07 \quad \text{for the case when } S\text{-}T \text{ interference exists}.$$

([3]) In the case of pure tensor interaction, the height of the first peak h_1 is always lower than the height of the second peak h_2. If the bimodal feature is the real one and h_1 is higher than h_2; this is the indication of scalar interaction in addition to the tensor interaction.

The accumulation of the experimental data of K^+_{e3} so far reported is given in Fig. 1 (4).

The data seem to show the bimodal feature and the preponderance of low energy electrons over high energy ones.

The small R value of the present experimental data ($R \sim 17/26 \sim 0.65$) (5) can be only explained by the existence of the S-T interference term. If the experiment can confirm $R < 1$, then it will afford some critical information for the arguments of the type of decay interaction.

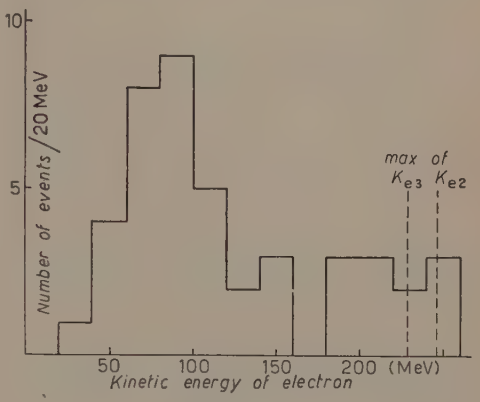

Fig. 1.

The importance of the K^+_{e3} spectrum must be especially emphasized in connection with the present situation that there is no strong evidence which is unfavorable for the universal weak Fermi V-A theory (6), while the present experimental data of K^+_{e3} give the suggestion that their decay interaction contains S and T and the V-A theory has rather small chance to explain the spectrum.

We remark that if the relative phase of S and T is $(2n+1)\pi/2$ which means the maximum violation of time-reversal invariance (7), the S-T interference vanishes and no solution consistent with the present experiment is obtainable. In such case we must consider other possibilities such as a Konopinski-Uhlenbeck type of weak interaction. Further investigation on these points will be discussed elsewhere.

---

(4) M. W. Friedlander, D. Keefe, M. G. K. Menon and L. Van Rossum: *Phil. Mag.*, **45**, 1043 (1954); M. G. K. Menon and C. O'Ceallaigh: *Proc. Roy. Soc.*, **221** A, 292 (1954); C. Dahanayake, P. E. Francois, Y. Fujimoto, P. Iredale, C. J. Waddington and M. Yasin: *Phil. Mag.*, **45**, 1219 (1954); R. H. Johnston and C. O'Ceallaigh: *Phil. Mag.*, **46**, 393 (1955); D. M. Ritson, A. Pevsner, S. C. Fung, M. Widgoff, G. T. Zorn, S. Goldhaber and G. Goldhaber: *Phys. Rev.*, **101**, 185 (1956); J. Crussard, V. Fouché, J. Hennessy, G. Kayas, L. Leprince-Ringuet, D. Morellet and F. Renard: *Nuovo Cimento*, **3**, 731 (1956); **4**, 1195 (1956); G-stack collaboration: *Nuovo Cimento*, **2**, 1063 (1955); W. A. Cooper, H. Filthuth, J. A. Newth and R. A. Salmeron: *Nuovo Cimento*, **4**, 390 (1956); R. W. Birge, D. H. Perkins, J. R. Peterson, D. H. Stork and M. N. Whitehead: *Nuovo Cimento*, **4**, 834 (1956); J. Orear, G. Harris and S. Taylor: *Phys. Rev.*, **104**, 1463 (1957); G. Alexander, R. H. W. Johnston and C. O'Ceallaigh: *Nuovo Cimento*, **6**, 478 (1958).

(5) This value will be reduced if the K_{e3} mode of K-meson decay exists.

(6) R. P. Feynman and M. Gell-Mann: *Phys. Rev.*, **109**, 193 (1958).

(7) S. Furuichi: *Nuovo Cimento*, **7**, 269 (1958).

IL NUOVO CIMENTO Vol. X, N. 3 1° Novembre 1958

Symmetry Properties of Clebsch-Gordon's Coefficients.

T. Regge

Istituto Nazionale di Fisica Nucleare - Sezione di Torino

(ricevuto il 23 Settembre 1958)

It has been known since long that the coefficients for the composition of angular momenta possess a symmetry group of 12 elements. This group consists of the 6 permutations of 3 angular momenta and of the space reflection.

The physical significance of these symmetries is evident and it led very early to their discovery. However a more elaborate analysis shows that they are part of a much larger group of 72 elements. Unnecessary details of the proof will be omitted here. For a better understanding of the symmetry properties we shall employ a different notation for the coefficients as follows:

$$(1)\qquad \begin{pmatrix} a & b & c \\ \alpha & \beta & \gamma \end{pmatrix} = \begin{array}{|ccc|} \hline b+c-a & c+a-b & a+b-c \\ a-\alpha & b-\beta & c-\gamma \\ a+\alpha & b+\beta & c+\gamma \\ \hline \end{array}\ .$$

The 9 elements of the square symbol at the right are bound by 4 equations. In fact all sums by rows and columns are equal to $a+b+c=J$. Moreover all elements are non-negative integers. We shall define also a square symbol in the case when it does not satisfy the above restrictions by letting it vanish. Clebsch-Gordon coefficients are defined by the expansion (1):

$$(2)\quad (v_1u_2-u_1v_2)^{a+b-c}(w_1v_2-w_2v_1)^{b+c-a}(u_1w_2-w_1u_2)^{c+a-b} =$$
$$= \sqrt{(J+1)!\,(a+b-c)!\,(b+c-a)!\,(c+a-b)!}\sum_{\alpha\beta\gamma}\begin{pmatrix} a & b & c \\ \alpha & \beta & \gamma \end{pmatrix}\cdot$$
$$\cdot\frac{u_1^{a-\alpha}u_2^{a+\alpha}}{\sqrt{(a+\alpha)!\,(a-\alpha)!}}\,\frac{v_1^{b-\beta}v_2^{b+\beta}}{\sqrt{(b-\beta)!\,(b+\beta)!}}\,\frac{w_1^{c-\gamma}w_2^{c+\gamma}}{\sqrt{(c-\gamma)!\,(c+\gamma)!}}\cdot$$

By multiplying both sides of this equation by:

$$u_3^{b+c-a}\,v_3^{c+a-b}\,w_3^{a+b-c}\,\frac{1}{(a+b-c)!\,(b+c-a)!\,(c+a-b)!}\,,$$

where u_3, v_3, w_3 are parameters and summing upon all values of a, b, c compatible with the triangular inequality, the left term, if J is kept fixed, becomes the J-th power of a determinant. The right term assumes a most symmetrical form upon introduction of the square symbol:

$$(3)\qquad \begin{vmatrix} u_1 & v_1 & w_1 \\ u_2 & v_2 & w_2 \\ u_3 & v_3 & w_3 \end{vmatrix}^J =$$

$$= \binom{2J-1}{J!}^{\frac{1}{2}} \cdot \sum_{\sum_{is} A_{is} = 3J} \boxed{\begin{matrix} A_{11} & A_{21} & A_{31} \\ A_{12} & A_{22} & A_{32} \\ A_{13} & A_{23} & A_{33} \end{matrix}} \frac{u_1^{A_{11}} u_2^{A_{12}} u_3^{A_{13}} v_1^{A_{21}} v_2^{A_{22}} v_3^{A_{23}} w_1^{A_{31}} w_2^{A_{32}} w_3^{A_{33}}}{(A_{11}!\, A_{12}!\, A_{13}!\, A_{21}!\, A_{22}!\, A_{23}!\, A_{31}!\, A_{32}!\, A_{33}!)^{\frac{1}{2}}}.$$

Under this form the properties of $C\cdot G$ symbols appear in full light:

a) The square is multiplied by $(P)^J$ $(P=\pm 1)$ by permutations of columns of parity P. These are known symmetries.

b) The same happens for rows. The exchange of the lowest rows is space reflection. The others are entirely new.

c) Rows can be exchanged with columns. Also this symmetry is new.

Wigner's $9-j$ symbol shows similar properties.

Thus far we cannot justify these symmetries using simple physical arguments. Work is in progress in order to check whether these additional properties entail some consequences for Racah's W coefficients and Wigner's $9-j$ symbols.

* * *

I wish to thank particularly Prof. G. Racah for many fruitful discussions and kind encouragement.

IL NUOVO CIMENTO Vol. X, N. 3 1° Novembre 1958

A Remark on Conservation Rules.

P. Roman

Department of Theoretical Physics - The University - Manchester

(ricevuto il 26 Settembre 1958)

This note investigates the unambiguity of the differential dynamical quantities of a system.

Suppose a physical system is characterised by the action integral

$$W = \int_R L(x_\mu, \psi_a(x), \partial_\mu \psi_a(x))\, \mathrm{d}x ,$$

extended over an arbitrary space-time region. The equations of motion, following from Hamilton's principle, are then the Euler-Lagrange equations. It is well known (see *e.g.* [1-3]) that if W is invariant under some symmetry transformation

$$x_\mu \to x'_\mu ,$$

$$\psi_a(x) \to \psi'_a(x') ,$$

then

$$(1) \quad \delta W \equiv 0 = \int_{R'} L'(\psi'(x'), \ldots)\, \mathrm{d}x' - \int_R L(\psi(x), \ldots)\, \mathrm{d}x =$$

$$= \int_R \left\{ D_\mu \left[\left(L\delta_{\mu\nu} - \frac{\partial L}{\partial \partial_\mu \psi} \partial_\nu \psi \right) \delta x_\nu + \frac{\partial L}{\partial \partial_\mu \psi} \delta \psi \right] \right\} \mathrm{d}x ,$$

i.e. the *conservation rule*

$$(1a) \qquad D_\mu f_\mu = 0 ,$$

---

[1] E. Noether: *Nachr. d. kgl. Ges. d. Wiss. Göttingen*, p. 235, (1918).
[2] E. L. Hill: *Rev. Mod. Phys.* **23**, 253 (1951).
[3] P. Roman: *Acta Phys. Hung.*, **5**, 143, (1955).

follows, with

$$f_\mu = \left(L\delta_{\mu\nu} - \frac{\partial L}{\partial \partial_\mu \psi}\, \partial_\nu \psi \right) \delta x_\nu + \frac{\partial L}{\partial \partial_\mu \psi}\, \delta\psi \,. \tag{2}$$

Here

$$\delta x_\nu = x'_\nu - x_\nu \,,$$

$$\delta\psi = \psi'(x') - \psi(x) \,,$$

are the changes of x and ψ under the infinitesimal element of the symmetry group and D_μ is the « complete » partial differentiation symbol

$$D_\mu \equiv \partial_\mu + \partial_\mu \psi \frac{\partial}{\partial \psi} + \partial_\mu \partial_\nu \psi \frac{\partial}{\partial \partial_\nu \psi} \,, \tag{2a}$$

which we will use consistently to avoid confusion.

It is also known that if one replaces L by $L^{(1)} = L + F$ where

$$F = D_\mu \Phi_\mu \,,$$

and the arbitrary functions Φ_μ may depend on the ψ but not on their derivatives, then $W^{(1)} = \int_R L^{(1)} \mathrm{d}x$ leads to the same equations of motion. Indeed, one can show (see ref. (2), p. 256) that F alone satisfies the Euler-Lagrange equations:

$$\frac{\partial F}{\partial \psi} - D_\mu \frac{\partial F}{\partial \partial_\mu \psi} = 0 \,. \tag{A}$$

Also, the addition of F should not destroy the symmetry properties of W. The criterion that a transformation group is a symmetry group of the system, has been explicitly demonstrated by Hill (2), eq. (36). As L satisfies this condition, we need for F

$$\delta x_\mu \partial_\mu F + \delta\psi \frac{\partial F}{\partial \psi} + \delta \partial_\mu \psi \frac{\partial F}{\partial \partial_\mu \psi} + F \partial_\mu \delta x_\mu = - D_\mu \delta \Omega_\mu \,, \tag{B}$$

where the Ω_μ are arbitrary functions which may depend on ψ.

Now it is clear that even though the replacement of W by $W^{(1)}$ will still lead to the same conservation rule, the actual form of the « conserved » density quantities f_μ will be in general changed to same $f_\mu^{(1)}$. This seems to be rather unsatisfactory because it makes the definition of the differential dynamical quantities ambiguous. In the following we want to find *a criterion which the added four divergence F must satisfy in order to leave the differential dynamical quantities unchanged.*

Remembering (1), (1*a*) and (2), clearly we must *demand* that

$$\delta W^{(1)} - \delta W = \delta \int_R F \,\mathrm{d}x = \int_R \left\{ D_\mu \left[\left(F\delta_{\mu\nu} - \frac{\partial F}{\partial \partial_\mu \psi}\, \partial_\nu \psi \right) \delta x_\nu + \frac{\partial F}{\partial \partial_\mu \psi}\, \delta\psi \right] \right\} \mathrm{d}x \equiv \int_R I \,\mathrm{d}x = 0 \,. \tag{3}$$

Here

$$I = \delta x_\mu D_\mu F + \partial_\mu \delta x_\mu \cdot F - \left(D_\mu \frac{\partial F}{\partial \partial_\mu \psi} \right) \partial_\nu \psi \delta x_\nu - \frac{\partial F}{\partial \partial_\mu \psi} \partial_\mu \partial_\nu \psi \cdot \delta x_\nu -$$

$$- \frac{\partial F}{\partial \partial_\mu \psi} \partial_\nu \psi \cdot \partial_\mu \delta x_\nu + \left(D_\mu \frac{\partial F}{\partial \partial_\mu \psi} \right) \delta \psi + \frac{\partial F}{\partial \partial_\mu \psi} \partial_\mu \delta \psi .$$

Calculating the first term explicitly by applying (2*a*) and using eq. (A) in the third and sixth term, we obtain:

$$I = \delta x_\mu \partial_\mu F + \partial_\mu \delta x_\mu \cdot F - \frac{\partial F}{\partial \partial_\mu \psi} \partial_\nu \psi \cdot \partial_\mu \delta x_\nu + \frac{\partial F}{\delta \psi} \delta \psi + \frac{\partial F}{\partial \partial_\mu \psi} \partial_\mu \delta \psi .$$

By eq. (B) this reduces to

$$I = - D_\mu \delta \Omega_\mu - \frac{\partial F}{\partial \partial_\mu \psi} (\delta \partial_\mu \psi - \partial_\mu \delta \psi + \partial_\nu \psi \cdot \partial_\mu \delta x_\nu) . \tag{4}$$

Introducing now for a moment the « local » variation

$$\delta^* \psi(x) = \psi'(x) - \psi(x) ,$$

which is connected to the « complete » variation by

$$\delta \psi = \delta^* \psi + \partial_\nu \psi \cdot \delta x_\nu ,$$

we have

$$\partial_\mu \delta \psi = \partial_\mu \delta^* \psi + \partial_\mu \partial_\nu \psi \cdot \delta x_\nu + \partial_\nu \psi \cdot \partial_\mu \delta x_\nu .$$

Noting that $\partial_\mu \delta^* = \delta^* \partial_\mu$ and that

$$\delta \partial_\mu \psi = \delta^* \partial_\mu \psi + \partial_\mu \partial_\nu \psi \cdot \delta x_\nu ,$$

we obtain

$$\partial_\mu \delta \psi = \delta \partial_\mu \psi + \partial_\nu \psi \cdot \partial_\mu \delta x_\nu ,$$

so that the coefficient of the second term in (4) vanishes and we are left with

$$I = - D_\mu \delta \Omega_\mu .$$

Thus our eq. (3) leads to

$$\int_R D_\mu \delta \Omega_\mu \, \mathrm{d}x = 0 ,$$

and, as R is arbitrary, this gives (*):

$$D_\mu \delta\Omega_\mu = 0 .$$

Substituting into (B), we obtain the desired condition which F must satisfy:

(C) $$\boxed{\delta x_\mu \partial_\mu F + \delta\psi \frac{\partial F}{\partial\psi} + \delta\,\partial_\mu\psi \frac{\partial F}{\partial\,\partial_\mu\psi} + F\partial_\mu \delta x_\mu = 0 .}$$

We consider briefly some special cases.

a) *Energy and momentum density.*
The corresponding conservation rule follows from invariance under the translations with

$$\delta x_\mu = a_\mu = \text{const}; \qquad \delta\psi = 0 .$$

Thus (C) simplifies to

$$\partial_\mu F = 0 ,$$

i.e. F must not depend explicitly on the co-ordinates.

b) *Angular momentum density.*
Conservation follows from invariance under

$$\delta x_\mu = \tfrac{1}{2}\varepsilon_{\alpha\beta} I^{\mu\nu}_{\alpha\beta} x_\nu \qquad \text{and} \qquad \delta\psi_a = \tfrac{1}{2}\varepsilon_{\alpha\beta} K^{ab}_{\alpha\beta}\psi_b ,$$

where $(\alpha\beta)$ characterise the plane of rotation;

$$I^{\mu\nu}_{\alpha\beta} = \delta_{\mu\alpha}\delta_{\nu\beta} - \delta_{\mu\beta}\delta_{\nu\alpha} ,$$

and $K_{\alpha\beta}$ is the representation of the rotation operator in the ψ-space. (C) gives then the set of equations

$$x_\beta \partial_\alpha F - x_\alpha \partial_\beta F + K^{ab}_{\alpha\beta}\psi_b \frac{\partial F}{\partial\psi_a} + K^{ab}_{\alpha\beta}\partial_\mu\psi_b \frac{\partial F}{\partial\,\partial_\mu\psi_a} = 0 .$$

For a spinless (scalar) field this simplifies to

$$x_\beta \partial_\alpha F - x_\alpha \partial_\beta F = 0 .$$

(*) Incidentally we note that this is equivalent to saying that if the theory was originally *form*-invariant, this must not be destroyed by adding F.

c) *Gauge transformations.*
Here

$$\delta x_\mu = 0\,, \qquad \delta\psi = i\alpha\psi\,, \qquad \delta\psi^+ = -i\alpha\psi^+\,,$$

so that we have

$$\psi\frac{\partial F}{\partial\psi} - \psi^+\frac{\partial F}{\partial\psi^+} + \partial_\mu\psi\frac{\partial F}{\partial\partial_\mu\psi} - \partial_\mu\psi^+\frac{\partial F}{\partial\partial_\mu\psi^+} = 0\,.$$

* * *

The author is indebted to Dr. E. Wolf who asked a question which sparked this investigation.

IL NUOVO CIMENTO Vol. X, N. 3 1° Novembre 1958

Search for Particles of Mass 500 m_e.

S. J. Bosgra and F. Bruin

Natuurkundig Laboratorium - Universiteit van Amsterdam

(ricevuto il 29 Settembre 1958)

In 1953 Alihaniyan *et al.* [1] reported a number of particles heavier than pions which were found in cosmic radiation. Due to the nature of the selecting mechanism the particles all had a momentum between 200 and 300 MeV/c. They had an average mass of 550 m_e, were positively charged and seemed to decay into charged pions or muons. Later investigations [2,3] indicated that these so called ζ-particles are very rare. Recently we investigated a large stack of Ilford G-5 emulsion exposed to a K^+-beam of the Berkeley Bevatron. No trace of a ζ was found.

The stack was the one exposed by Birge *et al.* for their K^+-decay modes experiment [4]. In this stack they located and identified about 2000 K^+-mesons and kindly supplied us with the emulsion and their scanning data. First measurements were carried out by M. Bruin of our group on particles found by area scanning in the region where a possible ζ-admixture of the K-beam should stop. No ζ-particles were identified. The statistical inaccuracy of the result yielded an upper limit for the eventual intensity of ζ's amounting to less than 4% of the K-beam intensity. From this it has been concluded that the ζ's found in the first experiment [1] were either confused with pions or could not have been produced in the same way or at the same primary energy as *e.g.* K-mesons. One assumption is that they were decay products of the known strange particles. The problem then remains why they were never found in emulsion exposed to the various beams of high energy accelerators. A reason could be that their identity remained hidden because the criteria used for the identification of the nuclear emulsion tracks were insufficient. We have checked the latter possibility for K^+-mesons.

If an analysis is made of the way in which the various decay modes of the K-meson have been classified it appears that there are two modes in which the secondary particles could have

(1) A. Alihaniyan, V. Kirillov-Ugryumov, N. Šostakovich and V. Fedorov: *Dokl. Akad. Nauk SSSR*, **92**, 255 (1953), see also: *Žu. Eksper. Teor. Fiz.*, **31**, 955 (1956).

(2) J. Steinberger: *CERN Conference on High Energy Particles* (Geneva, 1958).

(3) M. Conversi, E. Fiorini, S. Ratti, C. Rubbia, C. Succi and G. Torelli: *Nuovo Cimento*, **9**, 740 (1958).

(4) R. W. Birge, D. H. Perkins, J. R. Peterson, D. H. Stork and M. N. Whitehead: *Nuovo Cimento*, **4**, 834 (1956).

been ζ's, which by mistake were identified as pions or muons. The first case was investigated by HARRIS *et al.* [5] who checked a number of 51 $K_{\mu 3}$ decays. The second possibility probably was first suggested by S. GOLDHABER [6], who pointed out that the decay

$$K^+ \to \zeta^+ + \nu(+\pi^0), \quad \zeta^+ \to \pi^0 + \mu^+,$$

could have been identified as a $K'_{\pi 3}$ (or τ') decay if the mass of ζ would be about 500 m_e.

Out of 31 $K'_{\pi 3}$ mesons analyzed by BIRGE *et al.* we found that 28 had a decay muon of which the range could be measured accurately. Their mean range was equal to the range of muons from ordinary pion decay, namely 596 μm. Only 24 of the $K'_{\pi 3}$ secondary tracks were sufficiently flat to allow reliable scattering measurements. These were carried out on a Koristka MS 2 microscope. All decay products were compatible with the range of the pion mass, so that no evidence is found for K^+-meson decay products having the mass of about 500 m_e. Combining the results of HARRIS *et al.* with ours we conclude that the abundance of ζ-particles originating from K^+-meson decay is less than 0.1%.

* * *

This investigation has been carried out as part of the program of the Netherlands Institution F.O.M. It is a pleasure to thank Dr. R. W. BIRGE for suggesting the analysis and Prof. Dr. G. W. RATHENAU for stimulating discussions.

[5] G. HARRIS, J. OREAR and S. TAYLOR: draft *Padua-Venice Conference*, **6**, 49 (1957).

[6] Private communications from Dr. R. W. BIRGE.

IL NUOVO CIMENTO Vol. X, N. 3 1° Novembre 1958

A Comparison of the Born and the Asymptotic W.K.B. Approximation for the Phase Shift.

T. Tietz

University Łódź Department of Theoretical Physics - Łódź.

(ricevuto il 29 Settembre 1958)

As known the phase shift may be obtained from the W.K.B. solution of the radial Schrödinger equation.

$$d^2R_l/dr^2 + [k^2 - U(r) - l(l+1)/r^2]R_l = 0 , \tag{1}$$

where

$$k = \sqrt{2mE}/\hbar = mv/\hbar \qquad \text{and} \qquad U(r) = (2m/\hbar^2)V(r) .$$

In the asynptotic W.K.B. approximation the phase shift is given by [1]

$$\eta_l\,(\text{W.K.B.}) = -\frac{1}{2}\int_{(l+\frac{1}{2})/k}^{\infty} \frac{U(r)}{[k^2 - (l+\frac{1}{2})^2/r^2]^{\frac{1}{2}}}\,dr , \tag{2}$$

The Born approximation for the phase shift η_l as known is given by the following formula

$$\eta_l\,(\text{Born}) = -\frac{\pi m}{\hbar^2}\int_0^{\infty} V(r)[I_{l+\frac{1}{2}}(kr)]^2 r\,dr . \tag{3}$$

The asymptotic approximation is valid when the centrifugal barrier is large compared to the potential at distances of about $[l(l+1)]^{\frac{1}{2}}/k$. The above mentioned condition for the W.K.B. asymptotic W.K.B. approximation is the same for the Born approximation. In this paper we compare the validity of the Born and asymptotic W.K.B. approximation for the Coulomb potentials of the nucleus, which is modified by the screening effect of the orbital electrons of the nucleus, *e.g.* the Thomas-Fermi potential, as also for the Yukawa potential. The interaction potential in the Thomas-

[1] W. Henneberg: *Zeits. f. Phys.*, **83**, 555 (1933).

Fermi theory (2) may be written as

$$V(r) = -\frac{Ze^2}{r}\Phi(x), \quad \text{where} \quad \frac{r}{x} = \mu = 0.88534 a_0 Z^{-\frac{1}{3}}. \tag{4}$$

Z is the atomic number and a_0 is the first Bohr radius of hydrogen. If we adopt for the Thomas-Fermi function $\Phi(x)$ the following expression

$$\Phi(x) = \sum_{i=1}^{3} a_i \exp[-b_i x], \tag{5}$$

where a_i and b_i are constants, and $\sum_{i=1}^{3} a_i = 1$, then equations (4), (5) and (2) give (3) us for η_l (W.K.B.) the following formula (4).

$$\eta_l\,(\text{W.K.B.}) = \frac{Z}{\sqrt{E}} \sum_{i=1}^{3} a_i K_0(u_i), \quad \text{where} \quad u_i = \frac{b_i(2l+1)}{2\mu\sqrt{E}}. \tag{6}$$

In the last formula K_0 is the modified Bessel function of the second kind. For the Born approximation η_l (Born) we obtain (5) the following formula.

$$\eta_l\,(\text{Born}) = \frac{Z}{\sqrt{E}} \sum_{i=1}^{3} a\, Q_l[w_i], \quad \text{where} \quad w_i = 1 + \frac{1}{2}\left(\frac{b_i}{\mu\sqrt{E}}\right)^2.$$

Q_l are the Legendre functions of the second kind. In Table I we have a comparison of η_l (W.K.B.)/η_l (Born) as a function of $1/2\mu\sqrt{E}$.

TABLE I. – $\eta_l\,(W.K.B.)/\eta_l\,(Born)$ *as a function of* $1/2\mu\sqrt{E}$.

l	$1/2\mu\sqrt{E}$	η_l (W.K.B.)/η_l (Born)	l	$1/2\mu\sqrt{E}$	η_l (W.K.B.)/η_l (Born)
0	1	1.1249	0	0.1	1.0505
1		1.0127	1		1.0109
2		1.0039	2		1.0049
0	0.5	1.0988	0	0.01	1.0245
1		1.0187	1		1.0044
2		1.0058	2		1.0020

Table I shows that only for $l=0$, $l=1$, η_l (Born) differs from η_l (W.K.B.) and the difference decreases if E increases. In Table II we have a comparison for

(2) For reference see P. GOMBÁS: *Die statistische Theorie des Atoms und ihre Anwendungen* (Wien, 1949).

(3) In this paper we calculate in atomic units $e=1$, $a_0=1$ and the energy E in units of $e^2/2a_0$. We adopt these units in order to compare them with HENNEBERG's results.

(4) This formula we have obtained using the formula (4), of J. BERTRAND: *Traité de calcul différentiel et de calcul intégral* (Paris, 1870), p. 190.

(5) G. N. WATSON: *Theory of Bessel Functions* (Cambridge, 1952), p. 389.

η_l (Born) and η_l (W.K.B.) with the numerical results of Henneberg for $E = Z^2$ and $Z = 80$. For the constants appearing in equations (6) and (7) we adopt the Molière values $a_1 = 0.35$; $a_2 = 0.55$; $a_3 = 0.1$; $b_1 = 0.3$; $b_2 = 1.2$; $b_3 = 6$.

TABLE II. – *A comparison of* η_l *(W.K.B.) and* η_l *(Born) with the numerical values of Henneberg for* $E = Z^2$; $Z = 80$.

l	Numerical values of Henneberg	Molière approximate solution of the Thomas-Fermi function	
		η_l (W.K.B.)	η_l (Born)
0	203°	215° 04′	208° 20′
1	157°	153° 20′	152° 01′
2	129° 50′	125°	124° 38′
3	111° 30′	107° 05′	106° 57′

Table II shows that η_l (W.K.B.) and η_l (Born) differ from each other for $l > 1$ very little, and the difference between η_l (W.K.B.) and η_l (Born) as also the numerical values of Henneberg decrease if l increases.

If we adopt for the Yukawa potential the notation of Fogel ([6]) namely

$$U(r) = -b \exp[-r]/r \qquad \text{and} \qquad \varkappa = 2k\,, \tag{8}$$

then we obtain for the asymptotic W.K.B. approximation the following formula for the phase shift.

$$\eta_l\,(\text{W.K.B.}) = \frac{b}{\varkappa} K_0\left(\frac{2l+1}{\varkappa}\right). \tag{9}$$

In Table III in order to compare with the last formula for η_l (W.K.B.) we have collected several values for the phase shift for $l = 0$ and $l = 1$, *e.g.* the values of FOGEL ([7]) ($\eta_{l\text{F}}$), KÄLLÉN ( ) ($\eta_{l\text{K}}$), HANSON ([9]) ($\eta_{l\text{H}}$), RAMSEY ([10]) ($\eta_{l\text{R}}$) and numerical values ([11]) ($\eta_{l\text{num}}$).

Table III shows that the η_l (W.K.B.) are the better when $\varkappa$ increases and b decreases. The results for η_l (W.K.B.) are generally not worse than $\eta_{l\text{F}}$. For $l < 1$ the agreement for η_l (W.K.B.) with the exact values for η_l will be better. One can easily show taking into consideration the Watson's relation ([12]) for the Q_l that for $l \geqslant 10$ formula (7) is identical with formula (6). A more detailed discussion about the W.K.B. and the Born approximation we will published later on.

([6]) K. G. FOGEL: *Acta Acad. Aboensis*, **19**, 1 (1954).
([7]) See reference ([6]).
([8]) G. KÄLLÉN: *Ark. f. Fys.*, **4**, 42 (1952).
([9]) K. HANSON: *Fysiogr. Sallsk. Lund. Forhandl.*, **18**, 12 (1948).
([10]) W. RAMSEY: *Proc. Camb. Phil. Soc.*, **44**, 87 (148).
([11]) See reference ([6]).
([12]) G. N. WATSON: *Messenger. Math.*, **47**, 151 (1918).

TABLE III. – *Comparison of* $\operatorname{tg}\eta_l$ *(W.K.B.) with different results for* $l=1$ *and* $l=2$.

l	$\varkappa$	b	$\operatorname{tg}\eta_l$
1	1.2	— 0.9	$\operatorname{tg}\eta_l$ (W.K.B.) = — 0.04716 $\operatorname{tg}\eta_{lF}$ = — 0.04508 $\operatorname{tg}\eta_{lH}$ = — 0.04600
1	1.6	— 0.9	$\operatorname{tg}\eta_l$ (W.K.B.) = — 0.07430 $\operatorname{tg}\eta_{lF}$ = — 0.06775 $\operatorname{tg}\eta_{lH}$ = — 0.06906 $\operatorname{tg}\eta_{lK}$ = — 0.06850
1	1.6	2.7	$\operatorname{tg}\eta_l$ (W.K.B.) = 0.2235 $\operatorname{tg}\eta_{lF}$ = 0.1466 $\operatorname{tg}\eta_{lH}$ = 0.2911 $\operatorname{tg}\eta_{lK}$ = 0.267
1	0.8	2.7	$\operatorname{tg}\eta_l$ (W.K.B.) = 0.0501 $\operatorname{tg}\eta_{lF}$ = 0.0373 $\operatorname{tg}\eta_{lH}$ = 0.0863
1	1.2	2.7	$\operatorname{tg}\eta_l$ (W.K.B.) = 0.1414 $\operatorname{tg}\eta_{lF}$ = 0.1479 $\operatorname{tg}\eta_{lH}$ = 0.1925
1	1.13	— 5.12	$\operatorname{tg}\eta_l$ (W.K.B.) = — 0.2401 $\operatorname{tg}\eta_{lF}$ = — 0.1473 $\operatorname{tg}\eta_{lK}$ = — 0.156 $\operatorname{tg}\eta_{\text{num.}}$ = — 0.190
2	1.37	2.52	$\operatorname{tg}\eta_l$ (W.K.B.) = 0.0306 $\operatorname{tg}\eta_{lF}$ = 0.0305 $\operatorname{tg}\eta_{lH}$ = 0.0368 $\operatorname{tg}\eta_{lR}$ = 0.0366

IL NUOVO CIMENTO Vol. X, N. 3 1° Novembre 1958

Mesonic Decay of Helium Hyperfragment.

P. L. Jain

Physics Department, University of Buffalo - Buffalo, N. Y.

(ricevuto il 2 Ottobre 1958)

We have observed an event which is interpreted as a mesonic decay of a ^{4}He hyperfragment. This event was found in Ilford G-5 6 in. $\times$ 4 in. stripped emulsions of 400 μm thickness which were flown near Guam (Marian Island 6° N geomagnetic latitude) in 1957.

The interaction is observed in one emulsions with the exception of two particles which go into the facing emulsion. Fig. 1 shows the projection drawing of the events. A π-meson, which unfortunately could not be traced back beyond a range of 1237 μm collides with an emulsion nucleus and produces a primary star A, of type $2+1\pi$. From this nuclear disintegration, tracks b and c show the characteristic appearances of a heavy particle of charge one. Track d is due to a slow unstable particle in the forward hemisphere which comes to rest in the emulsion after 59.8 μm, thereupon giving rise to a secondary star B of three prongs. Because of the short length of the primary track d, no useful mass measurements could be made. There are no measurable δ-rays along the track, which exhibits only a very small amount of scattering along its path. This suggests that the charge of the hyperfragment was greater than one and by comparing with the other tracks in the same emulsion it was found to be due to an isotope of charge two.

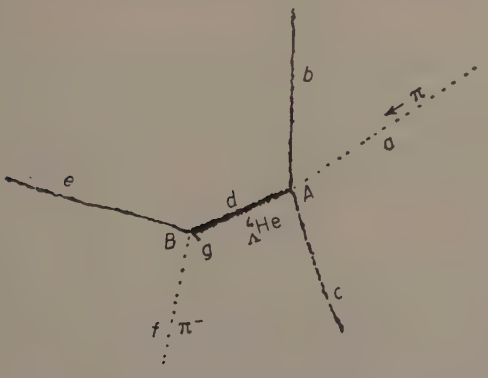

Fig. 1. - A nuclear fragment d from a primary star A stops in the emulsion and produces a secondary star B which has three prongs. Tracks e, f and g were produced by a proton, a π-meson and a ^{3}He nucleus respectively.

Track e is 657 μm long and ends in the same emulsion. The general appearance of the track e, along with the measurements of both δ-ray density and gap density against residual range along this track, indicates that it is due to a proton. The track f continues through eight pellicles and exhibits the characteristics of a π-meson. A « blob » accompanies the track ending which indicates that the π-meson was negative. A short

black track g is due to the recoil of a nucleus. The secondary star could not have been produced by a scattered proton because the short recoil is in the backward hemisphere. For the conservation of charge in the secondary particles it is required that track g must have been produced by a particle of charge two. Three tracks in the secondary star are coplanar within the limits of measurements ($\pm 2°$), and coplanarity of the track strongly suggests that only these three particles were involved in the disintegration of the hyperfragment, and no neutral particle was emitted in the decay; also the hyperfragment decayed from rest.

The data relating to this event are given in Table I. The energies and momenta of the singly charged particles were evaluated from the energy-range relation of FAY *et al.* [1], while for the doubly charged particle the range-energy relationship of WILKINS [2] was used. The energies of tracks e and f, from range measurement are found to be 11.0 MeV and 24.0 MeV respectively, and their corresponding momenta are 144.08 MeV/c and 85.3 MeV/c respectively. The momentum imbalance opposite to the recoil track g is 71.02 MeV/c which is within the error in angular measurements. If the recoil is assumed to be due to a ^{3}He nucleus, its momentum lies between 63 and 75 MeV/c as determined from its range. If the track is due to a ^{4}He nucleus its momentum lies between 73 and 85 MeV/c. The momentum balance would imply that the track was due to ^{3}He. Fragment d with a bound Λ^0 decays mesonically. The disintegration scheme which best satisfies all the measurements can be expressed by the equation

$$(1) \qquad {}^4\mathrm{He}_\Lambda \rightarrow {}^3\mathrm{He} + \mathrm{p} + \pi^- + Q_1 ,$$

where Q_1 is found to be (35.8 ± 0.34) MeV.

TABLE I.

Track	Identity	Range (μm)	Energy (MeV)	Momentum (MeV/c)	Angles
a	π	—	—	—	—
b	p	1180	15.5	171.5	—
c	p	285	6.7	112.8	—
d	$^4\mathrm{He}_\Lambda$	59.8	10.2	294.1	—
e	p	657	11.0	144.1	95.0
f	π^-	10752	24.0 ± 0.3	85.3 ± 0.2	53.2°
g	^{3}He	$2.6 < R < 3.1$	$0.7 < E < 0.9$	$63 < M < 75$	

The energy of the ^{3}He nucleus was obtained from momentum balance. It has been shown [3] that the value of Q_Λ from the following Λ^0 hyperon decay scheme

$$(2) \qquad \Lambda^0 \rightarrow \mathrm{p} + \pi^- + Q_\Lambda ,$$

is $Q_\Lambda = (36.9 \pm 0.2)$ MeV.

The close similarity between these Q values, together with the coplanarity

[1] H. FAY, K. GOTTSTEIN and K. HAIN: *Suppl. Nuovo Cimento*, **11**, 234 (1954).

[2] J. J. WILKINS: Atomic Energy Research Establishment, Harwell Report G/R 664 (unpublished).

[3] M. W. FRIEDLANDER, D. KEEFE, M. G. K. MENON and M. MERLIN: *Phil. Mag.*, **45**, 533 (1954).

already mentioned, strongly suggests that the observed phenomenon corresponds to break up of a meson active ^{4}He nucleus. In calculating the binding energy of Λ^0 particle in ^{4}He nucleus we have used Barkas' [4] mass values of different particles. The mass value of Λ^0 particle used is $M^0_\Lambda = 1114.82$ MeV, and the value of the binding energy of Λ^0 particle is found to be (1.1 ± 0.2) MeV. This value is in excellent agreement with the values appearing in the literature. This value may be compared with the much larger binding energy 20.6 MeV of the «last neutron» in ordinary ^{4}He.

If we consider the errors in the charge and mass, there exist alternate possible interpretations of the decay scheme of the hyperfragment of charge one. If the recoil was due to a proton, deuteron or a triton, one can write the following equations respectively.

(3) $\quad {}^2\mathrm{H}_\Lambda \to {}^1\mathrm{H} + \pi^- + {}^1\mathrm{H}\,,$

(4) $\quad {}^3\mathrm{H}_\Lambda \to {}^1\mathrm{H} + \pi^- + {}^2\mathrm{H}\,,$

(3) $\quad {}^4\mathrm{H}_\Lambda \to {}^1\mathrm{H} + \pi^- + {}^3\mathrm{H}\,.$

The expected ranges for these nuclei as obtained from the momentum imbalance of π^--meson and proton along track g are 14 μm, 16 μm, and 10.8 μm respectively. These ranges are much longer than the observed one, so the event observed is interpreted satisfactorily by equation (1).

* * *

We would like to thank Drs. K. E. Davis, N. M. Duller and C. A. Randall for sharing with us their plates which were exposed near Guam. We would also like to thank Prof. M. Schein for our stimulating introduction to this field in his laboratory during the summer of 1956.

(4) W. H. Barkas and D. M. Young: University of California Radiation Laboratory Report UCRL 2579 Rev. (unpublished).

IL NUOVO CIMENTO Vol. X, N. 3 1° Novembre 1958

Interaction entre un petit et un grand système Hamiltonien effectif; polarisation et absorption.

F. Englert

Université Libre de Bruxelles - Bruxelles

(ricevuto il 4 Ottobre 1958)

Considérons un système binaire dont les particules constituant le premier sous-système, appelé s, sont beaucoup moins nombreuses que celles formant le second, appelé S; soit $V(r)$ l'énergie potentielle d'interaction entre une particule de s et une particule de S.

On peut mettre l'hamiltonien du système sous la forme

$$H = H_0 + H_{\text{int}}, \tag{1}$$

où

$$H_0 = H^s + H^S, \tag{2}$$

et on peut écrire

$$H_{\text{int}} = \sum_{\vec{q}} V(q)\, \varrho^S_{\vec{q}}\, \varrho^s_{-\vec{q}}, \quad (*) \tag{3}$$

où $V(q)$, $\varrho^S_{\vec{q}}$, $\varrho^s_{-\vec{q}}$ sont des transformées de Fourier du potentiel $V(r)$ et des densités de particules dans s et S.

D'une manière générale, on peut toujours, à l'aide d'une transformation unitaire, obtenir un hamiltonien $\tilde{H}$ équivalent à H au second ordre en H_{int}

$$\tilde{H} = H_0 + {}^{\Lambda}H_{\text{int}} + \mathcal{R} \lim_{\varepsilon \to +0} \sum_m H_{\text{int}} \frac{1}{E_m - H_0 \pm i\varepsilon} H_{\text{int}} |m\rangle\langle m|, \tag{4}$$

où E_m et $|m\rangle$ sont relatifs à H_0 et ${}^{\Lambda}H_{\text{int}}$ est la partie de H_{int} connectant les états de même énergie de H_0; le signe $\mathcal{R}$ indique que seule la partie hermitienne de l'opérateur considéré doit être conservée.

(*) La méthode exposée ici est en fait valable pour un H_{int} quelconque.

Négligeons les transitions résonantes dues à ${}^{\Lambda}H_{\text{int}}$; portant (3) dans (4) et prenant une moyenne statistique sur les états du grand système, on obtient alors, si S est invariant par rapport aux translations, un hamiltonien effectif pour le petit système s

$$H_{\text{eff}} = H^s + \mathcal{R} \sum_{\bar{q}} V^2(q)\, \varrho^s_{\bar{q}}\, \varrho'^s_{-\bar{q}}\,, \tag{5}$$

où

$$\langle m^s | \varrho'^s_{-\bar{q}} | n^s \rangle = \langle m^s | \varrho^s_{-\bar{q}} | n^s \rangle \, \Phi^{\pm}_s(\bar{q}, \omega_{n^s m^s}; T)\,. \tag{6}$$

La fonction $\Phi^{\pm}_s(\bar{q}, \omega; T)$, dont les parties réelles et imaginaires sont liées par des relations de causalité, est caractéristique du système S à la température T et vaut

$$\Phi^{\pm}_s(\bar{q}, \omega; T) = \frac{1}{\hbar} \lim_{\varepsilon \to +0} \sum_{n^S} p_{n^s}(T) \sum_{m^S} \frac{|\langle m^S | \varrho^S_{\bar{q}} | n^S \rangle|^2}{\omega - \omega_{m^S n^S} \pm i\varepsilon}\,, \tag{7}$$

où $p_{n^s}(T)$ est le poids statistique affectant l'état $|n^S\rangle$ à la température T. Désignant par $T^{\omega,\bar{q}}\, f(\bar{r}, t)$ la transformée de Fourier quadridimensionnelle de $f(\bar{r}, t)$, on a

$$\Phi^{-}_S(\bar{q}, \omega; T) = \frac{i}{\hbar} T^{\omega,\bar{q}}\, G_S(\bar{r}, t; T)\, U(t)\,, \tag{8}$$

où $G_S(r, t; T)$ est la fonction de corrélation de paire de Van Hove [1] à la température T et $U(t)$ est la fonction qui vaut 0 pour $t < 0$ et 1 pour $t > 0$.

On peut écrire

$$\Phi^{\pm}_S(\bar{q}, \omega; T) = A^{\pm}_S(\bar{q}, \omega; T) + B^{\pm}_S(\bar{q}, \omega; T)\,, \tag{9}$$

où les deux termes de (9) sont définis par (8) en remplaçant successivement $G_S(\bar{r}, t; T)$ par sa partie imaginaire pure et par sa partie réelle; le terme $B^{\pm}_S$ intervient alors dans (5) uniquement par suite du traitement non symétrique des systèmes s et S et multiplie un commutateur; le terme $A^{\pm}_S$ au contraire, subsiste lorsque le petit système s peut être considéré comme classique. La fonction $\Phi^{\pm}_S(\bar{q}, \omega; T)$ détermine les propriétés de polarisation et d'absorption du système S; toutefois lorsque le petit système pourra être considéré comme classique, il suffira de considérer la fonction $A^{\pm}_S(q, \omega; T)$.

Envisageons maintenant le cas où s et S sont composés d'électrons interagissant par un potentiel coulombien; si on néglige les interactions d'échange entre s et S, on peut écrire (5) sous la forme

$$H^{\text{eff}} = H^{0s} + \mathcal{R} \sum_{\bar{q}} \frac{2\pi e^2}{q^2} \left\{ \varrho^s_{\bar{q}}\, \varrho^s_{-\bar{q}\,0} - n \right\}, \tag{10}$$

où n est le nombre de porteurs minoritaires, H^{0s} leur énergie cinétique et

$$\langle m^s | \varrho^s_{-\bar{q}\,0} | n^s \rangle = \langle m^s | \varrho^s_{-\bar{q}} | n^s \rangle \left\{ 1 + \frac{8\pi e^2}{q^2} \Phi^{\pm}_S(\bar{q}, \omega_{n^s m^s}; T) \right\}. \tag{11}$$

[1] L. VAN HOVE: *Phys. Rev.*, **95**, 249 (1954).

L'équation (10), où les éléments de matrice (11) sont pris en principe entre états propres de H^s est la généralisation de celle obtenue par PINES et NOZIÈRES [2]; l'expression

$$\left\{1+\frac{8\pi e^2}{q^2}A_s^{\pm}(\bar{q},\omega;T)\right\}^{-1}, \tag{12}$$

peut être identifiée à la constante diélectrique complexe classique du système S; elle est égale, pour $T=0$, à celle définie par PINES et NOZIÈRES [3] et est la même que celle de FANO [4].

D'autres applications et une discussion plus détaillée des résultats précédents feront l'objet d'une prochaine publication.

* * *

Nous remercions vivement Monsieur le Professeur GÉHÉNIAU qui nous a aidé par d'intéressantes discussions.

[2] P. NOZIÈRES et D. PINES: *Phys. Rev.*, **109**, 762 (1958).
[3] P. NOZIÈRES et D. PINES: *Nuovo Cimento*, **9**, 470 (1958).
[4] U. FANO: *Phys. Rev.*, **103**, 1202 (1956).

IL NUOVO CIMENTO Vol. X, N. 3 1° Novembre 1958

On the Radiation Emitted by Charged Particles Interacting with Complex Nuclei.

B. Bosco

Istituto di Fisica dell'Università - Torino
Istituto Nazionale di Fisica Nucleare - Sezione di Torino

(ricevuto il 27 Ottobre 1958)

A good deal of attention has been paid in recent years to the optical model with a complex potential.

Its application has furnished a simple and sufficiently general model to deal with the scattering of any kind of particles with complex nuclei when such phenomena are more or less anelastic as in the case of antinucleon-nucleus or meson-nucleus interaction (1).

It seems therefore to be worthwhile to analize whether it is possible to use the optical model in order to evaluate the radiation emitted in such interactions. Substantially there are two questions connected with such a problem:

1) The conventional electric current associated to a flux of charged particles when the hamiltonian is hermitian is given for a transition from a state a to a state b by:

$$\boldsymbol{j}_c = \frac{e\hbar}{2im}\{\bar{\Psi}_b \nabla \Psi_a - (\nabla \bar{\Psi}_b)\Psi_a\} \quad (2). \tag{1}$$

If now a and b are continuum states, and the Hamiltonian is not hermitian the problem is to know what kind of function has to be put in (1) for Ψ_b in order to obtain the proper asymptotical condition, or in other words if we write, as usually, Ψ_b by means of the phase-shifts, the problem is to determine if the phase-shifts of Ψ_b are due to the potential $V(r)$ of H or to $V^c(r)$ of H^c where the superscript c means complex coniugate.

---

(1) See for ex: J. Kessler and L. Lederman; *Phys. Rev.*, **94**, 689 (1954); H. Feshbach, C. Porter and V. Weisskopf: *Phys. Rev.*, **96**, 449 (1954). There are also many analysis of π-ncleus scattering in terms of complex potential. These analysis have been published in *J.E.P.T.* in the 1957.

(2) The antisymmetrization in necessary in order that j_c may satisfy the continuity equation.

2) It is well known that if complex potential is present the continuity equation reads:

$$\frac{\partial \varrho}{\partial t} + \operatorname{div} \boldsymbol{j}_c = -\frac{2e}{\hbar} V_i(r) \overline{\Psi}_b \Psi_a \,, \tag{2}$$

$$\varrho = e \Psi_b \Psi_a \,, \tag{1'}$$

and $\boldsymbol{j}_c$ is given by (1), where $V_i(r)$ is the imaginary part of the potential.

Clearly the term which appears on the r.h.s. of (2) represents the absorption by the nucleus of some charge of the beam: therefore also this term will contribute to create radiation. We begin with the first question.

Let us repeat step by spet the proof given in BETHE and MAXIMON [3], taking into account the fact that the phase-shifts are complex. We get for Ψ_b the expression:

$$\Psi_b(r) = \sum (2l+1) i^l \exp\left[-i\eta_c^*\right] L_l(r) P_l(\theta) \,,$$

where the functions are defined in the same paper.

Now since η_c is a real function of the potential we have $\eta_l^* = \eta_l^c$ where η_l^c are the phase-shifts due to the potential $V^c(r)$.

Then we can say that Ψ_b has to be an incoming wave corresponding to the potential $V^c(r)$.

The same results can be of course obtained with the more general argument of BETHE and BREIT [4].

We turn now attention to the second question; *i.e.* how to evaluate the radiation due to the absorption of charge.

The function $+(2e/\hbar) V_i(r) \overline{\Psi}_b \Psi_a$ can be considered as the divergence of a vector $\boldsymbol{j}_N$ which we can interprete as the nuclear current created by the absorption of charge from the beam of colliding particles.

The continuity equation (2) takes the form:

$$\frac{\partial \varrho}{\partial t} + \operatorname{div} (\boldsymbol{j}_C + \boldsymbol{j}_N) = 0 \,, \tag{3}$$

with:

$$\operatorname{div} \boldsymbol{j}_N = \frac{2e}{\hbar} V_i(r) \overline{\Psi}_b \Psi_a \,.$$

In other terms if we consider together with the conventional current also a nuclear current responsible for charge exchange between the nuclear matter and the beam particles we must obtain conservation of charge.

Unfortunally the knowledge of $\operatorname{div} \boldsymbol{j}_N$ does not determine completely the vector $\boldsymbol{j}_N$.

However, whilst $\boldsymbol{j}_c$ is important in all the space $\boldsymbol{j}_N$ is different from zero only in a limited region. This fact enables us at least for not too high energy of the

[3] H. A. BETHE and L. C. MAXIMON: *Phys. Rev.*, **93**, 768 (1954).
[4] H. A. BETHE and G. BREIT: *Phys. Rev.*, **93**, 888 (1954).

emerging photon to determine the matrix element of all the the electric multipole transitions.

In fact if $(kR)^2 < 4l + 6$ we have [5]: (l is the order of multipole).

$$a_E(l, m) = \frac{i}{c} \frac{4\pi}{(2l+1)!!} \left(\frac{l+1}{l}\right)^{\frac{1}{2}} k^{l+1} \int r^l Y^*_{lm}(\theta, \varphi) \operatorname{div} \boldsymbol{j}_N \, \mathrm{d}V .$$

The magnetic effect of such a current is completely indetermined from the previous arguments but from qualitative evaluation of such effects we can argue that such effect is quite small. In fact we know that the order of magnitude of multipoles magnetic transitions are

$$a_M(l, m) \simeq \frac{V}{c} a_E(l, m) ,$$

where V is the velocity of the charge of the particles absorbed by the complex nucleus and therefore is practically zero.

In order to complete the model we must add a prescription on the incoherence of the amplitude of $\boldsymbol{j}_c$ and $\boldsymbol{j}_N$; in fact since $\boldsymbol{j}_N$ will change the charge number of nuclear wave function its amplitude will certainly be incoherent with the amplitude of $\boldsymbol{j}_c$ which conserves such a number.

* * *

The author is greatly indebted to Prof. V. WEISSKOPF for many illuminating discussions; he also wishes to thank Prof. M. VERDE and S. FUBINI for useful suggestions and criticism.

---

(5) J. M. BLATT and V. F. WEISSKOPF: *Theoretical Nuclear Physics* (New York, 1952), p. 807.

LIBRI RICEVUTI E RECENSIONI

J. D. Fast, H. G. van Buren. J. Philibert – *La diffusion dans les métaux*, Bibliotèque Thecnique Philips – Eindhoven, 1957. pp. 124

Si tratta degli atti di un convegno di un piccolo gruppo di specialisti francesi, belgi e olandesi su alcuni aspetti della diffusione nei solidi. Più esattamente due lavori trattano l'influenza dei difetti strutturali sulla diffusione; quattro vertono sull'effetto Kirkendall, qualche altro sulla diffusione intergranulare, con un totale di otto lavori. Precede una chiara introduzione di A. D. Le Claire.

G. Careri

Michel Bayet – *Physique électronique des gas et des solides*. Masson et Cie. - Paris, 1958 (pag. 246).

Questo libro è sostanzialmente un corso universitario sui fenomeni di trasporto delle cariche elettriche nei gas e nei solidi.

Parte dei capitoli ha un valore introduttivo e tratta le nozioni di statistica quantica, la teoria degli urti, la cinetica dei gas, la teoria elettronica dei metalli, ecc., in modo elementare ed, a volte, un poco incompleto. Altri capitoli invece, si staccano nettamente e sono di livello assai più elevato. In modo particolare quelli che trattano il gas di Lorentz non degenere e le proprietà elettromagnetiche dei plasmi dal punto di vista meccanico statistico. In questo campo l'autore ha portato anche dei contributi personali.

Ne risulta un libro, che, pur mancando di unità, può riuscire utile sia agli studenti che agli specialisti.

G. Careri

V. Hlavaty – *Geometry of Einstein's unified field theory* Noordhoff Ltd. Groningen-Holland pag. xxxii, 341, $ 9.

Questa monografia di Hlavaty costituisce certamente uno dei contributi più notevoli alla discussione dell'ultima teoria di Einstein del campo unificato. Le equazioni della teoria furono postulate da Einstein poco prima della sua morte e si trovarono riportate nell'appendice II del volume *The meaning of Relativity*. È noto che la deduzione delle conseguenze di tali equazioni ha presentato e presenta tuttora notevoli difficoltà matematiche e difficile appare anche il problema di individuare predizioni specifiche della teoria che sia possibile sottoporre a verifica sperimentale.

Hlavaty cura essenzialmente in questo volume di sviluppare una base geometrica per l'interpretazione delle equazioni di Einstein. In vista della natura essenzialmente geometrica della teoria questo studio è già sufficiente ad offrire una visione molto dettagliata delle principali conseguenze fisiche. Il primo capitolo del volume considera le conseguenze ed i relativi sviluppi geometrici di quello che l'autore chiama postulato A della teoria, cioè che il campo unificato sia descritto da 16 potenziali, come suggerito dal computo dei potenziali necessari nelle teorie non unificate. Pertanto viene esaminata in dettaglio la struttura algebrica dello spazio-tempo dovuta al tensore non simmetrico $g_{\lambda\mu}$. Dallo studio della struttura del tensore $g_{\lambda\mu}$ si ricava una classificazione dei possibili spazio-tempo in tre classi a seconda della natura delle soluzioni del problema ad autovalori relativo al tensore misto ricavabile dalla parte antisimmetrica di $g_{\lambda\mu}$, usando quale tensore metrico la parte simmetrica di $g_{\lambda\mu}$. Questa classificazione è importante in tutto il seguito e l'interpretazione fisica delle equazioni del campo va condotta con metodi diversi nei tre casi. Il campo elettromagnetico $f_{\lambda\mu}$, è diverso dalla parte antisimmetrica del tensore $g_{\lambda\mu}$, ma entrambi questi tensori appartengono alla stessa classe.

Nei seguenti due capitoli vengono esaminate le conseguenze del cosiddetto postulato B della teoria cioè, che i potenziali determinino la curvatura e la torsione dello spazio-tempo. L'espressione matematica del postulato si trova nelle 64 equazioni che definiscono la connessione $\Gamma^{\nu}_{\lambda\mu}$ dello spazio-tempo attraverso $g_{\lambda\mu}$ e le sue derivate prime, analogamente a quanto avviene per i simboli di Cristoffel nella teoria della gravitazione. Anche qui la discussione dell'esistenza della soluzione per i $\Gamma^{\nu}_{\lambda\mu}$ è subordinata alla distinzione degli spazio-tempo nelle tre classi menzionate, e diverse sono le condizioni per l'esistenza nei tre casi.

Nel capitolo quarto l'autore affronta il problema centrale della teoria, cioè la discussione delle conseguenze di quello che egli chiama postulato C, che richiede al tensore $g_{\lambda\mu}$ di essere soluzione di un sistema di equazioni differenziali equivalenti a precise condizioni per la curvatura e la torsione dello spazio-tempo. La specificazione di tali condizioni, dovuta ad Einstein, porta a condizioni per il tensore di curvatura $R^{\nu}_{\omega\mu\lambda}$ che possono venire interpretate come equazioni differenziali per il tensore non simmetrico $g_{\lambda\mu}$ (equazioni del campo). In questo capitolo vengono solo discusse le conseguenze di tali condizioni sulla struttura geometrica dello spazio-tempo.

Le conseguenze fisiche del postulato C e della sua specificazione in termini delle equazioni di Einstein vengono esaminate nel capitolo quinto. Anzitutto viene mostrata l'esistenza e l'unicità di un tensore $f_{\lambda\mu}$ (campo elettromagnetico) che sia antisimmetrico, che sia una funzione di $g_{\lambda\mu}$, ma non delle sue derivate, ottenibile da $g_{\lambda\mu}$ mediante costruzione tensoriale, e che soddisfi le equazioni di Maxwell come conseguenza delle equazioni di Einstein. Si trova che $f_{\lambda\mu}$ può esprimersi esplicitamente in termini della parte antisimmetrica di $g_{\lambda\mu}$, ma non coincide mai con essa. Il tensore del campo gravitazionale può quindi identificarsi con la parte simmetrica di $g_{\lambda\mu}$, dal confronto dell'equazione per il suo tensore contratto con le vecchie equazioni del campo nella teoria della gravitazione. L'autore mostra come, nell'ipotesi in cui sia trascurabile il campo elettromagnetico del sole, si ottengano dalla teoria del campo unificato le equazioni della teoria gravitazionale.

Completano il volume tre lunghe appendici. Nella prima l'autore studia la geometria dei segnali luminosi. Il risultato importante di questo studio è la previsione di possibili campi elettromagnetici per cui, pur sotto l'ipotesi di costanza della velocità della luce e trascurando effetti gravitazionali, non deve valere necessariamente il risultato della

esperienza di Michelson-Morley. È noto che una discrepanza era stata riportata in passato tra i risultati di Michelson-Morley e i risultati di analoghe esperienze di Miller. Riteniamo molto probabile che la discrepanza sia dovuta piuttosto ad errori sperimentali. È chiaro però che un riesame e un perfezionamento dell'esperimento potrebbero risultare utili. La seconda appendice sull'algebra degli spinori a quattro componenti è particolarmente interessante per il fisico teorico. L'autore mostra come il tensore non simmetrico $g_{\lambda\mu}$ si presti molto convenientemente all'algebra ed all'analisi degli spinori a quattro componenti. Infine l'appendice terza, utile per la lettura di certe parti del volume, contiene l'esposizione degli elementi essenziali della geometria della retta in uno spazio proiettivo a tre dimensioni.

Da questa, pur rapida e incompleta esposizione del contenuto, il lettore si renderà conto dell'importanza del volume che crediamo riuscirà molto utile agli studiosi della teoria del campo unificato. Come abbiamo già accennato, l'autore si propone anzitutto di chiarire le basi geometriche della teoria. Pertanto il volume presuppone già una educazione geometrica nel lettore, purtroppo non molto diffusa tra i fisici, ivi compresi i fisici teorici. È improbabile tuttavia che si possa ricavare una comprensione sufficiente della teoria del campo unificato senza pieno uso degli strumenti geometrici necessari. L'esame delle conseguenze fisiche della teoria presuppone invece una conoscenza altrettanto accurata di molte questioni astronomiche, e di questo aspetto del problema possono trovarsi nel volume solo cenni brevissimi.

R. Gatto

Direttore responsabile: G. POLVANI Tipografia Compositori - Bologna

Questo fascicolo è stato licenziato dai torchi il 27-XI-1958